EXPERIMENTAL STUDY OF PLASMA OSCILLATIONS IN IMPED

By

SAYAK BOSE
PHYS06200804002

Institute for Plasma Research, Gandhinagar

A thesis submitted to the

Board of Studies in Physical Sciences
In partial fulfillment of requirements

for the Degree of

DOCTOR OF PHILOSOPHY

of

HOMI BHABHA NATIONAL INSTITUTE

August, 2015

Homi Bhabha National Institute

Recommendations of the Viva Voice Board

As members of the Viva Voice Board, we certify that we have read the dissertation prepared by **Sayak Bose** entitled "**Experimental study of plasma oscillations in IMPED**" and recommend that it may be accepted as fulfilling the dissertation requirement for the Degree of Doctor of Philosophy.

18/01/16 Date: 18/01/2016

Chairman: Prof. Y. C. Saxena

18.01.16 Date: 18/01/2016

Guide / Convener: Prof. P. K. Chattopadhyay

18.1.2016 Date: 18/01/2016

Examiner: Prof. R.P. Dahiya

18/01/16 Date: 18/01/2016

Member: Prof. Sudip Sengupta

18/01/16 Date:18/01/2016

Member: Dr. Joydeep Ghosh

Final approval and acceptance of this dissertation is contingent upon the candidate's submission of the final copies of the dissertation to HBNI.

I hereby certify that I have read this dissertation prepared under my direction and recommend that it may be accepted as fulfilling the dissertation requirement.

Date: 18/01/2016

18.01.16

Place: Gandhinagar **Guide**

STATEMENT BY AUTHOR

This dissertation has been submitted in partial fulfillment of requirements for an advanced degree at Homi Bhabha National Institute (HBNI) and is deposited in the Library to be made available to borrowers under rules of the HBNI.

Brief quotations from this dissertation are allowable without special permission, provided that accurate acknowledgement of source is made. Requests for permission for extended quotation from or reproduction of this manuscript in whole or in part may be granted by the Competent Authority of HBNI when in his or her judgment the proposed use of the material is in the interests of scholarship. In all other instances, however, permission must be obtained from the author.

Sayak Bose

Sayak Bose

DECLARATION

I, hereby declare that the investigation presented in the thesis has been carried out by me. The work is original and has not been submitted earlier as a whole or in part for a degree/diploma at this or any other Institution/University.

Sayak Bose

Sayak Bose

List of Publications arising from the thesis

A. **Published:**

1. Inverse mirror plasma experimental device (IMPED) – a magnetized linear plasma device for wave studies, Sayak Bose, P.K. Chattopadhyay, J. Ghosh, S. Sengupta, Y.C. Saxena and R. Pal, *Journal of Plasma Physics*, **2015**, 81 345810203.

2. Inverse mirror plasma experimental device - A new magnetized linear plasma device with wide operating range, Sayak Bose, Manjit Kaur, P.K. Chattopadhyay, J. Ghosh and Y.C. Saxena, *Review of Scientific Instruments*, **2015**, 86, 063501.

B. **To be communicated:**

1. Design and plasma characteristics of a magnetized linear plasma device with a multi-filamentary plasma source, Sayak Bose *et al., To be submitted.*

2. Langmuir probe algorithm for automated and semi-automated measurement of plasma parameters, Sayak Bose *et al., To be submitted.*

3. Interactions in a magnetized plasma column, Sayak Bose *et al., To be submitted.*

4. Interaction of plasma oscillation with a background ion density perturbation, Sayak Bose *et al., To be submitted.*

Sayak Bose

Sayak Bose

DEDICATED

TO

MY PARENTS

Acknowledgement

I would like to start by thanking my parents for their unending support and constant motivation during my PhD. I would also like to thank them for being a constant source of love, concern, strength and patience all these years. I would like to express my heart-felt gratitude to my family.

I would also like to express my sincere gratitude to my thesis supervisor Prof. Prabal K. Chattopadhyay for his continuous support during my PhD work and for his patience, motivation, enthusiasm, and immense knowledge. His guidance helped me in all the time of research and writing of this thesis. I am deeply grateful to him for the discussions that helped me sort out the technical details of my work.

I am also thankful to Prof. Y. C. Saxena and Dr. J. Ghosh for their help and discussion. Their patience and support helped me overcome many crisis situations and finish this thesis. They have been always there to listen and give advice. Their insightful comments and constructive criticisms at different stages of my research were thought provoking and they helped me focus my ideas. I humbly appreciate their motivating ideas and fruitful discussions we had.

I would like to thank Prof. Sudip Sengupta for his continuous support, encouragement and guidance throughout this thesis, which kept me on track. I would also like to thank Prof. Rabindranath Pal, of Saha Institute of Nuclear Physics, for various stimulating discussions on different occasions during the tenure of my PhD. I am also thankful to Prof. P.K. Kaw and Prof. D. Bora for giving me this wonderful opportunity.

I specially thank Dr. Mani Subramanian for allowing me to use some of his Laboratory equipments. I would like to thank Prof. Amita Das, Dr. R. Ganesh, Dr. M. Kundu, *Dr. D. Sharma, Dr R. Goswami and Dr. M. Warrier for teaching me during my 1st year course work. I would like to thank Prof. S. Mukherjee for his guidance and quick response on things related to HBNI.*

I am grateful to my colleagues in Basic Plasma Laboratory Manjit, Kshitish, Soumen, Sonu and Hiral for various fruitful discussions on different occasions regarding the experimental results of other devices in the laboratory. This enabled me to develop a better understanding of experimental plasma physics. I would like specially thank my colleague Manjit for allowing me to carry out experiments in her experimental device (Complex Plasma Experimental Device) when my device was under construction. The hands on experience that I gained while working with Manjit proved to be very helpful. I would like thank my summer school students, Nasreen Banu, Gaurav Nalini Datttaraya, Harshit Agrawal, Tanmay Macwan, Safikul Alam, Niketa Joshi, Shruti Thakkar, Anjali Panchwanee and Shikha Binwal for working on their summer projects very enthusiastically and also for asking very insightful questions.

I am also grateful to the staff members from electronics lab, workshop, computer centre, library, stores, purchase section, administration, drafting section canteen and security at Institute for Plasma Research for their co-operation and help during the entire duration of my PhD. I would like to thank Rajni, Radhe and Rashik for working with me to make and install Inverse Mirror Plasma Experimental Device.

I would like to thank to my seniors Vikrant, Maya, Kishor, Vikram, Ujjwal, Gurdatt, Prabal, Sita, Ashwin, Sunita, Satya, Sharad, Pravesh, Rameshwar, Shekar, Jugal, Sanat, Sushil, Debu da and juniors Aditya for their support, valuable inputs during PhD and providing friendly environment in scholar hall and hostel. I would also like to thank my juniors, Vikram, Veda, Vara, Roopender, Chandrashekar, Bhibhu, Neeraj, Mangilal, Deepa, Akanksha, Vidhi, Harish, Meghraj, Sameer, Arghya, Surbahi, Bhumika, Narayan, Ratan, Modhu, Amit, Debraj, Umesh, Sonu, Sagar, Atul, Jervis, Deepak, Prabhakar, Meenakshi, *Pallavi, Alamgir, Sandeep, Harshita, Chetan, Arun and others for their humour without which our hostel would have been a very dull place. Last but not the least, I would like to thank my dear friends Dr. Subir Biswas and Dr. Animesh Kuley for their support during my PhD.*

Table of Contents

Synopsis

Plasma supports a number of modes and understanding of these various modes is crucial for understanding of basic plasma physics. Electrostatic plasma oscillation is one of the fundamental modes in plasma where the electrons oscillate with a frequency close to electron plasma frequency (ω_{pe}). Plasma density oscillates longitudinally with high frequency when the quasineutrality of the plasma is violated locally. Tonks and Langmuir[1] experimentally observed this oscillation and provided a basic theoretical explanation; however, they restricted their treatment to cold plasma and small amplitude oscillation. The effect of thermal motion of particles was studied theoretically by Vlasov and Landau. In fact Landau[2] showed that it is possible to damp electron plasma waves even without collisions. A physical picture of this Landau damping was later given by Dawson[3] who explained the phenomena as exchange of energy between the wave and the particles having velocity close to wave phase velocity (resonant wave particle interaction). Malmberg *et al.*[4] established the collisionless damping of electron plasma wave experimentally. They measured the spatial damping of longitudinal electron plasma wave, excited by applying a high frequency voltage to a Langmuir probe in collisionless plasma. The authors also verified the role of resonant electrons in the collisionless damping by cutting off the tail of the Maxwellian distribution of electrons and observed a sharp decrease in damping. O'Neil[5] extended the collisionless damping of nonlinear plasma oscillations to time (t) greater than $\tau_B \left(= \sqrt{m/eEk}\right)$, the bounce period of the trapped particles in the wave having electric field amplitude E and wave number k. The damping coefficient has an oscillatory behaviour when t/τ is of the order of unity, and its phase mixes to zero as $t/\tau \to \infty$. This nonlinear behaviour of the damping coefficient was experimentally proven by Malmberg and Wharton[6]. They investigated the damping of a large amplitude plasma wave and observed amplitude oscillation at large distances from the exciter. In the course of their experiment, Wharton *et al*.[7] observed side bands separated from the transmitter frequency by bounce frequency $\omega_B \left(=1/\tau_B\right)$ associated with large amplitude electron plasma wave. Subsequently, different aspects of nonlinear electron plasma wave, namely, electron trapping effects, wave–wave interaction and side band instability, were investigated by Franklin *et al.*[8 - 10].

It is observed that on increasing the amplitude of electron plasma wave, different nonlinear effects become dominant. But plasma does not sustain wave having arbitrarily high amplitude, and beyond certain limit, wave breaks. The maximum electric field amplitude that a plasma can sustain is a topic of fundamental importance to many areas of plasma physics particularly, plasma based particle acceleration schemes[11-12] and some laser fusion schemes[13 – 14]. In laser fusion experiments, energetic electrons generated by wave breaking eventually leads to heating of the core and in plasma based particle accelerators, the maximum energy of the particles accelerated by resonant wave–particle interaction is dictated by the wave breaking amplitude. In cold plasma, wave breaking occurs when the electron excursion length becomes comparable to the wavelength and which is characterized by sharp rise in the local electron density and its gradient[15]. Bauer *et al*.[16] reported experimental observation of wave breaking of electron plasma wave in radiofrequency (RF) afterglow plasma. They observed energetic electrons associated with wave breaking. However, a detailed experimental study of wavebreaking of plasma oscillation establishing the parametric dependence of the wavebreaking amplitude on other plasma parameters like density and temperature are to be carried out.

Besides wave breaking, a wave may lose its coherence by another less violent process namely, phase mixing of plasma oscillation/wave. Phase mixing is the loss of coherence of plasma oscillation/wave due to fine scale mixing of various parts of the oscillation/wave when there is a spatial variation of local plasma frequency. This can happen due to the presence of inhomogeneity in the background plasma density that may occur due to a number of reasons. It may be caused by the presence of an ion wave in the background [17]. It may also occur in homogeneous plasma in the presence of nonlinear plasma oscillations because of the response of ions to ponderomotive forces either directly or through low frequency self consistent fields[18].

A number of theoretical work[17 -23] have been carried out in the field of nonlinear plasma oscillation especially pertaining to wavebreaking and phase mixing of plasma oscillation. However, only a few experiments have been carried out, and a comprehensive experimental study testing, various predictions of theory and simulation is still elusive. For example, Sengupta *et al*[18] theoretically showed that phase mixing of plasma oscillation can occur in homogeneous plasma and time (t_{mix}) in which the oscillations phase mix is dependent on the mass of the ions, $t_{mix} \propto \left(\Delta / \sqrt{1+\Delta}\right)^{1/3}$, where Δ is the electron ion mass ratio. Recently, Verma *et al.* [23] using one dimensional particle in cell (PIC) simulation of large amplitude of plasma oscillations in cold plasma showed the excitation of residual Bernstein-Greene-Kruskal like waves after electron wavebreaking in cold plasma. With these perspectives in mind a new machine, Inverse Mirror Magnetized Plasma Device (IMPED), has been designed and fabricated in-house at Institute for Plasma Research, India, in which phase mixing and wave breaking of nonlinear plasma oscillation/wave can be investigated comprehensively in a controlled manner.

The primary objective, of the work described in this thesis, is to identify the plasma window necessary for comprehensive experimental study of wavebreaking and phase mixing of plasma oscillation followed by design, fabrication of an experimental device that satisfies all the necessary criteria for successfully carrying out these experiments. Plasma in IMPED is thoroughly characterised to establish the capability of the device producing plasmas required for the proposed experiments. This is followed by experimental study of phase mixing of plasma oscillation carried out within the requisite window of operation.

The thesis is organized in eight chapters. Chapter 1 gives the introductory description of plasma oscillation and different linear and nonlinear phenomena associated with it. Chapter 2 includes theoretical review of phase mixing and wavebreaking of nonlinear plasma oscillation. Phase mixing of plasma oscillation leads to loss of coherence as a result of which the oscillation decays. In laboratory plasma, the oscillation/wave may decay due to Landau damping or collisional damping. Phase mixing is not a violent process like wave breaking and in noisy plasma, it might be very difficult to do a controlled study of phase mixing. Additionally, phase mixing may occur in a number of physical situations, so the plasma device should be able to accommodate such physical conditions. Therefore, a calculation is carried out to determine experimental conditions necessary for observing phase mixing of plasma oscillation in terms of density range, temperature range, operating pressure, quiescence, magnetic field, required plasma uniformity and other requirements that the plasma source needed to satisfy. In the light of the experimental requirements, a detailed review of the existing schemes of plasma production is carried out to identify which scheme of plasma production can be further developed to meet the experimental requirements. The above mentioned theoretical review and the subsequent calculation to determine a suitable window for the proposed experiments are published in Journal of Plasma Physics, 81, 345810203 (2015).

In Chapter 3, the development of the experimental device is described in detail. The development of the device is carried out in two stages. In the first stage, a ~ 2.7 m long prototype device is made. The prototype is called Magnetised Linear Plasma Device (MLPD). It consists of a source chamber of length and diameter 0.5 m followed by a 2.2 m long main chamber of diameter 0.161 m. Ten air cooled wire wound magnets were placed coaxially along the length of the main chamber for producing a uniform magnetic field over a distance of ~ 1.4 m. Plasma is produced by the multifilamentary plasma source [24] located in the low magnetic field region of the source chamber. During the course of operation of the prototype device, modifications were made in plasma source to improve the performance and also primary diagnostics were developed. This was followed by the upgradation of the prototype to the final design. The upgraded device is named Inverse Mirror Plasma Experimental Device (IMPED). The upgraded device is 3.4 m long, it consist of a source chamber, source chamber extension and main chamber. Uniform magnetic field is produced by placing 10 electromagnets coaxially around the main chamber for producing a maximum field 1.2 kG. The upgraded device has four additional electromagnets between the source and the main chamber for independent variation of magnetic field. Design considerations, fabrication and operation of the system and subsystems have been described in this chapter. The diagnostics developed for measuring plasma parameters are discussed in this chapter. The diagnostics include Langmuir probe, emissive probe, ion wave exciter and exciter and detector of plasma oscillation. In order to process the Langmuir probe data quickly, a code has been developed to process the data automatically and semi-automatically.

In Chapter 4, plasma characteristics of MLPD and IMPED are presented. The variation of the plasma parameters with different control features in both the devices is discussed. Particularly wide range of density and temperature variation has been achieved in IMPED. Lowest operating pressure in IMPED is 1.7×10^{-5} mbar which is well within the collisionless regime of plasma production. Plasma density is found to vary ~ 20 times when pressure is varied from 1.7×10^{-5} mbar to 10^{-3} mbar at 1090 G axial magnetic field. On varying the magnetic field from 109 to 1090 G at 10^{-4} mbar pressure, the density is again found to vary ~ 20 times. Plasma density can also be varied without changing the pressure and magnetic field in the uniform magnetic field region. This is done by using the flexible transition magnetic field between the plasma source and the uniform magnetic field in the main chamber. By changing the magnetic field near the source holding the magnetic field in the main chamber constant, the density in the main chamber can be varied. Plasma density is varied ~ 10 times by changing the magnetic field near the source, holding magnetic field constant at 1090G and pressure 10^{-4} mbar. The plasma produced is uniform, length of the axially uniform plasma is L ~ 120 cm and radial uniformity extends over 4 cm diameter typically. However, the diameter of the radially uniform plasma can be varied in this device. The density in IMPED ranges from 10^{9} to 10^{12} cm^{-3}, temperature 1.5 to 5 eV and operating pressure ranges from 1.7×10^{-5} mbar to 10^{-3} mbar. The above mentioned plasma characteristics of IMPED along with details of the experimental set-up, its novelties and its capabilities are to be published in Rev. Sci. Instrum. vol 86, issue 6 (2015). The paper has been accepted for publication.

Chapter 5 is focussed on quiescent plasma production in IMPED. Quiescent magnetized plasma with background density fluctuations around and less than 1% is produced over a wide pressure range (5×10^{-5} to 10^{-3} mbar) covering both collisional and collisionless regime for magnetic field values ranging from 109 to 1090 G. IMPED employs a unique flexible transition magnetic field in between the plasma source and the main chamber to maintain plasma density fluctuations around and below 1% in the above mentioned range. The effectiveness of this method over the entire operating range is discussed and reason for the control over the density fluctuation is explored. Quiescent collisionless plasma ${}^{\delta n}/_{n}$ ~ 0.2 % is produced at ~ 10^{-4} mbar operating pressure and 872 G magnetic field in the main chamber for the intended wave experiments.

In Chapter 6, the experimental results of wave experiments are presented and discussed. The wave experiments include initial excitation and detection of ion density perturbation and plasma oscillation separately. This was followed by excitation of plasma oscillation in the presence of a controlled ion density perturbation in the background. The power in the coherent oscillation was found to decrease with increase in the magnitude of the ion density perturbation. A manuscript is being written on the interaction of plasma oscillation with a background ion density perturbation for publication.

The summary of the main results presented in this thesis and the future scope of this work is discussed in chapter 7.

The main results of this thesis are as follows

1. Based on the extensive review of phase mixing and wavebreaking of plasma oscillations, an experimental device has been designed to study the above mentioned phenomena experimentally.
2. The device has been developed from elementary sub-component in two stages along with essential diagnostic systems. Initially, a prototype is made followed by the final version of the device named IMPED. IMPED is a 3.4 m long device with a flat top uniform magnetic field extending ~ 1.3 m. It has a wide operating range, density range is 10^9 – 10^{12} cm^{-3}, magnetic field range 109 G to 1.2 kG, pressure range covers both collisional and collisionless regime. The entire device has been developed in-house.
3. Inverse Mirror Plasma Experimental device employs a unique feature for production of quiescent plasma $\delta n/n \leq 1\%$ from 5×10^{-5} mbar to 10^{-3} mbar covering a wide density range. Controlling the quiescence of the plasma by controlling the radial density gradients over a wide density range, makes this device one of its kind in existing linear magnetised plasma devices in the world.
4. Experiments on the interaction of plasma oscillation with a background ion density perturbation have been successfully conducted in this device. The power in the

coherent oscillation was found to decrease with increase in the magnitude of the ion density perturbation, indicating the occurrence of phase mixing of plasma oscillations.

References

[1] L. Tonks and I. Langmuir, *Phys. Rev*. 33, 195 (1929).

[2] L. D. Landau, *J. Phys.* 10, 25, (1946).

[3] J. Dawson, *Phys. Fluids (1958 - 1998)* 4, 869 (1961).

[4] J. H. Malmberg *et al. In: Proc. Conf. Plasma Physics and Controlled Nuclear Fusion Research*, IAEA Vienna, 485 (1966).

[5] T. O. Neil, *Phys. Fluids (1958 - 1998),* 8, 2255 (1965)

[6] J. H. Malmberg and C. B. Wharton, *Phys. Rev. Lett*. 19, 775 (1967).

[7] C. B. Wharton *et al. Phys. Fluids (1958 - 1998),*11,1761(1968).

[8] R. N. Franklin *et al. Proc. R. Soc. A*, 347, 1 (1975).

[9] R. N. Franklin *et al*. *Proc. R. Soc. A*, 347, 25 (1975).

[10] R. N. Franklin *et al*. *Proc. R. Soc. A*, 360, 229 (1978).

[11] T. Tajima, *Phys. Rev. Lett.* 43, 267 (1979).

[12] E. Esarey *et al. Rev. Mod. Phys.* 81, 1229 (2009).

[13] M. Tabak *et al. Phys. Plasmas (1994 - present),*1, 1626 (1994).

[14] R. Kodama *et al. Nature,* 412, 798 (2001).

[15] J. M. Dawson, *Phys. Rev.*113, 383 (1959).

[16] B. S. Bauer *et al. Phys. Rev. Lett.* 68, 3706 (1991).

[17] P. K. Kaw *et al. Phys. Fluids* 16, 1967 (1973).

[18] S. Sengupta and P. K. Kaw, *Phys. Rev. Lett.* 82, 1867 (1999).

[19] T. P. Coffey, *Phys. Fluids (1958 - 1988)* 14, 1402 (1971).

[20] C. Nappi and d. Nicola, *Europhys. Lett* 19, 381(1992).

[21] E. Infeld and G. Rowlands, *Phys. Rev. A* 42, 838 (1990).

[22] E. Infeld *et al*, *Phys. Rev. Lett.* 62, 2269 (1989).

[23] P.S. Verma *et al. Phys. Rev. E* 86 016410 (2012).

[24] W. Gekelman and R. L. Stenzel, *Rev. of Sci. Instrum.* 46, 1386 (1975).

List of Figures

List of Tables

Chapter 1 Introduction

1.1 Overview and motivation

Plasma supports a number of modes and a detailed understanding of these modes are essential for understanding basic plasma physics and to foster its application for benefit of mankind. Electrostatic plasma oscillation is one of the fundamental modes in plasma where the electrons oscillate with a frequency close to electron plasma frequency(ω_{pe}). Here, a high frequency longitudinal density oscillation is excited when quasineutrality of the plasma is violated locally. Tonks and Langmuir [1] experimentally observed this oscillation and provided a basic theoretical explanation; however, they restricted their treatment to cold plasma and small amplitude oscillation. The effect of thermal motion of particles was studied theoretically by Vlasov and Landau. Landau [2], in fact, showed that it is possible to damp electron plasma waves even without collision. A physical picture of this Landau damping was later given by Dawson [3] who explained the phenomena as exchange of energy between the wave and the particles having velocity close to wave phase velocity (resonant wave–particle interaction). Experimentally Malmberg et al. [4] established the collisionless damping of electron plasma wave. They measured the spatial damping of longitudinal electron plasma wave, excited by applying a high frequency voltage to a Langmuir probe in a collisionless plasma. The authors also verified the role of resonant electrons in the collisionless damping by cutting off the tail of the Maxwell distribution of electrons and observed a sharp decrease in damping. O'Neil [5] extended the damping of collisionless nonlinear plasma oscillations to time (t)greater than $\tau_B\left(= \sqrt{m/eEk}\right)$, the bounce period of the trapped particles in the wave having electric field amplitude E and wave number 'k'. The damping coefficient has an oscillatory behaviour when t/τ_B is of the order of unity, and it phase mixes to zero as $t/\tau_B \rightarrow \infty$. This nonlinear behaviour of the damping coefficient was experimentally proven by Malmberg and Wharton [6]. They investigated the damping of a large amplitude plasma wave and observed amplitude oscillation at large distances from the exciter. In the course of their experiment, Wharton et al. [7] observed side bands separated from the transmitter frequency by bounce frequency $\omega_B(= 1/\tau_B)$ associated with large amplitude electron plasma wave. Subsequently, different aspects of nonlinear electron plasma wave, namely, electron trapping effects, wave–wave interaction and side band instability, were investigated by Franklin et al. [8, 9, 10].

It is observed that on increasing the amplitude of electron plasma wave, different nonlinear effects become dominant. As the amplitude of the wave increases, its waveform is no longer sinusoidal, i.e., it steepens. As per cold plasma theory when this steepening is so extreme that there are singularities in plasma density, the wave breaks. In laboratory plasmas with a finite temperature, the tendency of the plasma density to increase to infinity at the wave crest is opposed by plasma pressure and at some large wave amplitude, plasma electrons with large velocities along the direction of the phase velocity begin to be trapped and accelerated by the wave. A self-trapped electron is the one that already has velocity as large as the phase velocity of the wave and see a constant electric field and can be accelerated. Untrapped electrons are simply slow electrons that simply move with their thermal velocity in addition to taking part in coherent wave oscillations. At wavebreaking amplitude, numerous electrons are nonlinearly brought into resonance with the wave leading to a very strong irreversible damping of the wave and efficient acceleration of the charged particles. The wavebreaking amplitude of the wave, hence the maximum longitudinal electric field that can be supported by the plasma is a topic of fundamental importance as it dictates the maximum energy of the charged particles.

Besides wave breaking, a wave may lose its coherence by another less violent process namely phase mixing of plasma oscillation/wave. Phase mixing is the loss of coherence of plasma oscillation/wave due to fine scale mixing of various parts of the oscillation/wave when there is a spatial variation of local plasma frequency [11]. This can happen due to presence of inhomogeneity in the background plasma density that may arise due to a number of reasons. The nonuniformity in background plasma density may be caused by the presence of an ion wave in the background [12]. It may also occur in an inhomogeneous plasma in the presence of nonlinear plasma oscillations because of the response of ions to ponderomotive forces either directly or through self-consistent fields [13]. Phase mixing of plasma oscillation is characterized by transfer of energy [12] from lower to higher 'k' followed by transfer of energy from wave to particle by resonant wave particle interaction.

In addition to phase mixing and wavebreaking, a wave may also be damped collsionlessly by linear Landau damping as mentioned before. But linear Landau damping phenomenon in plasma with a finite temperature has no thresholds as required by wavebreaking. Wavebreaking and phase mixing of plasma oscillation/wave results in transfer of energy from the wave to the particle irreversibly. However collisionless linear Landau damping is a reversible phenomenon and experimental observation of plasma echo [14] conclusively supports this fact.

The physics of wavebreaking and phase mixing is a topic of considerable interest because it leads to transfer of energy from wave to particle. Energetic electrons generated by wave breaking in laser fusion experiments [15, 16] eventually leads to heating of the core. In plasma based particle accelerators [17, 18], the maximum energy of the particles accelerated by resonant wave–particle interaction is dictated by the wave breaking amplitude. Other potential uses of large amplitude plasma waves ranges from development of intense X-ray sources [19], to the modification of the ionosphere [20] and chemistry of upper atmosphere [21]. The concept of phase mixing of wave in an inhomogeneous medium leading to dissipation of wave energy serves as possible model for coronal heating. Phase mixing of Alfvén wave in a medium with a density gradient perpendicular to the magnetic field has been studied as a possible model for coronal heating [22].

1.2 Review of previous experiments on wavebreaking and phase mixing

A number of experiments have been carried out to study plasma oscillation and electron plasma wave in the last five decades. But most of the experiments have been concentrated in studying Landau damping of electron plasma wave and nonlinear effects associated with electron plasma waves as mentioned in section 1.1. Investigations of phase mixing and wavebreaking have mostly been limited to simulation [23, 24] and analytical [25, 26, 27, 28, 29, 30] works with very few experiments in between. Bauer et al. [31] reported experimental observation of wave breaking of electron plasma wave in a radiofrequency (RF) afterglow plasma. The wave experiments were carried out in a cylindrical, coaxial capacitor plate configuration by driving the central conductor with a $200\ MHz$ VHF burst. Large amplitude plasma waves are excited at the location in the plasma where the VHF resonates with the local plasma density($critical\ density\ n_c = 5 \times 10^8\ cm^{-3}$). They reported observation of energetic electrons from the breaking of these large amplitude waves. Wavebreaking of plasma wave in laser plasmas have been experimentally reported by different authors. Everett et al. [32] reported experimental observation of wavebreaking of non-relativistic plasma waves induced by Raman backscatter [33]. Scattered light from an external probe beam indicated destruction of wave's coherence and trapping and acceleration of background electrons (up to $4v_{ph}\ or \sim 1keV$) was inferred by computer simulations. Modena et al. [34] reported observations of relativistic plasma waves driven to breaking point by Raman forward scattering instability, induced by short, high intensity laser pulses. They observed acceleration of plasma electrons upto to a maximum energy of $44\ MeV$ by wavebreaking. However we shall not concentrate on laser plasma experiments in this review as spatial extent and temporal duration of such plasmas is very small which makes it very difficult to experimentally verify different aspects of nonlinear plasma theory.

To the best of our knowledge no direct experiment has been carried out to comprehensively study the phase mixing of plasma oscillation. Michelsen et al. [35] experimentally studied the propagation characteristics of long wavelength ion acoustic waves in presence of propagating short wavelength electron plasma waves in a single ended Q machine. Cesium plasma of density 5×10^{7} to $5 \times 10^{8}\ cm^{-3}$ was confined radially in a string magnetic field $(0.4\ T)$. Ion acoustic waves were excited using a grid immersed perpendicular to the plasma column and electron plasma waves were excited by a probe placed $1\ cm$ behind the grid. They observed a decrease in the damping distance and phase velocity of the ion acoustic wave, when the electron and ion acoustic wave were excited simultaneously. They did not report the effect of ion acoustic wave on the magnitude of the coherent power in electron plasma wave.

1.3 Unresolved issues

From the review in section 1.2, it appears that some experiments have been carried out to observe and characterize wave breaking phenomena, but a comprehensive study testing various predictions of theory and simulation is far from satisfactory. For example the experimental study of phase mixing in plasma oscillations in the presence of a controlled density gradient is yet to be done. Role of ion inertia [13] on phase mixing of plasma oscillation in uniform plasma is yet to be explored experimentally. Bauer et al. [31] observed wavebreaking of large amplitude electron plasma wave in the laboratory but a parametric study of the variation of wavebreaking amplitude on plasma density and temperature has not been carried out. Recently Verma et al. [24] using one dimensional particle in cell simulation of large amplitude plasma oscillations in cold plasma showed the excitation of residual Bernstein–Greene–Kruskal like waves after electron wave breaking in cold plasma. The amplitude of the residual BGK wave satisfies the Coffey's wave breaking limit for warm plasma [36]. Such theoretically predicted results, where the plasma heats up after electron plasma wave breaking and eventually supports a BGK like wave with an amplitude limit determined by Coffey's limit [36] needs to be experimentally verified. Further it is well known theoretically that electron plasma oscillations break via the process of wave breaking in an inhomogeneous plasma [11, 37] but an experimental study is yet to be carried out. It has been theoretically predicted that collisions can possibly prevent the breaking of waves [38]. This is another theoretical result whose experimental verification, to the best of our knowledge, does not exist.

1.4 Scope and outline of the thesis

The thesis describes the design and development of an experimental device for comprehensive study of phase mixing and wavebreaking. The first stage of the designing process involved a detailed calculation to identify the plasma parametric space necessary for experimental study of different aspects of phase mixing and plasma oscillations. The experimental demands as per the detailed calculation included formidable requirements such as production of quiescent plasma ($\delta n/n \lesssim 1\%$) over a wide operating range $5 \times 10^{8}\ cm^{-3} - 10^{11}\ cm^{-3}$ density, $2 - 5\ eV$ temperature with operating pressure varying from $5 \times 10^{-5}\ mbar$ to $10^{-3}\ mbar$ and magnetic field ranging from $50\ G$ to $1.2\ kG$. The plasma must be both radially and axially uniform with axial uniformity extending $L_{uniform} \geq$

$120\ cm$ and diameter of the uniform plasma $d_{uniform} \sim 4\ cm$. The plasma source has to be compatible with different ion species with effortless change over between different ion species to perform the experiments smoothly.

In order to meet the above mentioned criterias completely, such that a comprehensive experimental study of phase mixing and wave breaking can be carried out a new machine IMPED [39], has been designed and fabricated in house at Institute for Plasma Research, India. However, the device is so designed that it is not limited to only wave breaking and phase mixing studies, and several other plasma waves and instabilities can be investigated thoroughly in this device. Quiescent magnetized collisionless plasma which is one of the prerequisites for phase mixing studies is produced in IMPED using a multifilamentary plasma source [40, 41, 42, 39] over a wide pressure range spanning both collisional and collisionless regime. Using the different control parameters, a large density variation in the range of 10^9–10^{12} cm^{-3} is obtained. The novelty of the device lies in the fact that the level of quiescence is controlled by mirror ratio ($R_m = B_{main}/B_{source}$) using a unique flexible transition magnetic field between the source and the uniform high magnetic field region (main chamber) over a wide range of densities. The mirror ratio is varied either by varying the source magnetic field (B_{source}) or magnetic field in the main chamber (B_{main}). Quiescent plasma with $\delta n/n \leq 1\%$ has been achieved even with ∼30 G magnetic field near filaments demonstrating the possibility of quiescent plasma production with ambient magnetic field near the filament >10 G [41]. Another uniqueness of this device is its capability of achieving density and temperature variations without varying pressure or magnetic field in the main chamber using the transition magnetic field.

After successfully producing the plasma necessary for the proposed wave experiments in IMPED, experiments on the interaction of plasma oscillation with a background ion density perturbation are successfully carried out in this device. The coherent power in the plasma oscillation is found to decrease with the increase in the amplitude of the background perturbation.

The thesis is divided into seven chapters. First chapter gives the overview, motivation and outline of this thesis. The second chapter describes the detailed calculation carried out to determine the plasma parametric regime necessary for a detailed study of phase mixing and wavebreaking along with a survey of different plasma sources to identify a suitable plasma source for the proposed wave study. The third chapter gives a detailed account of the design of the experimental device and a brief description of the fabrication procedure adopted to make the device. The diagnostics used to measure the plasma parameters and for exciting and studying the propagation characteristics of the wave is also described in chapter three. The different plasma control features of the newly built experimental device that enable it to accommodate a four order density variation is described in the fourth chapter. The method employed for quiescent plasma production in the experimental device is reported in chapter five. The effectiveness of this method for quiescent plasma production has been substantiated with experimental data. Chapter six describes the experimental result of plasma oscillation in the presence of background density gradient. The conclusion of the work carried out in this thesis and its future scope is written in chapter seven.

Chapter 2 Designing of the experimental device

Designing of an experimental device for the study of a physics phenomenon involves first the development of theoretical understanding of the phenomena to be studied followed by the determination of the window of operation that must be satisfied experimentally such that the phenomenon to be observed is dominant. This is to be followed by careful designing of the different components and the subcomponents of the experimental set up such that the required window of operation can be achieved experimentally.

The present chapter is divided into four sections. Different aspect of plasma oscillations to be studied experimentally is described in section 1. In section 2 the different requirements that an experimental device must satisfy for a comprehensive experimental study of phase mixing and wave breaking of plasma oscillation/wave is determined. A survey of different laboratory plasma sources for identification of a suitable plasma source that can be employed to produce the plasma necessary for the proposed wave studies is described in section 3. It is followed by a discussion on the choice of the plasma source for the proposed experimental device in section 4.

2.1 Physics basis of the design

Plasma oscillations are one of the fundamental modes of plasma that is excited when the plasma is perturbed locally. In the presence of finite temperature these oscillations propagate and constitute a wave. These are longitudinal density oscillations/wave, the oscillators (electrons) constituting the oscillation move parallel or anti parallel to the direction of propagation. A plasma oscillation/wave breaks when the electron excursion length becomes of the order of plasma wavelength i.e. $ekE/m\omega_{pe}^2 \sim 1$, or in other words the oscillation/wave breaks when fluid velocity ($eE/m\omega_{pe}$) becomes of the order of the phase velocity (ω_{pe}/k). Physically this results in the crossing of neighbouring electron trajectories. At the point of breaking intense wave–particle interaction occurs resulting in transfer of energy from the wave to random particle kinetic energy. A plasma oscillation/wave may break suddenly when it is excited in a way such that the breaking condition is satisfied within a plasma period or it may occur gradually through a process known as phase mixing. Phase mixing of an oscillation/wave implies decay of the oscillation/wave by fine scale mixing of various parts of the oscillation due to temporal dependence of the phase difference between individual oscillators constituting the oscillation/wave. This temporal dependence of the phase difference between oscillating fluid elements arises, when the plasma frequency because of some physical reason acquires a spatial dependence. Phase mixing eventually results in crossing of electron trajectories thus causing the oscillation/wave to break. Spatial dependence of plasma frequency, which is the underlying cause of phase mixing may arise either due to the presence of a static inhomogeneous background [11, 12, 43, 37] (infinitely massive ions) or due to gradual development of an inhomogeneity which results from the excitation of a low frequency self-consistent field in the presence of finite ion mass background [13]. In the presence of a static inhomogeneity, cold plasma oscillations phase mix at arbitrarily small amplitudes in a time scale [11] given by $t_{mix} \sim \pi/\{2(d\omega_{pe}/dx)X\}$, where X is the displacement from the equilibrium position. For a sinusoidal inhomogeneity ($n_i = n_0 + n_0\epsilon\ cos k_i x$), the phenomenon of phase mixing in the form of mode coupling of a long wavelength mode to short wavelength modes was discussed by Kaw et al. [12] , they showed that energy irreversibly goes from the low 'k' mode to high 'k' modes in a time scale $t_{mix} \sim 2/(\epsilon\omega_{pe})$. The exact solution for cold plasma oscillations in a fixed sinusoidal background was given by Infeld et al. [37], the authors described phase mixing in term of electron density burst. As stated above, inhomogeneity in the ion background may also gradually arise in a homogeneous plasma in the presence of nonlinear plasma oscillations due to the response of the background species to ponderomotive forces either directly or through low frequency self-consistent fields [13]. For this case, it has been shown that plasma oscillations phase mix in a time scale $\omega_{pe} t_{mix} \sim \left\{ (A^2/24)\left(\Psi/\sqrt{1+\Psi}\right)\right\}^{-1/3}$, where $A = \delta n/n$ and $\Psi = m_e/m_+$. In the following subsections we briefly illustrate the physics of wave breaking and phase mixing (resulting in breaking) using a physically intuitive sheet model proposed by Dawson [44].

2.1.1 Breaking of nonlinear plasma oscillations

According to the one dimensional sheet model [44], the evolution of any coherent mode in plasma can be studied in terms of oscillating motion of electron sheets about their equilibrium position. These electron sheets are assumed to be embedded in a cold immobile positive ion background. Dawson [11] showed that a coherent mode will maintain its coherence provided the electron sheets, while oscillating, do not cross each other. Crossing of electron sheets leads to a phenomenon called wavebreaking which completely destroy the coherence of the wave.

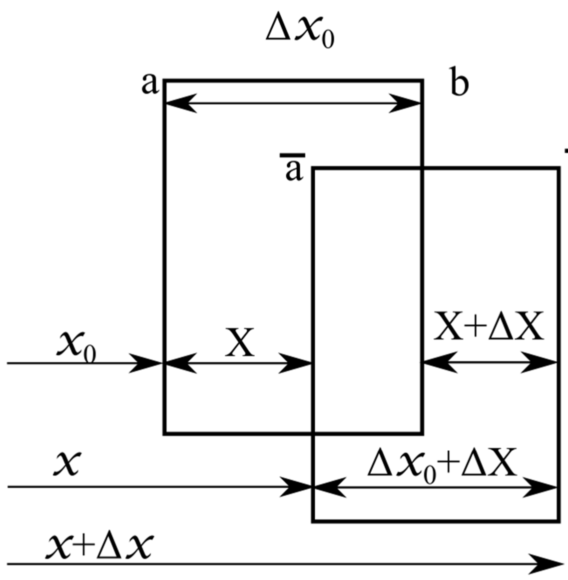

Figure 2.1: One dimensional sheet model describing plasma oscillation

Consider the adjoining Figure 2.1. Let the electron originally placed at an equilibrium position x_0 be displaced by an amount $X(x_0, t)$ and the electron originally at the equilibrium position $x_0 + \Delta x_0$ be displaced by $X + \Delta X$. Here x_0 is the Lagrange coordinate of the electron. Equating the number of electrons originally contained between Δx_0 to the number of electrons contained between $\Delta x_0 + \Delta X$, we get the electron density as

$$n(x_0, t) = \frac{n_0}{\left[1 + \frac{\partial X(x_0, t)}{\partial x_0}\right]} \tag{2.1}$$

where n_0 is the equilibrium density. Further, the width of the ion slab crossed by the electron sheet which was originally at x_0 is X, which by using Gauss's law, yields equation of the electric field as

$$E(x_0, t) = \frac{n_0 e}{\epsilon_0} X(x_0, t) \tag{2.2}$$

Therefore, the equation of motion of the electron sheet can now be written as

$$m\ddot{X} = -eE$$

$$m\ddot{X} = -\frac{n_0 e^2}{\epsilon_0} X \tag{2.3}$$

Which finally gives

$$\ddot{X} + \omega_{pe}^2 X = 0 \tag{2.4}$$

where ω_{pe} is the plasma frequency. This is the equation of motion for a simple harmonic oscillator whose general solution has the form

$$X(x_0, t) = X(x_0, 0)\cos(\omega_{pe} t) + \frac{v(x_0, 0)}{\omega_{pe}} \sin(\omega_{pe} t) \tag{2.5}$$

In order to study nonlinear plasma oscillation and its breaking, we use the following intial conditions, which in terms of Euler coordinate x are given by, where Δ represents the perturbation

$$n(x_0, 0) = n_0(1 + \Delta\cos(kx) \tag{2.6}$$

$$v(x_0, 0) = 0 \tag{2.7}$$

Where the Euler coordinate x is related to Lagrange coordinate x_0, as $x = x + X(x_0, t)$. The above initial conditions immediately lead to

$$X(x_0, t) = X(x_0, 0)\cos(\omega_{pe} t) \tag{2.8}$$

Which when substituted in **(2.1)** gives the number density as

$$n(x_0, t) = \frac{n_0}{\left[1 + \frac{\partial X(x_0, 0)}{\partial x_0}\cos(\omega_{pe} t)\right]} \tag{2.9}$$

Here $X(x_0, 0)$ is implicitly obtained by using **(2.6)** in Gauss's law and equating it to the electric field at $t = 0$ given by **(2.2)**, as

$$X(x_0, 0) = -\frac{\Delta}{k}\sin(k\tilde{x}_0) \tag{2.10}$$

where $\tilde{x}_0 = x_0 + X(x_0, 0)$. For the density to remain positive at all times (or in other words, for no sheet crossing),

$$\frac{\partial X(x_0, 0)}{\partial x_0}\cos(\omega_{pe} t) > -1 \tag{2.11}$$

Using **(2.10)**, the no crossing condition now stands as

$$\frac{\Delta\cos(k\tilde{x}_0)}{1 + \Delta\cos(k\tilde{x}_0)}\cos(\omega_{pe} t) < 1 \tag{2.12}$$

The maximum value of the L.H.S. is $\Delta/(1-\Delta)$, which gives $\Delta < 1/2$ for sustained coherent nonlinear oscillations. Hence in terms of electric field, the maximum value is limited to $\mathrm{keE_{max}}/m\omega_{pe}^2 = \Delta < 1/2$ [45]. Therefore, if the initial conditions are such that $\Delta \geq 1/2$, then cold plasma oscillations break within a plasma period, at an amplitude $E_{max} = m\omega_{pe}^2/2ke$. In the next subsection, we consider the case, where wave breaking occurs at arbitrarily low amplitudes via the gradual process of phase mixing.

2.1.2 Phase mixing of nonlinear plasma oscillations

As mentioned in the beginning of this section, plasma oscillations phase mix and eventually break if the plasma frequency becomes spatially dependent. Spatial dependence arises because of a background inhomogeneity, which in turn, may either be due to static ion inhomogeneity or may arise self-consistently in the presence of electron-ion oscillations. As the electrons and ions move about their out own centre of mass, they eventually create a low frequency electrostatic field, which further affects the motion of ions thus creating inhomogeneities in space. This in turn affects the electron wave motion causing it to phase mix. In this subsection, we illustrate the phase mixing phenomenon using a static background ion inhomogeneity. Taking a sinusoidal inhomogeneity as $n_i = n_0(1+\epsilon\sin(k_i x_0))$, $\epsilon \ll 1$ (2.4) approximately becomes (taking $k_i X \ll 1$)

$$\ddot{X}(x_0,t) + \omega_{pe}^2\{1+\epsilon\sin(k_i x_0)\}X(x_0,t) \approx 0 \tag{2.13}$$

Choosing $n_e = n_0\{1+\epsilon\cos(k_i x_0)\} + \delta n_0\cos(k_e x)$ and $v(x,0)=0$ $(k_e \ll k_i)$ as initial conditions [12], solution of the above equation can be written as

$$X(x_0,t) = X(x_0,0)\cos\left(\omega_{pe0}t\sqrt{1+\epsilon\sin(k_i x_0)}\right) \tag{2.14}$$

Where $X(x_0,0)$ is approximately given by

$$X(x_0,0) \approx -\frac{\delta\sin(k_e x_0)}{k_e(1+\epsilon\sin(k_i x_0)) + \delta\cos(k_e x_0)} \tag{2.15}$$

For $\epsilon \ll 1$, (2.14) can further be approximated as

$$X(x_0,t) \approx -\frac{\delta}{2k_e}\sum_{n=-\infty}^{\infty} J_n\left(\frac{\epsilon\omega_{pe0}t}{2}\right)\left[\sin\left\{\omega_{pe0}t + (nk_i + k_e)x_0\right\} - \sin\left\{\omega_{pe0}t + (nk_i - k_e)x_0\right\}\right] \tag{2.16}$$

Since the electric field is directly related to $X(x_0,t)$ as

$$E(x_0,t) = \frac{m\omega_{pe0}^2}{e}(1+\epsilon\sin(k_i x_0))X(x_0,t) \tag{2.17}$$

(2.16) shows that the field energy put in the fundamental mode diminishes as $\sim J_0^2\left(\epsilon\omega_{pe0}t/2\right)$ and the coherence is lost in a time scale [12] $t_{mix}\sim 2/(\epsilon\omega_{pe0})$. Physically, since each electron sheet oscillates with a frequency which depends on their position, as time progresses, they slowly go out of phase [11] and the initial coherence is lost. As the energy goes into higher modes, the density profile becomes steeper, eventually resulting in the crossing of trajectories of neighbouring electron sheets which causes the oscillations to break.

The nonlinear problem of plasma oscillations in a static periodic ion background was exactly solved by Infeld et al. [37], the authors analytically showed that, because of the spatial dependence of the plasma frequency, the electron number density will eventually explode. This is nothing but a signature of wave breaking. Thus the phenomenon of phase mixing ultimately causes the oscillations/waves to break at arbitrarily low amplitudes. If the inhomogeneity is self-consistently generated, then as stated above, plasma oscillations phase mix (wave break) in a time scale $\omega_{pe}\tau_{mix}\sim\left\{(A^2/24)\left(\Psi/\sqrt{1+\Psi}\right)\right\}^{-1/3}$. Here A is the amplitude of perturbation and Ψ is the electron to ion mass ratio.

2.2 Identification of operating window of the experimental device

Phase mixing is a gradual process. It happens over several plasma periods. In addition to phase mixing a wave may be lost in the plasma due to collisional damping and Landau damping [46]. So it is necessary to find out the range of experimental parameters over which phase mixing of nonlinear plasma oscillations may be expected to dominate over other competing processes i.e. the phase mixing length is less than collisional damping or Landau damping length. In the following, we will estimate the maximum length within which phase mixing is expected to occur as well as all different length scales of the relevant damping mechanisms. From these calculations one arrives at the suitable plasma parameters the device should provide.

2.2.1.1 Phase mixing length

Phase mixing of plasma oscillation may occur in a non-uniform plasma [11, 12] as well as in a uniform plasma [13] to start with. The length of time in which plasma oscillation is expected to phase mix is more in case if plasma oscillations are excited in uniform plasma. So for designing purpose, phase mixing of plasma oscillations in homogeneous plasma is considered for determining the maximum phase mixing length. The maximum length within which phase mixing is expected to occur for various plasma densities and temperatures are determined from the expression: $\lambda_{mix} = t_{mix} v_{the}$.

$$\lambda_{mix} = \frac{1}{\omega_{pe}} \left[\left(\frac{A^2}{24} \right) \left(\frac{\Psi}{\sqrt{1+\Psi}} \right) \right]^{-\frac{1}{3}} v_{the} \tag{2.18}$$

The expression for t_{mix} is valid for electron plasma oscillation in a uniform background. For non-uniform background or in the presence of ion wave in the background the phase mixing length is even lower. Thus from the expression for maximum phase mixing length (2.18) it is observed that it's a function of plasma density, electron temperature, fluctuation level (A = δn/n) and electron to ion mass ratio $\Psi = m_e/m_+$. As the plasma density increases, the phase mixing length decreases. A plot of the variation of the maximum phase mixing length with change in A is given in Figure 2.2 with different values of T_e. From the figure, it is seen that for A = 0.05 the maximum λ_{mix} is 0.94 m at T_e = 5 eV and $n = 5 \times 10^8 cm^{-3}$. Hence, from the perspective of maximum phase mixing length, operation at densities greater than $5 \times 10^8\ cm^{-3}$ is preferred, as for lower densities phase mixing length will increase. For example, for same parameters as mentioned above, the maximum phase mixing length is 2.94 m for electron density of $5 \times 10^7 cm^{-3}$. For higher densities, say, $10^{10} cm^{-3}$, the maximum phase mixing length will be much less, but with increase in density the plasma frequency also increases ($f_{pe} \propto \sqrt{n}$) thus increasing the demand on diagnostics. Thus, the density window from mid $10^8\ cm^{-3}$ to mid $10^9 cm^{-3}$ is preferred for the phase mixing experiment. However experiments can be carried out at higher densities. The plasma temperature (T_e) should be around few eV, as for large T_e the maximum phase mixing length increases considerably. This is so because as the temperature increases the group velocity of the wave also increases thus increasing the phase mixing length.

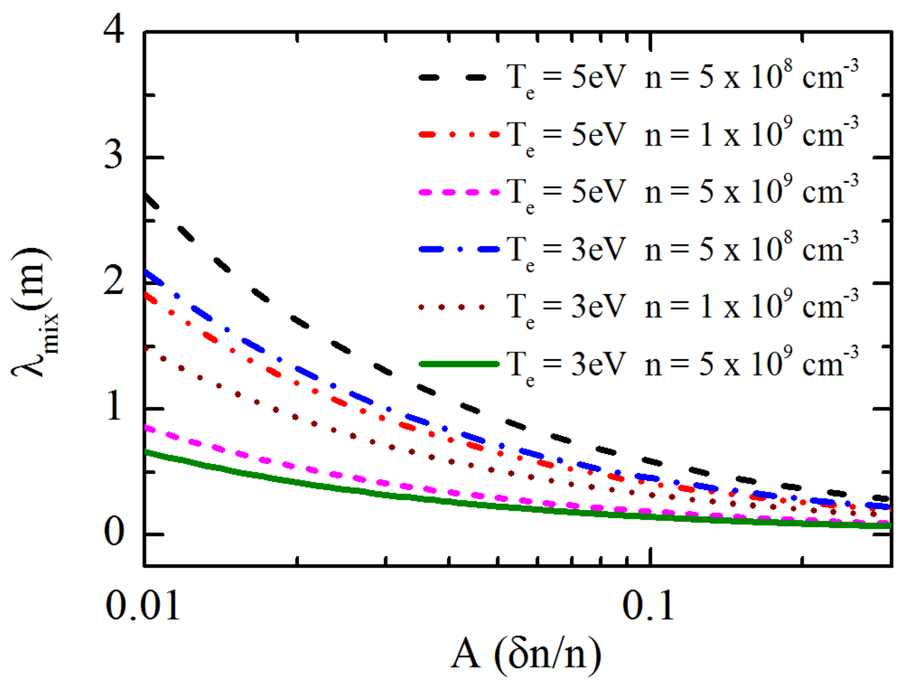

Figure 2.2: variation of maximum phase mixing length with induced density perturbation $A=\delta n/n$ for argon plasma of different density and temperature.

2.2.1.2 Collisional damping

Experimental study on phase mixing requires all collision lengths to be greater than the maximum phase mixing length. This implies that the plasma has to be collisionless in order to observe the phase mixing phenomena. To ensure this, the electron-neutral mean free path $\lambda_{mf} (= \frac{1}{n_n \sigma_{en}})$, which is the dominant collision mechanism in laboratory plasmas, must be several times the maximum phase mixing length. To get an estimate of the collisional damping length, the damping length of a linear Langmuir wave is calculated using the fluid equations.

The governing equations for determining the collisional damping length of a linear Langmuir wave are equation of motion of the electron fluid, continuity equation and Gauss's Law. The equation of motion of the electron fluid after taking electron neutral and electron ion collisions into account becomes

$$m_e n_e \left[\frac{\partial \overrightarrow{v_e}}{\partial t} + (\overrightarrow{v_e} . \nabla)\overrightarrow{v_e}\right] = -\gamma k_B T_e \nabla n_e - e n_e \vec{E} - m_e \nu_{en} n_e \overrightarrow{v_e} - m_e \nu_{ei} n_e \overrightarrow{v_e} \quad (2.19)$$

The equation of continuity for electron density and Gauss's law can be written as

$$\frac{\partial n_e}{\partial t} + \nabla . (n_e \overrightarrow{v_e}) = 0 \quad (2.20)$$

$$\nabla . \vec{E} = \frac{e(n_i - n_e)}{\epsilon_0} \quad (2.21)$$

The last two terms on the right hand side of (2.19) represents the momentum gained per unit volume by electrons due to collisions with neutrals and ions respectively. Other symbols have their usual meaning. Solving (2.19), (2.20) and (2.21) by the process of linearization, where $n_e = n_0 + n_1$, $\overrightarrow{v_e} = \overrightarrow{v_0} + \overrightarrow{v_1}$ and $\vec{E} = \overrightarrow{E_0} + \overrightarrow{E_1}$. Subscript zero represents the equilibrium quantities and the subscript one represents first order perturbation. At equilibrium $\overrightarrow{v_0} = \overrightarrow{E_0} = \nabla n_0 = 0$. Therefore (2.19), (2.20) and (2.21) takes the form

$$\frac{\partial \overrightarrow{v_1}}{\partial t} = -\frac{\gamma k_B T_e}{m_e n_0}\nabla n_1 - \frac{e}{m_e}\vec{E} - \nu_{en}\overrightarrow{v_1} - \nu_{ei}\overrightarrow{v_1} \quad (2.22)$$

$$\frac{\partial n_1}{\partial t} + \nabla(n_0\overrightarrow{v_1}) = 0 \quad (2.23)$$

$$\nabla.\overrightarrow{E_1} = \frac{en_1}{\epsilon_0} \quad (2.24)$$

Fourier analysing the above equations and performing a little algebra one gets

$$\omega^2 = \omega_{pe}^2 + \frac{\gamma}{2}v_{th}^2 k^2 - i(\nu_{ei} + \nu_{en})\omega$$

For one dimensional adiabatic process $\gamma = 3$, the dispersion relation becomes

$$\omega^2 = \omega_{pe}^2 + \frac{3}{2}v_{th}^2 k^2 - i(\nu_{ei} + \nu_{en})\omega \quad (2.25)$$

Let $\omega = \omega_r + i\omega_{im}$

After a little algebra one gets

$$\omega = \sqrt{\left\{\omega_{pe}^2 + \frac{3}{2}v_{th}^2 k^2 - \frac{(\nu_{ei} + \nu_{en})}{4}\right\}} - i\,\frac{\nu_{ei} + \nu_{en}}{2} \quad (2.26)$$

Therefore

$$E_1 \propto e^{-i\omega t}$$

$$E_1 \propto e^{-i\omega_r t} e^{-(\nu_{ei}+\nu_{en})t/2} \quad (2.27)$$

The time in which the electric field decreases to $1/e$ of its original value

$$\tau_{damping} = \frac{2}{\nu_{ei} + \nu_{en}} \tag{2.28}$$

The group velocity of the electron plasma wave is given by

$$v_g = \frac{1}{2} \frac{3v_{th}^2 k}{\sqrt{\left\{\omega_{pe}^2 + \frac{3}{2}v_{th}^2 k^2 - \frac{(\nu_{ei} + \nu_{en})^2}{4}\right\}}} \tag{2.29}$$

The distance in which the amplitude decreases to $1/e$ of its original value (damping length) is

$$\lambda_{coll} = v_g \tau_{damping}$$

$$\lambda_{coll} = \frac{2}{\nu_{ei} + \nu_{en}} \frac{\frac{3}{2}v_{the}^2 k}{\sqrt{\left\{\omega_p^2 + \frac{3}{2}v_{the}^2 k^2 - \frac{(\nu_{ei} + \nu_{en})^2}{4}\right\}}} \tag{2.30}$$

The variation of the collisional damping length with pressure, density, temperature and wavelength is shown in Figure 2.3.

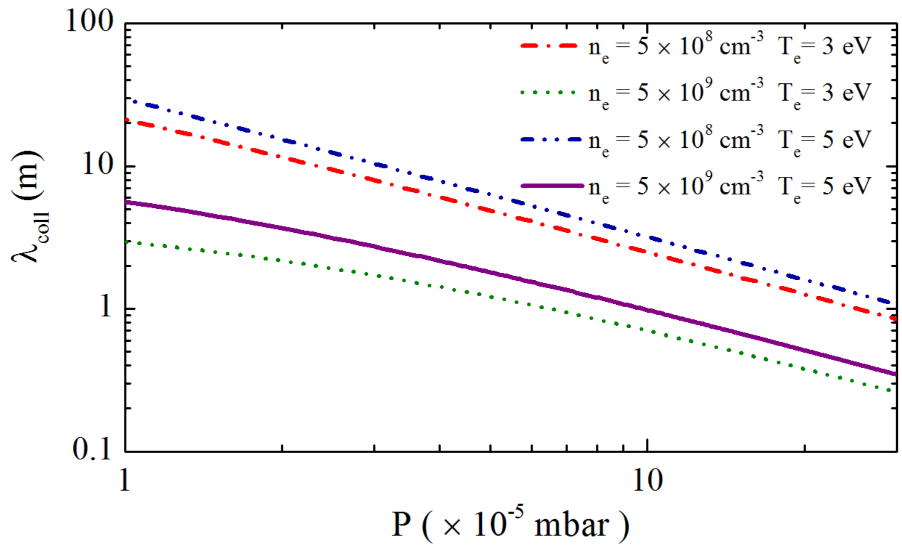

Figure 2.3: Variation of collisional damping length of linear Langmuir wave of wavelength 2.5 cm with pressure for different plasma densities and temperature.

2.2.1.3 *Landau Damping length*

The phase mixing length should be less than Landau damping length. The landau damping length of the wave can be increased, by increasing the wavelength of the wave. This may be achieved by exciting wave near the plasma frequency. Landau damping for a wave exhibiting weak damping [8] may be estimated by

$$k_i = \gamma_L \left(\frac{\partial \omega}{\partial k}\right)^{-1} \tag{2.31}$$

where γ_L is the Linear landau damping rate in the time domain.

2.2.1.4 *Desirable features of the plasma*

Based on the discussion in the previous sections we now arrive at the most suitable features of the plasma that are necessary for observing phase mixing and wavebreaking phenomena in the laboratory. They are listed as follows:

a) **Quiescence**: Ideally one would require plasma with background fluctuation level $\delta n_{noise}/n$ much less than the perturbation level that is going to be excited. Hence one would require a quiet plasma. Taking practical difficulties into consideration, this background level should be ≤ 0.01 at least.

b) **Uniformity**: The plasma must be uniform, as phase mixing of nonlinear oscillation as per the route described by Sengupta and Kaw [13] requires uniform plasma to begin with. The length of the uniform plasma must be greater than the maximum phase mixing length. Considering that the maximum phase mixing length for A = 0.05 in 5 eV argon plasma having density $5 \times 10^8\ cm^{-3}$ is 0.94 m. So, the uniform plasma length must be greater than 0.94 m. Radially uniform plasma with radius of the uniform plasma greater than equal to the wavelength of the wave to be excited is preferred.

c) **Axial magnetic field**: One way of ensuring uniform plasma of length greater than 0.94m is to use an axial magnetic field for confinement. The addition of magnetic field further enriches the wave phenomena that one may look at experimentally. Hence a variability of the magnetic field such that one may vary ω_{ce} (cyclotron frequency) from less than ω_{pe} to greater than ω_{pe} is desired.

d) **Compatibility with different ion species**: The maximum phase mixing length is a function of the electron–ion mass ratio (Ψ). This implies that in order to experimentally investigate the parametric dependence of the phase mixing time on Ψ, one requires a plasma source compatible with different ion species.

e) **Reproducibility**: The plasma should exhibit the same physical characteristics under the identical operating conditions. This is a necessity for studying the different aspects of the wave phenomena in a controlled manner.

f) **Ease of operation**: Since the proposed experiments require parametric study with different ion species, it is desirable to change the ion species easily in between experiments without any major changes in the set up.

Therefore the experimental requirements for the study of phase mixing and wavebreaking experiments are as follows.

a. Quiescence : $\delta n/n \sim 0.01$ or less
b. Density range : $5 \times 10^8 - 10^{11}\ cm^{-3}$ (for experimental purpose a three order density variation within the mentioned range may suffice)
c. Temperature : few eV
d. Operating pressure : $5 \times 10^{-5} - 10^{-3}\ mbar$
e. Magnetic field: $50G$ to $1.2kG$
f. Extent of the flat top magnetic field: $1.2\ m$
g. Axial uniformity of the plasma : $L_{uniform} > 1.2\ m$

h. Plasma source to be compatible with different ion species

2.3 Selection of Plasma source

Over the years several plasma sources and devices have been built for conducting different plasma physics experiments. Different laboratory plasma sources have different characteristics. In order to identify a potential plasma source for carrying out the proposed wave experiments a number of laboratory plasma sources have been reviewed. The suitability of a plasma source has been judged keeping in mind the required plasma features as described in the previous section along with technical complexity involved in building the plasma source and cost of building and maintain the same.

The different plasma sources that have been reviewed are discussed as follows.

1. Positive Column of parallel plate DC glow discharge: Production of the plasma by the application of a potential difference between two electrodes is one of the oldest forms of plasma production. Plasma is produced by electron impact ionization of the neutral gas and the discharge is sustained by secondary emission of electrons from the cathode surface because of ion bombardment [47]. The structure of such a discharge is complicated near the cathode [47], but away from the cathode in the positive column, fairly uniform weakly ionised plasma is obtained. The positive column has a longitudinal electric field which is fairly constant along the column. DC glow discharge can be used to produce long plasma columns (> 1m) if sufficient voltage is applied between the anode and the cathode. Plasma density typically ranges from 10^9 to $10^{11}\ cm^{-3}$. The electron temperature typically vary from $1 - 5\ eV$, depending on the ionization potential of the gas, fill pressure and column radius [48]:

$$\frac{exp(eE_i/k_B T_e)}{\sqrt{eE_i/T_e}} = (Cpr)^2 \tag{2.32}$$

where C is a tabulated constant [49]. The ions are generally in thermal equilibrium with neutrals. A longitudinal magnetic field reduces radial diffusion but a field larger than few hundred gauss can cause instabilities in the plasma column [50]. The fill pressure typically ranges from hundreds of mbar to ~ $10^{-1}\ mbar$. At low pressures quiescence is often limited by ionization instabilities (striations). Hence for quiescent plasma production operation is limited to higher neutral pressures. Thus in DC glow discharge the plasma is highly collisional and it is not suitable for the proposed wave experiments at all.

2. Hollow cathode discharge: The limitation of the ordinary glow discharge in terms of higher operating pressure can be surmounted in a hollow cathode discharge by the use of differential pumping. The schematic of the plasma source is shown in Figure 2.4.

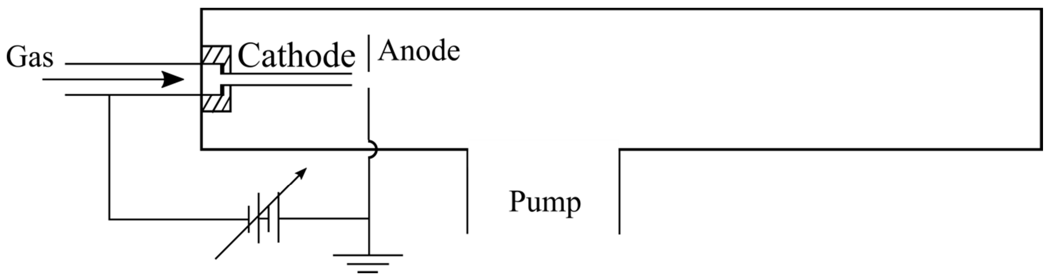

Figure 2.4: Schematic of hollow cathode discharge

The hollow cathode is a thin walled metal tube (~ typical diameter 1 cm) which electrically serves as the cathode and simultaneously acts as the input for the neutral gas, which is to be ionized. The neutral pressure inside the cathode tube can be 10^3 times higher than in the main chamber. Ignition is typically achieved by overvolting. Generally hollow cathode is operated at high current densities typically in the range ~1 – 10 A cm^{-2}. Intense ion bombardment of the cathode at such current densities leads to high cathode temperatures causing thermionic emission. Most of the ionization occurs in the high pressure region inside the cathode. Ionization efficiency can be is high ~ 80% and is generally used for high density plasma density production [51] (10^{13} – 10^{14} cm^{-3}). However lower plasma densities around $\sim 5 \times 10^{9}\ cm^{-3}$ which is more suitable for the proposed wave experiments has been reported by Sato et al [52]. Hollow cathode discharge can be operated both in the presence and absence of an axial magnetic field. Plasma temperature ranges typically from 2 – 4 eV. However plasma temperature can be decreased continuously by an order of magnitude by installing pins in hollow cathode discharge [52]. This can be advantageous from the point of view of parametric wave studies. A number of gases can be used for plasma production. The lower operating pressure in hollow cathode discharge is ~ 10^{-4} mbar. Since the lowest operating pressure required for the proposed wave experiment is around $5 \times 10^{-5}\ mbar$, hollow cathode discharge may not be suitable for the proposed experiment. Additionally the life time of the metal tube that acts as the hollow cathode is also less and may require frequent replacements, this increase the down time of the experimental device.

3. **Duoplasmatron**: Like hollow cathode discharge, collisionless plasma in this case is

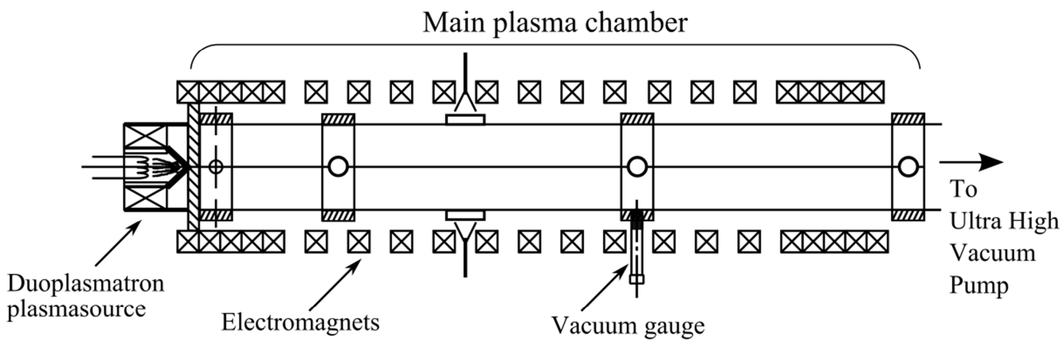

Figure 2.5: Schematic of an experimental device using a duoplasmatron source for magnetized plasma production .

also produced by differential pumping. The schematic of a duoplasmatron plasma source for production of collisionless plasmas is shown in Figure 2.5. Plasma is produced by filament discharge at high pressure ~ $5 \times 10^{-2}\ mbar$ and injected through a 1 – 3 mm diameter hole through a magnetic mirror into the main chamber which is held at a much lower pressure (~ 10^{-3} to 10^{-5} mbar). Long plasma column can be sustained (>1m) in the presence of a strong axial magnetic field of value of few kG [53]. Plasma having density 10^{8}–10^{9} cm^{-3}, temperature 5–20 eV using a duoplasmatron source have been reported in the literature [54]. But the radial uniformity of the plasma produced using duoplasmatron is poor [50].

4. **Reflex discharge**: The geometry of a typical Reflex discharge is shown Figure 2.6 schematically. Plasma is produced by electron impact ionization. The ionizing electrons are confined axially by negatively biased electrodes and radially by an axial magnetic field. Instead of using hot cathodes as shown in Figure 2.6, cold cathodes can also be used for plasma production. Plasma can be produced over a wide density range ~$10^{9} - 10^{12}\ cm^{-3}$. Plasma temperature typically ranges from 2 – 10 eV. This plasma source is compatible with an axial magnetic field. The main disadvantage with reflex discharge is lack of quiescence for greater part of the parametric range of operation. Density fluctuations level can be > 10 % depending on the instabilities present. However it is possible to produce quiet plasma over a small parametric space. When the axial magnetic field and the operating pressure are such that the electron loss rate due to classical diffusion is equal to the ion loss rate, instabilities are suppressed [55]. The density fluctuation level decreases to $\delta n/n \cong$ 0.01%. This strictly restricts the available operating parametric space for wave studies. Hence reflex discharge cannot be used for the proposed wave studies.

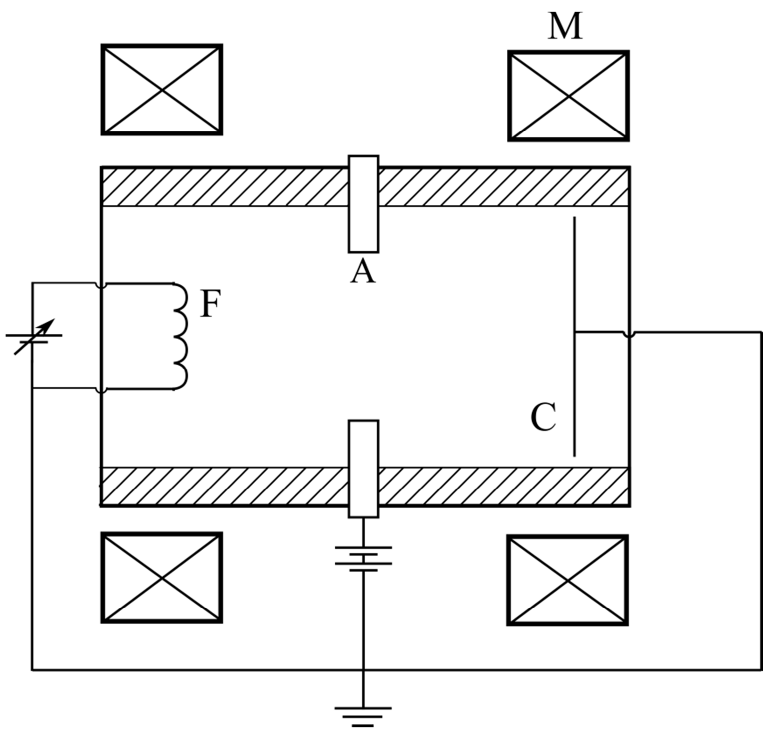

Figure 2.6: Schematic of a typical reflex discharge using a hot cathode. F = filament, A = anode, C = cathode and M = magnet

5. Radio Frequency discharge: A plasma can be produced inside a vacuum chamber by means of an oscillating electric and magnetic field. RF range commonly used in discharge practice is $f \cong 1 - 100\,MHz$. 13.56 MHz RF generators are most commonly used for plasma production. RF discharges can be subdivided into capacitive, inductive and helicon discharges depending on the way in which RF energy is deposited in the plasma. In capacitive discharges, the voltage from the RF generator is applied to the electrodes, the electrons gains energy from the oscillatory electric field. Plasma is produced by electron impact ionization of neutrals. The operating pressure range using the parallel plate configuration is typically $10^{-2} - 10^{-1}\,mbar$ and densities are obtained in the range $10^{9} - 10^{10}\,cm^{-3}$. Typically in inductive discharges, RF is fed to helical coils wound axially around a cylindrical dielectric plasma vessel as shown in Figure 2.7b. The power is coupled to the discharge by transformer action. The oscillating current in the coil produces an oscillating magnetic field along the axis of the coil which inturn produces an induced vortex electric field with closed lines of force. The electrons are accelerated by this induced electric field and oscillations occur in curved orbits. The density range for efficient inductive discharge is typically 10 times greater than capacitive range. Typically inductive discharges are operated at pressures above $10^{-3}\ mbar$. Helicon discharges [56] are wave heated discharges and absorption of energy from waves to particles is responsible for deposition of RF power into the plasma. This plasma source is highly efficient and can be used to produce high density plasmas $\sim 10^{12} - 10^{13}\ cm^{-3}$. Figure 2.7c shows the different antennas that have been developed for helicon plasma production.

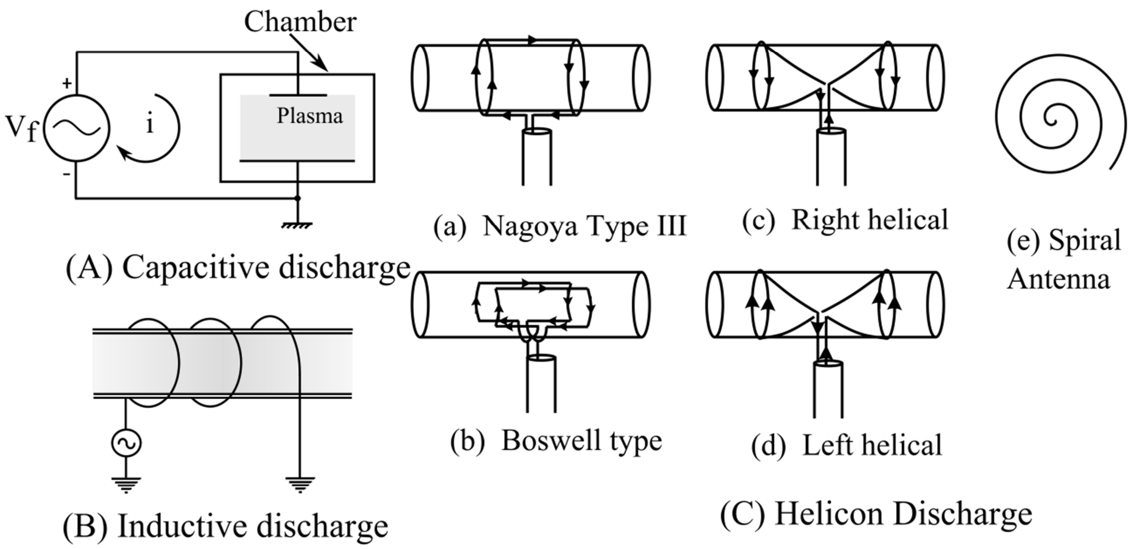

Figure 2.7: Different types of RF discharge. (A) Capacitive discharge, (B) Inductive Discharge, (C) Different types of antenna used in Helicon discharge.

Using the same antenna capacitive, inductive and helicon discharges can be produced in a device, this increases the plasma density range ($10^{9} - 10^{12} cm^{-3}$) available for experimental purpose. Long plasma columns [57] can be produced by using helicon plasma source in the presence of an axial magnetic field. Helicon plasmas may be quiescent or noisy depending on the operating regime [58]. Typically the lowest operating [59] pressure for devices using a helicon plasma source is $\sim 10^{-4}\ mbar$. But helicon plasma column may not be radially uniform under all operating conditions. In addition to the conventional methods described above, power from the RF generator can be coupled to produce plasma under a variety of other configuration. For example, Earl and Mackenzie [60] produced reasonably uniform cylindrical plasma in the presence of uniform magnetic field ($\leq 500G$) by applying 200V RF at 80 MHz to a fine wires stretched across the diameter. They produced argon plasmas of densities $10^8 - 10^9\ cm^{-3}$ and electron temperature up to 12 eV with noise level $\delta n/n \sim 0.3\%$. The lowest operating pressure reported by Earl and Mackenzie is around $10^{-4}\ mbar$. Plasmas of different gases can be produced using an RF source.

6. **ECR plasma**: Long magnetized uniform plasma column [61] can be generated by exploiting the fundamental electron cyclotron resonance condition. The applied axial magnetic field may be uniform [62] or non-uniform [63]. Typical non uniform profiles being either that of a mirror or half mirror. Microwave is generally launched axially; it couples to a mode of the plasma and is absorbed in the resonance layer where $\omega \approx \omega_{ce}$, this absorption of the wave energy by the plasma particles helps in maintaining the plasma. Figure 2.8 shows the schematic of a microwave discharge system for production of uniform magnetized plasma. A magnetron is used as a microwave source. It is connected to a circulator followed by a dual directional coupler. The circulator protects the magnetron from the reflected power while the dual directional coupler is used to sample the forward and reflected power. Linearly polarized microwave is launched directly from an open ended waveguide into the plasma chamber through a mica window.

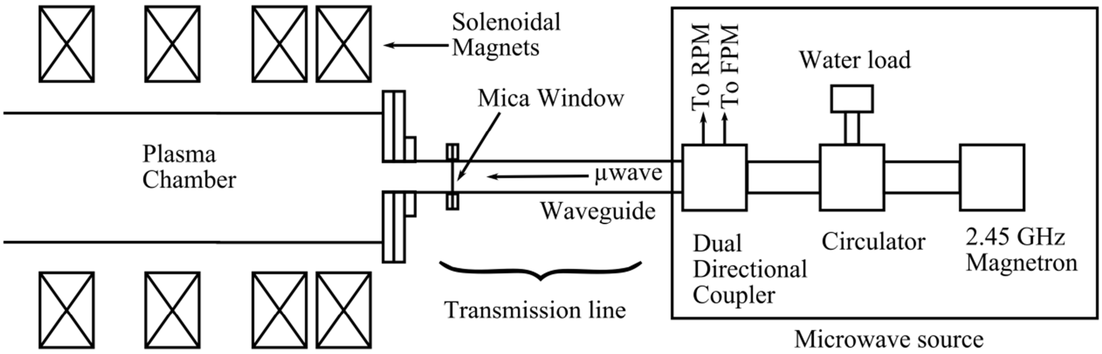

Figure 2.8: Schematic of linear plasma device with a microwave source for magnetized plasma production. RPM = Reflected power meter, FPM = Forward power meter.

Typical frequencies of microwave sources for ECR based applications range from a few GHz to several tens of GHz. In tokamaks, ECR pre-ionization and heating are usually carried out at frequencies between 30 to 100 GHz depending on the value of the toroidal magnetic field. However, 2.45 GHz microwave source is the most commonly used because they are easily available, cheap and magnetic field requirement is less (876 G). The ECR produced plasmas are generally efficiently ionized and of moderate density. There is a critical density (n_c) determined by the cut-off condition of ordinary wave: $\omega \approx \omega_{pe} = \sqrt{n_c e^2/\epsilon_0 m_e}$, where ω_{pe} is the plasma frequency and ϵ_0 is the vacuum permittivity. At 2.45 GHz the value of n_c is $7.4 \times 10^{10}\ cm^{-3}$. This limitation can be surmounted by feeding power using a circularly polarized microwave. Tanaka et al. [64] using a 2.45 GHz microwave source produced plasma having density $n > 10^{13}\ cm^{-3}$ by converting the linear polarized microwave to circularly polarized one by using a circular polarizer. Thus it is observed that plasma over a wide density range [64, 62] i.e. $10^9 - 10^{13}\ cm^{-3}$ can be produced in ECR discharge. The lowest operating pressure is typically ~ $10^{-5}\ mbar$. ECR plasmas with low density fluctuations [65] ($\delta n/n \sim 1 - 2\%$) have been reported in literature. Plasma temperature can vary from few to few tens of eV. Plasma of different gases can be produced using ECR discharge.

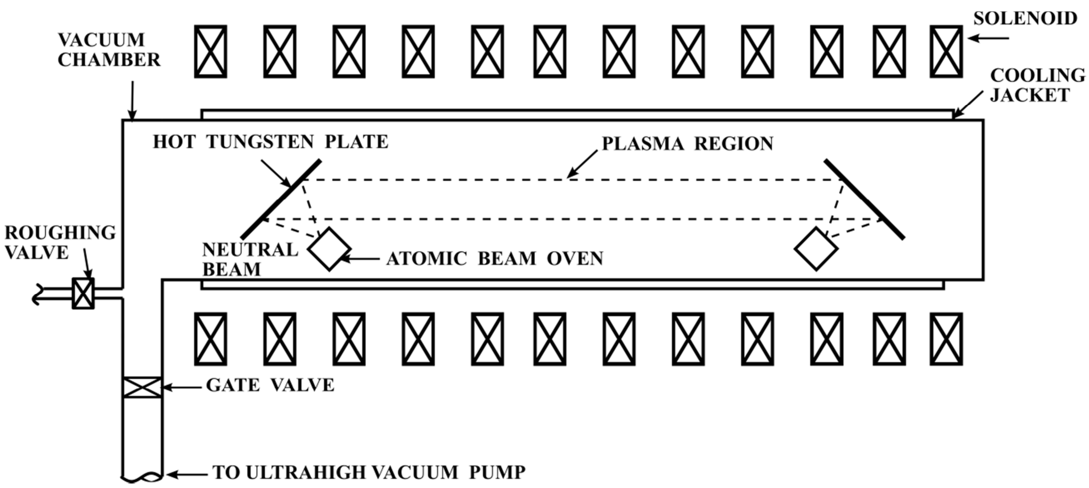

Figure 2.9: Schematic of a double ended Q machine.

7. Q machines: In the Q machine plasma is produced by contact ionization [66] of an alkali or alkali earth metal vapour on a hot metal plate and thermionic emission of electrons from the hot plate at high temperatures. The schematic of a Q machine is shown in the Figure 2.9. Figure shows a double ended Q machine however, plasma can also be produced in a single ended configuration with the hot plate at one end and a terminating metal plate at the other end of the column. Plasmas of different ion species can be produced. The ion species is limited to neutrals having low enough ionization energies like Na (5.14 eV), K (4.34 eV), Cs (3.89 eV), Ba (5.21 eV) etc. Hot plate is made from materials with high melting points like tungsten (3380^0C), tantalum (3000^0C) and rhenium ($3182^0\ C$). This is so because the plate is to be maintained at high enough temperatures to give an appreciable Richardson emission of electrons to maintain plasma neutrality. The hot plate is generally maintained at temperatures around 2100^0C. Both electrons and ions have the same temperature as that of the hot plate just above ~ 0.2 eV. This can be varied by application of auxillary heating. For example Levine et al. [67] varied the electron temperature from 0.2 eV to ~ 1 eV by resonant absorption of energy at electron cyclotron frequency by application of ~ 1W of power at 10GHz. Plasmas over a wide range of densities [68, 69, 70, 71] 10^7 to $10^{13} cm^{-3}$ have been produced in Q machines. In order to produce collisionless plasma one has to operate the device in the low density range ~ $10^7 - 10^9\ cm^{-3}$ because of the high electron-ion collision frequency due to lower temperatures. The plasma produced is radially uniform and the radial uniformity is dependent on the diameter of the hot plate. Long plasma column (> 1 m) can be easily produced by confining the plasma by magnetic field of the order of kG aligned along the axis of the device. The plasma produced in Q machines is generally very quiet as most of the free energy sources which can excite instabilities can be avoided. For example nonuniform heating of the hot plate will give rise to a temperature gradient on the plate which can cause a large potential gradient in the plasma. The resulting electric field may cause ion and electron drifts. This can be solved by using a carefully designed cathode system [72, 73]. Finally it can be concluded that the required quiescence, uniformity, density and temperature range for the proposed wave experiments can be satisfied in Q machine.

8. **Multifilament discharge**: In filament discharge, plasma production is based on electron impact ionization of the gas by accelerated thermionic electrons emitted by heated filaments. The filaments are heated by passing current through it. The current density of the thermionically emitted electrons in the presence of high extraction field is determined by the Richardson Dushman law $J_{max} = AT^4\ exp\left(-\frac{eW}{k_B T_e}\right)$, where A is the Dushman's constant ($1.2 \times 10^6\ A\ m^{-2}\ K^{-2}$), T is the filament temperature in kelvin, W is the work function of the filament in volts and k_B is the Boltzmann's constant. If the extraction voltage is not large enough, the emission is space charge limited and the emission current density is given by Child's Law for a cylindrical diode $J_e \propto V^{3/2}$. The thermionically emitted electrons are accelerated by the biasing voltage applied to the filaments. These energetic (primary) electrons ionize the gas by electron impact ionization. The plasma forms sheath around the heated filaments and the plasma at the sheath edge forms the anode. The sheath region around the filaments is rich in ions and primary electrons.

Homogeneous plasma over a large volume can be produced by using multiple filaments such that the ionizing electrons are disposed symmetrically around the chamber. This concept was used by Taylor et al. [74] to produce uniform plasma over a large volume in their double plasma device. Densities were typically in the range $10^8 - 10^{10}\ cm^{-3}$, electron temperature varied from 0.5 to 5 eV and noise level $(\delta n/n)$ was 5×10^{-4}. The lower operating pressure in this type of devices is typically $\sim 10^{-4}\ mbar$. This is so because as the pressure decreases the mean free path increases, and when the mean free path becomes much greater than the system dimension most of the primary electrons escape to the vessel wall without ionizing the gas. This problem was solved by introducing multi-dipole confinement scheme, for confining the plasma and the primary ionizing electrons. Figure 2.10b shows a double plasma device, using permanent magnets to produce a multipolar magnetic field at the surface of the vessel. The primary electrons are reflected multiple times back into the plasma by the multi-dipolar magnetic field at the surface of the vessel. Thus the ionizing electrons travel a much greater length before it is lost to the vessel wall; as a result plasma can be produced at a much lower operating pressure. Limpaecher and Mackenzie [75] using multidipolar confinement produced quiescent collisionless argon plasma at $5 \times 10^{-6}\ Torr$ with $T_e \approx 5\ eV$, $T_i \approx 0.5\ eV$, $n_i \approx 8 \times 10^{10}\ cm^{-3}$, noise $\delta n/n \approx 2 \times 10^{-4}$. The reason for observation of such low density fluctuation was ascribed to the isotropization [48] of the primary electron population due to scattering by the permanent magnets lining the surface of the device. The Mackenzie bucket has been used in neutral beam injectors for tokamaks; it has been used for producing large volume uniform plasma for wave studies in the absence of axial magnetic field.

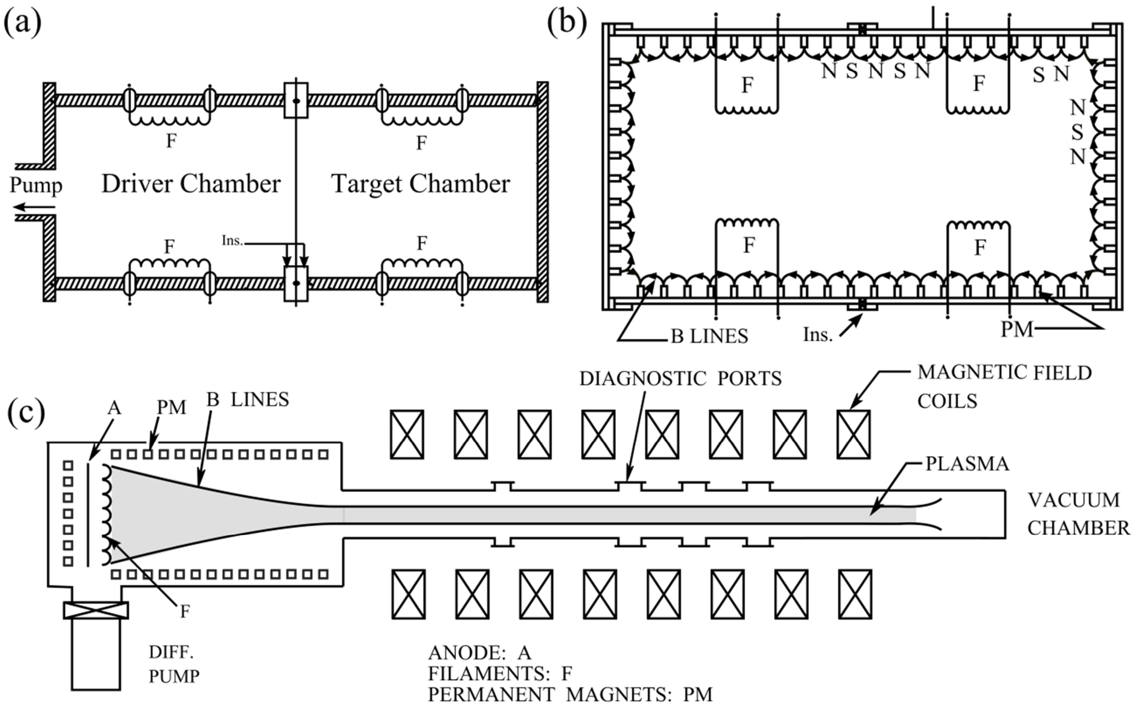

Figure 2.10 : Schematic of devices using multifilamentary discharge for plasma production, (a) Double Plasma Device, (b) Double plasma device with multidipolar confinement, (c) Device for production of magnetized filament plasma

Gekelman and Stenzel [40] produced magnetized plasma using a multifilamentary cathode. A schematic of a multifilamentary device with an axial magnetic field is shown in the Figure 2.10c. Primary electrons produced by the multifilament cathode in weak field region stream along the magnetic field lines to high field region producing plasma by electron impact ionization. The large source chamber is surrounded by permanent magnets which serve to confine the primary electrons enabling efficient plasma production. The magnetic field near the joule heated filaments is maintained at a low value around ~ 10 G such that twice the Larmor radius of the electrons emitted by the filaments is greater than the filament separation. This is done to ensure that the electrons emitted by adjacent filaments are able to thermalize. Gekelman and Stenzel were able to produce argon plasma with a density range ~ 10^{9} – 10^{11} cm^{-3} and operating pressure spanned form $\sim 6.7 \times 10^{-5}$ to $10^{-3}\ mbar$. They reported a density fluctuation $\delta n/n\ \lesssim 1\%$ in argon plasma at $\sim 4 \times 10^{-4}\ mbar$ and $1kG$ magnetic field. Plasmas of different gases like argon, helium, neon, etc., can be produced in filament discharge.

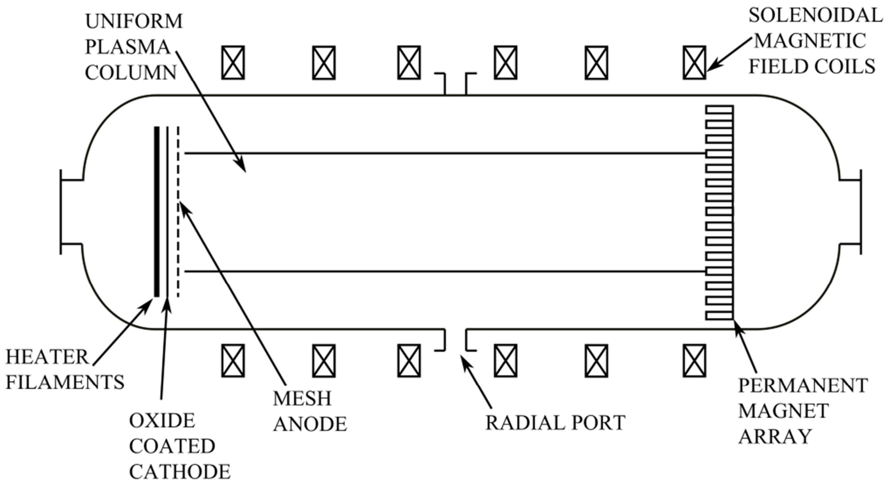

Figure 2.11 : Schematic of a device using Large oxide coated cathode for plasma production.

9. Large area oxide coated cathode: Oxides coated cathode of oxides of barium (Ba), strontium (Sr), calcium (Ca), are efficient emitters at low temperature ($800^{0}C$). The oxide-coated-cathode is stretched flat with springs and indirectly heated by filaments behind it. The emitted electrons are accelerated through a pulse anode grid to ionize the gas by electron impact ionization. Large diameter plasma over a long distance can be produced using an axial magnetic field. In LAPD [76] a large area oxide coated cathode is used to produce plasma of diameter 50 cm and 10 m length in a magnetic field up to $3\ kG$. Quiescent [77] plasmas ($\delta n/n \sim 1\%$) of different ion species like krypton, argon, etc. can be produced. Plasma can be produced at lower operating pressure [78] $\sim 10^{-4}\ mbar$. This source is particularly suitable for production of high density plasma $\sim 10^{11} - 10^{12} cm^{-3}$ with few eV temperatures. Oxide coated cathode suffers from deterioration of the cathode coating when exposed to O_2 and CO_2 [79]. Oxide coated cathode plasma source is more costly compared to other hot cathode sources [79].

10. Other sources: Some of the other type of plasma sources like laser produced plasma, atmospheric discharge [47] etc, as they are not suitable for the proposed wave experiments have not been described here. For example laser produced plasmas exist for a small duration of time and the spatial extent is also too small to study phase mixing of plasma oscillation in detail.

2.4 Proposed Device

From the review of different plasma sources only a few sources are found to be suitable for the proposed wave experiments. From the point of view of compatibility with magnetic field, production of collisionless uniform plasma with low density fluctuation and required density range (section 2.2 on page 33) only Electron cyclotron resonance discharge, Q machine and multifilamentary discharge with an axial magnetic field are suitable for the proposed wave experiments. One of the easiest ways to produce a long uniform plasma column using ECR is to launch the microwave in a uniform axial magnetic field. However the magnitude of the magnetic field is limited by the frequency of microwave source used for plasma production, such that the resonance condition is met ($\omega \approx \omega_{ce}$). Thus inorder to have the experimental flexibility of changing the uniform axial magnetic field a variable frequency microwave plasma source is necessary. But such a variable frequency microwave plasma source is very costly. The problem can be circumvented by producing plasma with a 2.4 GHz microwave source in a non-uniform magnetic field.

Q – machines satisfied all the plasma source criterias mentioned in section 2.2 except one and i.e. is ease of operation. For the proposed experiments plasmas of different species will have to be produced. Changing the ion species in Q machine will take time. Moreover Q machines are very costly.

Multifilamentary plasma source in the presence of an axial magnetic field can be used to produce uniform plasma at low operating pressure. Quiescence is a concern density fluctuation $\delta n/n \sim 1\%$ was reported by Gekelmann and Stenzel in SCAMP at $3 \times 10^{-4}\ torr$, but value of density fluctuations at lower operating pressure $\sim 5 \times 10^{-5}\ mbar$ is not available in published literature for this type of devices. A detailed study of multifilamentary plasma source compatible with an axial magnetic field shows that there is scope of carrying out a number of modifications in the existing designs for improving the performance. For example the axial confinement of primary ionizing electrons can be improved by lining the walls with permanents magnets in line cusp configuration for better confinement. The density range accessible for experiments in the main chamber can be increased by controlling radial diffusion in the source chamber. This can be achieved by removing the permanent magnets lining the curved surface of the source chamber and control the radial confinement of plasma in the source chamber by increasing or decreasing the axial magnetic field. To increase the maximum value of allowable axial magnetic field near the filaments, the filaments will have to be spaced closely such that filament spacing is greater than equal to twice the Larmor radius of the primary electrons emitted thermionically by the heated filaments. This is so because if the filaments are spaced at a distance greater than twice the larmor radius then the electrons emitted by two adjacent filaments may not be able to thermalize and this will result in parallel beams [80] inside the experimental device which is not desired for wave studies. It may be possible to reduce filament spacing to 1 cm thus increasing the magnitude of maximum allowable magnetic field near filaments to ~ 70 G at –

90 V discharge voltage. However it must be noted that Pierre et al. [80] pointed out that the ambient magnetic field near the filaments should be less than 10G for quiescent plasma production in a multifilamentary source compatible with an axial magnetic field based on the results of Taylor and Mackenzie in the double plasma device. This may not be quite true and further experiments are needed to verify this. As far as quiescence is concerned experiments can be carried out to reduce plasma fluctuations by minimizing sources of free energy.

Considering the low cost and scope of improvement available for a multifilamentary plasma source coupled with easy availability of materials required for the construction locally, a multifilamentary plasma source with an axial magnetic field is the preferred plasma source. Local availability of the materials required for the construction of the device is important as it reduces the time required to procure the materials hence cuts down the time required to fabricate the experimental device and carry out necessary trouble shooting.

Thus it was decided to make a magnetized linear plasma device with a multifilamentary plasma source having a number of modifications to suite our experimental requirements. Considering that experimental results may not always be as desired, the new device must have enough flexibility to accommodate an ECR source or be converted into a Q machine if absolutely necessary for the wave experiments. In order to ensure that the device can be converted into a Q machine if required, there must be provisions to increase the axial magnetic field values to 2.5 kG or above. Thus the solenoid magnets to be designed must be capable of producing higher magnetic fields than necessary for operation with multifilamentary source.

Chapter 3 Experimental device and diagnostics

An experimental device is designed and fabricated for controlled study of plasma waves and instabilities. It has a number of components which have been carefully planned to deliver a machine a) having wide plasma parameter regime, namely, low plasma density to high density, to allow plasma frequency to go from less to higher than electron cyclotron frequency, b) operable at wide range of pressure to cover collisionless to collisional regimes, c) having low quiescence plasma allowing wave excitation and detection experiments possible, d) flexible magnetic coils positioning to get different magnetic field configurations, e) operable in steady state or pulse mode to meet requirements of various experiments, and f) having options of connecting to various kinds of plasma sources.

The experimental device is developed in two stages. In the first stage, a prototype device is made to test the new designs, carry out troubleshooting wherever necessary and develop the primary diagnostics. The prototype device is called Magnetized Linear Plasma Device. In the second stage the upgraded version of the device is installed and operated. The upgraded version is called Inverse Mirror Plasma Experimental Device [42, 39]. This chapter describes the design and construction aspects of the experimental device. The diagnostics that has been developed to measure plasma parameters and carry out wave experiments is described. The diagnostics include Langmuir probe for measurement of plasma density, temperature, plasma potential, floating potential and EEDF, emissive probe for direct measurement of plasma potential, rack probes for measuring fluctuations in plasma, ion acoustic wave exciter and detector, Langmuir wave exciters and high frequency receiver probes.

3.1 Magnetized Linear Plasma Device (MLPD)

The design and construction aspects of magnetized linear plasma device are as follows.

3.1.1 Plasma production

Plasma is produced by electron impact ionization of the neutral gas. Schematic illustration of the plasma production method used in MLPD is shown in Figure 3.1. A two dimensional array of joule heated filaments is mounted on the axial end flange of the source chamber. The primary electrons emitted by the filaments stream along the magnetic field lines from the source to subsequent uniform high magnetic field region and ionize the gas. Loss of charged particles on the axial end flange on the source side is limited by lining its walls with permanent magnets in line cusp configuration [75]. In order to prevent local rise in the pressure due to outgassing from the permanent magnets [75], the permanent magnets are mounted on blind slots milled on the surface of this flange from the air side as shown in Figure 3.2. Two NdFeB (Neodymium Iron Boron) magnets of 6 mm height and 10 mm width are placed on top of each other. The surface field of each permanent magnet is ~ 3.5 kG. The distance between the magnet surface and the vacuum wall is 6 mm. The center-to-center separation between two adjacent line of magnets placed in the cusp configuration is 4 cm. NdFeB magnets are chosen because of their low price and high coercive force. The curie temperature of the magnets is 312^0C and the maximum operating temperature is 80^0C. Because of their low operating temperature the end flange is actively cooled by passing cold water in alternate slots as shown in Figure 3.2. The flow rate is maintained at $100\ litres\ per\ minute$ for effective cooling. This number is arrived at by thermal simulation in ANSYS software.

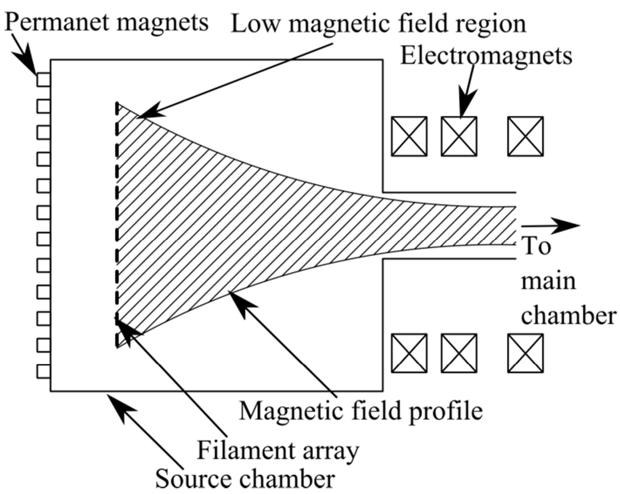

Figure 3.1 : Schematic illustration of the plasma production method used in MLPD. Joule heated filaments are located in the low magnetic field region followed by a subsequent high magnetic field region.

The multi-filamentary source consists of 48 filaments arranged in the form of a matrix. The filaments are attached to rectangular frames, which are supported inside the vacuum vessel using in-house developed water cooled current feed-throughs. All the filaments are electrically connected in parallel and are powered by a 500 Amp, 20V power supply and negatively biased by a 128V, 25A DC power supply for regular operations. The electrical connections are shown in the Figure 3.2. The filament to filament separation is 2 cm, which is less than twice the Larmor radius of the primary electrons near the filaments. There are provisions in the source to reduce the filament separation to 1cm if operational requirement demands. The filaments (tungsten wires of purity 99.95%, 0.125mm diameter and length 6 cm) are placed at a distance of 21.3 cm from the inner wall of the end flange, where the magnetic field due to the permanent magnets is few gauss only. The voltage drop across the filaments is ~ 6 V and the heating current for each filament for daily operation is maintained at ~ 2A.

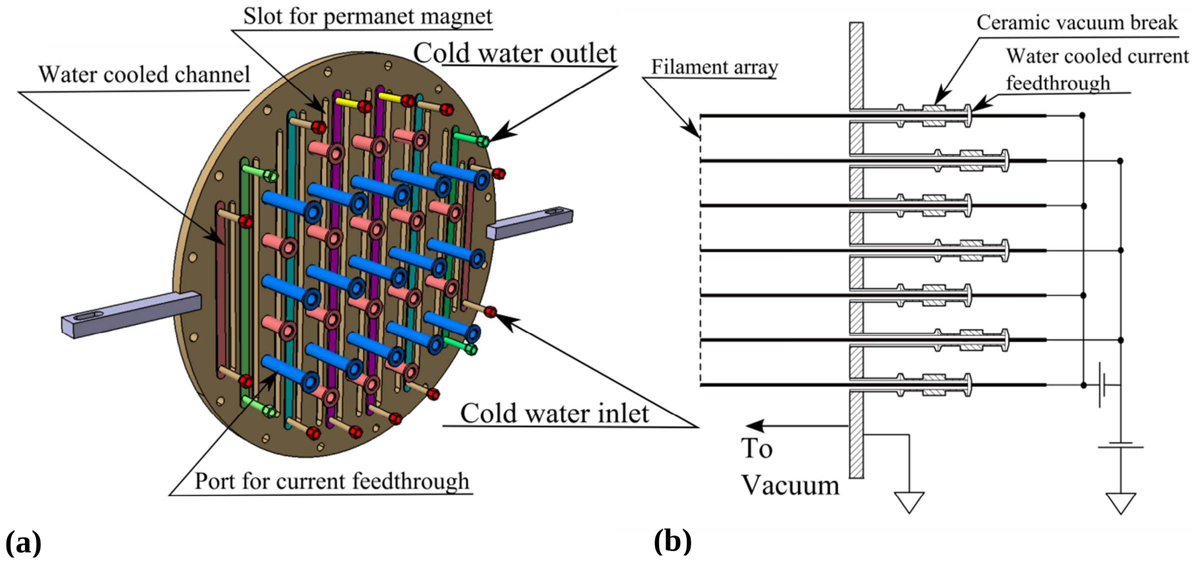

Figure 3.2: (a) Diagram of the plasma source flange showing its features. (b) Schematic of the plasma source showing the electrical connections.

3.1.2 Vacuum Vessel

The cylindrical vacuum vessel of MLPD, made of stainless steel SS304. It is 2.72 m and consists of two parts: a) Source chamber, and b) Main plasma chamber. The schematic of the vacuum vessel is shown in Figure 3.3.

The source chamber which houses the multi-filamentary plasma source is 0.5 m long and 0.5 m in diameter. It has four orthogonal side ports, each 155 mm in diameter and located midway between the two ends. C channels are welded on the surface of this chamber for passing chilled water for cooling during operation.

The main chamber is 2.22 m long and 161 mm in diameter. It consists of 5 smaller sub-chambers of varying lengths bolted serially. The first sub-chamber is the longest, 850 mm in length, whereas the others have smaller but similar lengths, namely, 360mm, 300mm, 264mm and 296 mm. The fifth chamber has a Tee section for connecting a vacuum pump. There are a total of 17 radial ports of different inner diameters welded at various axial locations and distributed azimuthally 90^0 apart. The eight ports in the first sub chamber are the largest in diameter (90 mm) and they are to be used for introducing three-gridded exciter for exciting waves in the plasma.

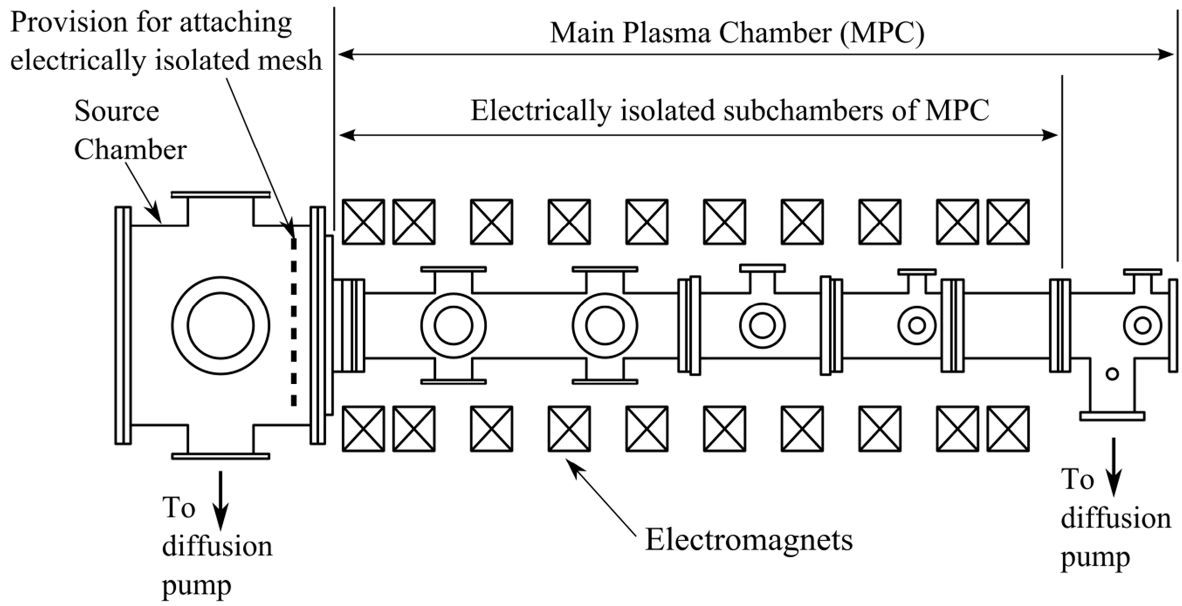

Figure 3.3 : Schematic of MLPD

The first four of the above five sub-chambers can be electrically isolated from the rest of the device and made to float or biased as per the needs of the experiment. There is provision for attaching an electrically isolated mesh to the 20 mm thick adapter flange between main plasma chamber and source chamber. This mesh may be biased to alter the downstream plasma parameters. The sub-chambers of the main chamber may also be biased with respect to one another as per requirements of the experiment.

Two high vacuum pumps are being used to pump the vacuum vessel. One 700 l/s (un-baffled speed) diffusion pump is connected to the source chamber. The second pump, a $1000\ l/s$ diffusion pump, is connected to the fifth sub chamber at other end of the system. Both diffusion pumps are isolated from the vacuum system by butterfly valve. Pressure is measured by three gauges, two Instrutech make hot cathode ionization gauge (IGM 401 hornet) and one Pfeiffer made cold cathode gauge (model no. IKR 251). All the gauges are placed away from the high magnetic field region using a suitable extension to reduce the stress on the filament due to the magnetic field. The base pressure achieved in the system in absence of the plasma source is $1\times 10^{-6} mbar$. Gas is fed to the system in a controlled manner using Pfeiffer make gas dosing valve (model EVN 116) located near the source chamber.

The whole vacuum system is mounted on a non-magnetic stand made from aluminum square bars. The KF (Klein Flange) clamps used in the system are also non-magnetic in nature. Differentially pumped vacuum feedthroughs are used for inserting probes in the vacuum vessel.

3.1.3 Magnet System

The magnet system of MLPD is designed to deliver a flat top axial magnetic field in the main chamber over a distance of $1.4\ m$. The magnetic field is to be varied from $0 - 200\ G$. The low ripple in the main chamber is achieved by placing the electromagnets magnets with center to center spacing less than the inner radius of the magnets. The width of the magnets is optimized to have enough space between the magnets for placing the diagnostics. The electromagnets magnets are 10.2 cm wide with inner diameter and outer diameter, 42 cm and 55.5 cm, respectively, and center to center spacing between consecutive regular magnets is 20 cm. The separation between last two regular magnets at either end is 2.8 cm. The material selection for the fabrication of the magnets and process employed to construct it are specifically chosen to minimize the cost and time of production. Poly Vinyl Chloride (PVC) coated copper wires of 16 sq mm conducting cross-sectional area are wound over a PVC pipe of 42 cm outer diameter, which is supported at both ends by rectangular hylam blocks

($80.5\ cm\ \times\ 86\ cm$) of 0.9 cm thickness. Each magnet has 77 turns. The magnets are air cooled and can be easily operated for 30 minutes with any damage due to temperature rise.

The magnets were designed using the freely available Poisson Superfish Code [81]. Figure 3.4 shows axial variations of magnetic field at three radial locations, measured using a Hall probe. The ripple in magnetic field in the axial direction in the flat top region is ~1%.

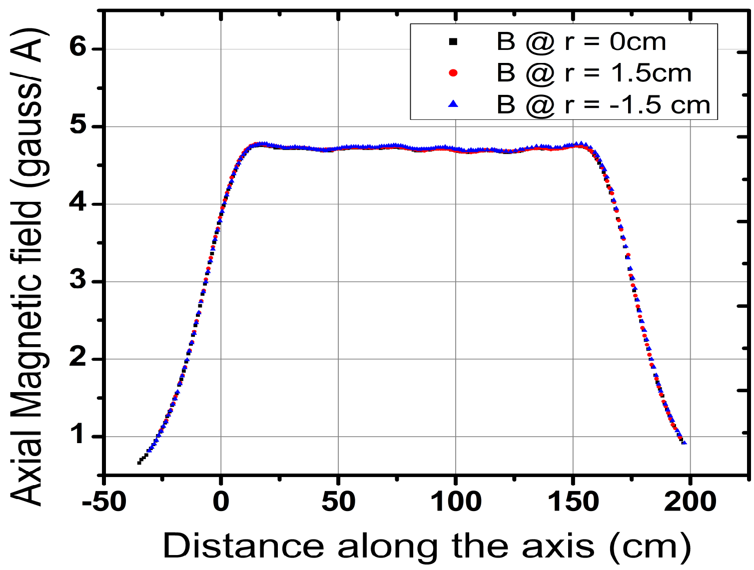

Figure 3.4 : Variation of axial magnetic field with distance at three radii.

A picture of the fully assembled experimental device consisting of the plasma source, vacuum vessel and magnet system is shown in the Figure 3.5.

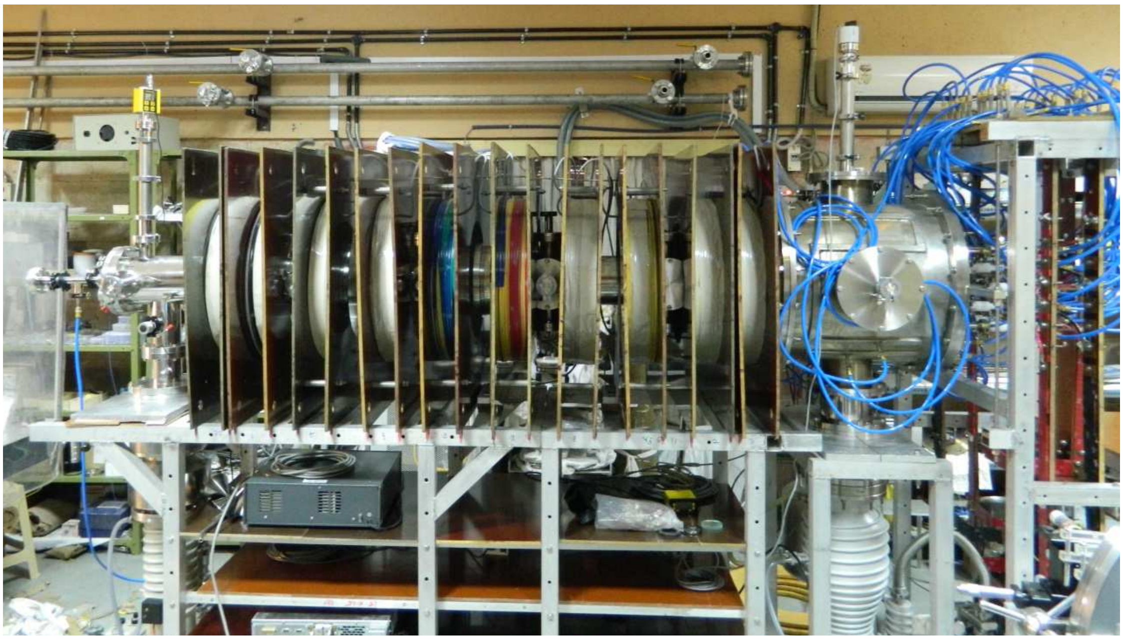

Figure 3.5: Picture of Magnetized Linear Plasma Device

3.2 Inverse Mirror Plasma Experimental Device (IMPED)

The Inverse Mirror Plasma Experimental Device is designed and fabricated for the experimental studies of waves and instabilities in collisional and collisionless plasma in the presence of magnetic field. The device has been developed with significant inputs from the experience gained during experiments in MPLD. Primary goal of IMPED is to meet the experimental requirements of the proposed wave studies as described in chapter 2 at the same time have enough operational flexibility for investigating other waves and instabilities like drift, Kelvin-Helmholtz and Rayleigh-Taylor instabilities.

Major upgrades were performed to make the Inverse Mirror Plasma Experimental Device. Some of the upgrades include replacement of the old air cooled magnets with the new steady state water cooled high magnetic field (2.4 kG continuous operation) electromagnets. The new magnet system has novel features for enhancing the plasma parametric space available for wave experiments which will be discussed in details later. The design and construction of upgrades are described below.

3.2.1 Plasma Source

A two dimensional array of joule heated filaments biased negatively with respect to the vacuum vessel is used to produce plasma in IMPED. As a part of the upgrade the dimensions of the filament holding structure is increased to accommodate 90 filaments instead of 48 filaments that were used to produce plasma in MLPD. The filaments are arranged at 2 cm spacing, the holding system can also accommodate filaments arranged at 1 cm separation if the requirement arises.

3.2.2 Vacuum Vessel

The length of the vacuum vessel is increased as a part of the upgrade. A new cylindrical chamber is added between the exiting source and the main chamber. This is done to increase the distance between the plasma source and the high magnetic field region of the main chamber. As the increased length between the source and main chamber will enable the user to decrease the magnetic field from high values in the main chamber (~1.2 kG) to low magnetic field values (< 60 G) the near plasma source slowly enough such that adiabatic invariance of the magnetic moment of the gyrating charge particles moving from source to main chamber is maintained.

The new cylindrical chamber is called the source extension chamber. It is 0.62 m long and ~ 0.346 m in diameter. The source chamber extension has three sets of 40KF radial ports located at three axial locations. Each set consists of three radial ports at 90^0 apart azimuthally with no ports on the bottom side. The source chamber extension is attached to the source chamber at one end and main chamber at the other end by water cooled adapter flanges. Provisions are made for attaching electrically isolated mesh on both the adapter flanges. The mesh may be biased to alter the downstream plasma parameters.

The length of the upgraded experimental device named IMPED is 3.38 m. The schematic of the cylindrical vacuum vessel is shown in the Figure 3.6.

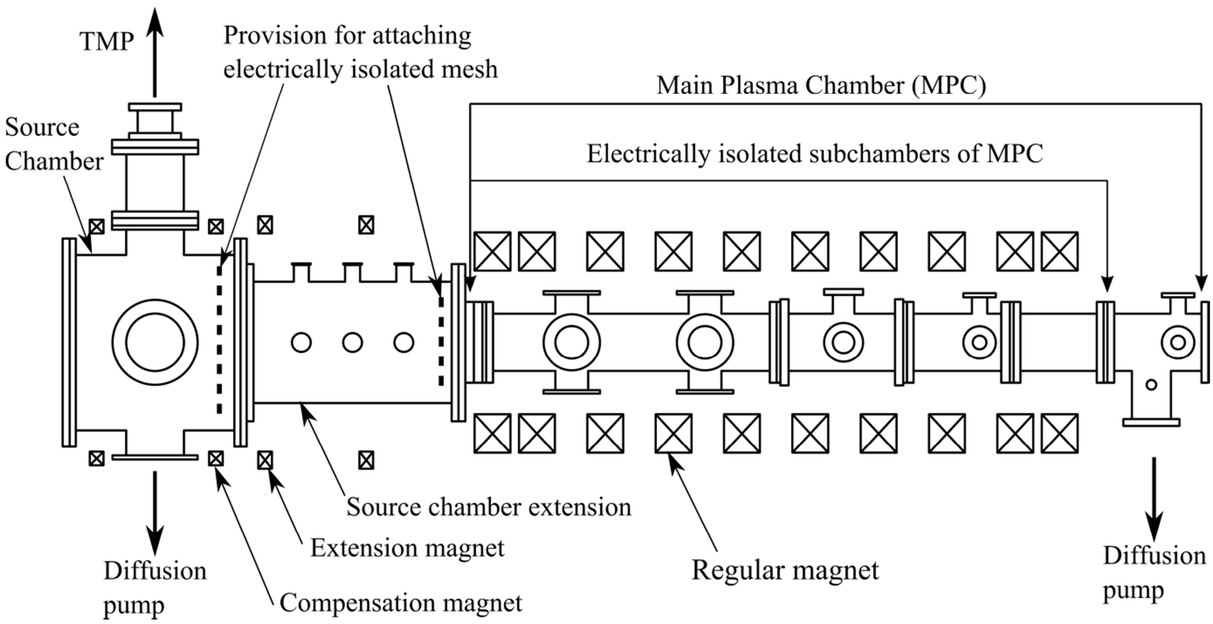

Figure 3.6 : Schematic of IMPED

Three high vacuum pumps are being used to pump the vacuum vessel. Two pumps, one 700 l/s (un-baffled speed) diffusion pump and one 200 l/s turbo molecular pump (Pfeiffer made Model no. TMU 261 Y P), are connected to diametrically opposite ports of the source chamber. The turbo molecular pump (TMP) is connected in an inverted position by an I-section as shown in the Figure 3.6. The long I section has been used to ensure the value of ambient magnetic field near the turbo molecular pump to be less than 60 G. The third pump, a 500 l/s diffusion pump, is connected to the fifth sub chamber at other end of the system. The base pressure achieved in the system in absence of the plasma source is $1.3 \times 10^{-6}\ mbar$, whereas with the plasma source attached it becomes $2 \times 10^{-6}\ mbar$.

3.2.3 Magnet system

The magnet system has been designed keeping in mind the multi-filamentary plasma source, magnetic field requirement for wave studies, maximizing diagnostic access while minimizing ripple in the magnetic field both in the radial and axial directions ($\delta B/B < 1\%$) in the uniform magnetic field region of the main plasma chamber. The multi-filamentary plasma source requires the magnetic field near the filaments to be kept below 38 G whereas the experimental flexibility demands a magnetic field variable in the range of 50 G to 1.2 kG in the main plasma chamber to enable changing electron cyclotron frequency (ω_{ce}) from less than to greater than plasma frequency (ω_{pe}). This variation should be independent of the magnetic field in the source chamber for greater controllability of plasma parameters in the system. The mechanical holding system must be flexible enough to allow the user to change the location of the magnets in order to achieve different geometrical configuration of the magnetic field. The magnet system should be able to produce steady state magnetic field to avoid dynamic stress related problem to all mechanical components and to reduce the demand on plasma diagnostics. The magnet system should be able to produce a high uniform magnetic field (~ few kG) such that other plasma sources like an alkali plasma source may be used in the future if the experiment demands.

With the above conditions in mind, the magnet system of the IMPED has been primarily designed with the help POSSON SUPERFISH [81]. The results of the POISSON SUPERFISH code are shown in Figure 3.7. The figure represents the variation magnetic field in the RZ plane. A total of ten magnets with NI = 1800 Amp turns are needed for producing an axial uniform magnetic field of value 1.1 kG extending over a length of 1.3m. These magnets termed as regular magnets placed coaxially around the main plasma chamber as shown in Figure 3.6. The successive regular magnets are separated by 9.5 cm, allowing enough space for diagnostics. Inner diameters of the magnets are kept at 42 cm.

Larger diameter coils could have given better uniformity in the main chamber, however, it would have added to the cost. The outer diameter and width of the regular magnets is 64.5 cm and 10.5 cm respectively. The last two regular magnets at either end of the main plasma chamber are separated by 2.5 cm. This is done to extend the uniform region in the axial magnetic field region in the main chamber. The other two types of electromagnets, namely the extension and compensation magnets are used to maintain the magnitude of the magnetic field near the emitting filaments at permissible values irrespective of the magnetic field in the main plasma chamber. The inner diameter and width of all the 4 coils are 64 cm and 4.5 cm respectively, while the outer diameter of the extension and compensation coils are 74.8 cm and 72.4 cm respectively.

The name of the system is derived from the magnetic field profile as shown in Figure 3.7. It is seen that the magnetic field profile extending from the main plasma chamber to the source chamber resembles an inverse of a magnetic mirror configuration.

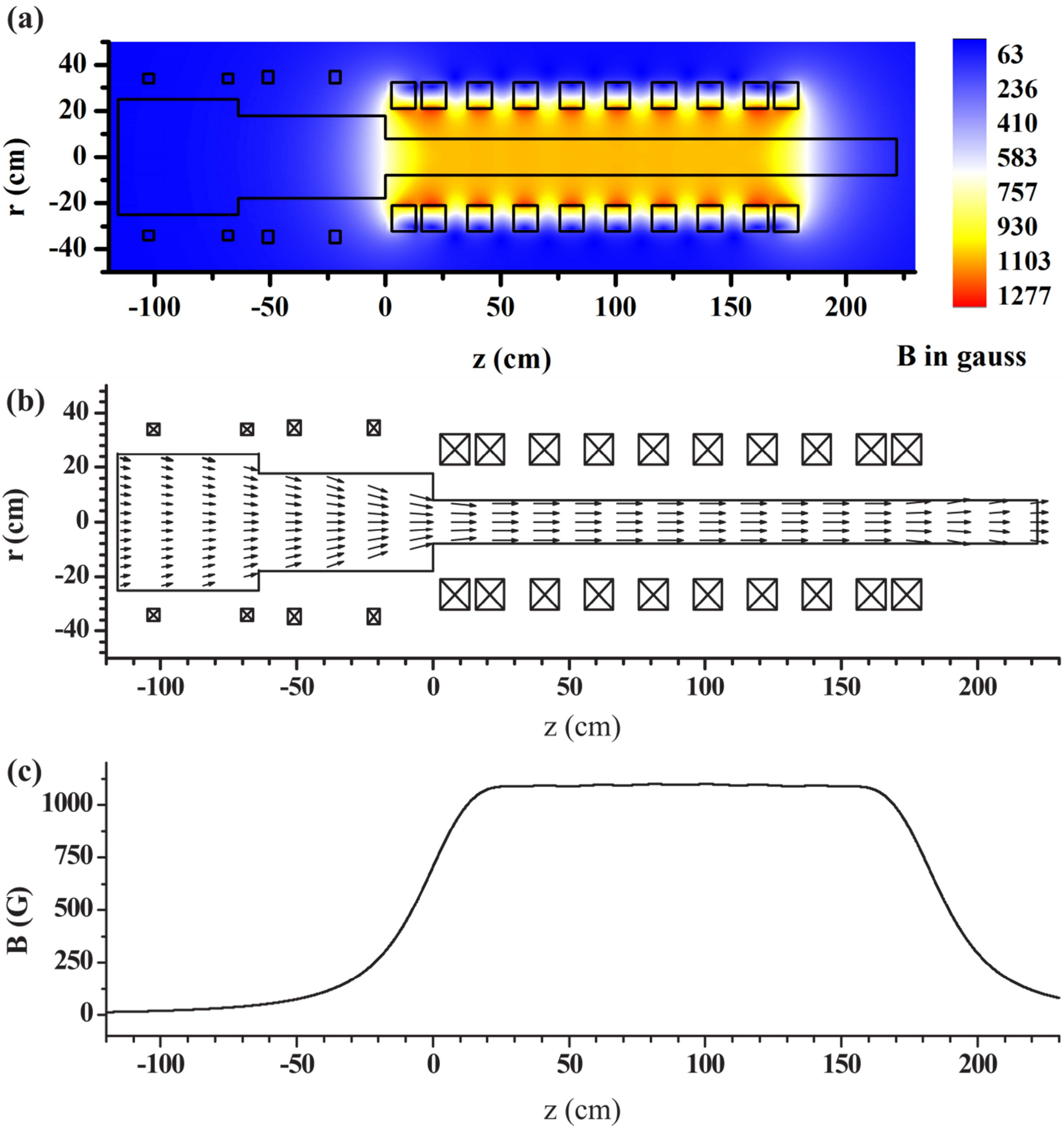

Figure 3.7 : (a) 2D color map of the simulated magnetic field showing the variation in the RZ plane. (b) Profile of the magnetic field produced by the regular magnets. The length of the arrows is proportional to $log|B|$ (c) Variation of the magnetic field along axis. All the three figures are for $NI = 18000$ amp-turns in the regular magnets. The current in the compensation and the extension magnet is zero.

3.2.3.1 Choice of conductor and magnet fabrication

The choice of the conductor for fabricating the magnets involves several trade-offs. First, one has to choose the conducting material to be used for making the magnets. Generally copper is used to make magnets for generating magnetic fields of value few ~ kG. This is so because copper magnets cost less to fabricate compared to its other counter parts like super conducting magnets. The magnetic field produced by a magnet is directly proportional to the total current (NI) flowing through it. Hence large currents must be driven by large power supplies to generate high magnetic fields. This will lead to generation of heat which must be dissipated by cooling the system. If the heat is not dissipated, the conductor temperature will rise as a result the resistance of the magnet will increase, requiring higher voltage to drive the same current. If the rise in temperature is not checked and the temperature rises beyond the maximum operating temperature of the materials used to make the magnet, the magnet may get damaged permanently. One of the most effective ways of cooling a current carrying conductor surrounded by other current carrying conductors is to pass liquid coolant like cold water through it. Hence a channel for water cooling is an additional requirement. The conductor material must be soft enough to be bent to form coils. Two variants of coper was considered for the fabrication of the magnets, electrolytic tough pinch (ETP) grade and Oxygen free High conductivity (OFHC) copper. ETP copper was selected for magnet fabrication because of its low price and local availability. OFHC copper do have a higher conductivity, (101% International Annealed Copper Standard) [82] compared to ETP grade [82] (100% IACS), but 1% reduction in conductivity is tolerable compared to significant price difference between the two grades of copper. Circular cross-section annealed copper tube of inner and outer diameter 8mm and 5 mm respectively is chosen for fabrication of the magnet coils. This dimension of copper tube is regularly used in the industry hence it is cheap and locally available, and annealed copper tubes are soft enough to be bent to form coils.

The magnets coils are made by fabricating sub coils in the form of double pancakes first and then the fabricated double pancakes are assembled to make the magnets that are to be used for the experiments. The coils were fabricated in-house with a 1.2 m diameter turn table having a motorized feed arrangement shown in Figure 3.8. The frequency of the turn table can be varied from 0.1 Hz to 5 Hz as per requirement. Winding was done on a steel bobbin placed on the turn table having a diameter equal to the inner diameter of the magnet being fabricated. For electrical insulation, the copper conductor was first wrapped around by double layer of 1 mil thick kapton tape, then by double layer of 0.25 mm thick cotton tape. Insulating and winding were done simultaneously with the help of motorized feed. Finally, after the completion of the winding, one double layer of cotton taping was given throughout the pancake. Two copper blocks of dimensions $80 \times 60 \times 15\ mm^{-3}$ were brazed on the two leads of each pancake for electrical connections whereas two brass nozzles were brazed at the ends of the lead for water connection. Each pancake was then subjected to several tests for interlayer insulation, high voltage withstand, water path blockage, water pressure withstand cum leakage and resistance measurement across the two leads of the pancake before applying epoxy to provide extra insulation and mechanical strength. The finished pancakes were assembled together to make required magnets. Regular magnets were made by assembling five double pancakes and extension and compensation magnets were made by assembling two double pancakes coaxially.

Figure 3.8: Machine for fabricating the double pancakes

3.2.3.2 Magnet cooling consideration

The magnet coils are cooled by passing demineralized water at 20^0C through the magnets at 5 bar pressure. Such high pressure ensures the water flowing through the tube in the turbulent regime for better heat transfer coefficient between the water and the conductor surface. The flow rate of the water through the system is about 100 litre per minute and the inlet water temperature is maintained at 20^0C for effective cooling.

3.2.3.3 Testing of the magnet system

The magnetic field extending from the main plasma chamber to the source chamber is measured using a gauss meter with a Hall probe. A comparison of the measured and simulated magnetic field as shown in in Figure 3.9 exhibits a remarkable agreement. The magnet system produces a flat top field over a distance of 1.3 m; in the main chamber. The variation of the magnetic field in the chamber is ~ 0.7% in the axial direction and ~0.46% in the radial direction. The magnet system is powered using four sets of magnet power supplies; this is done to enable magnetic field of different configurations in the system. By varying the currents in different coils one can produce different magnetic field gradients at different locations in the system.

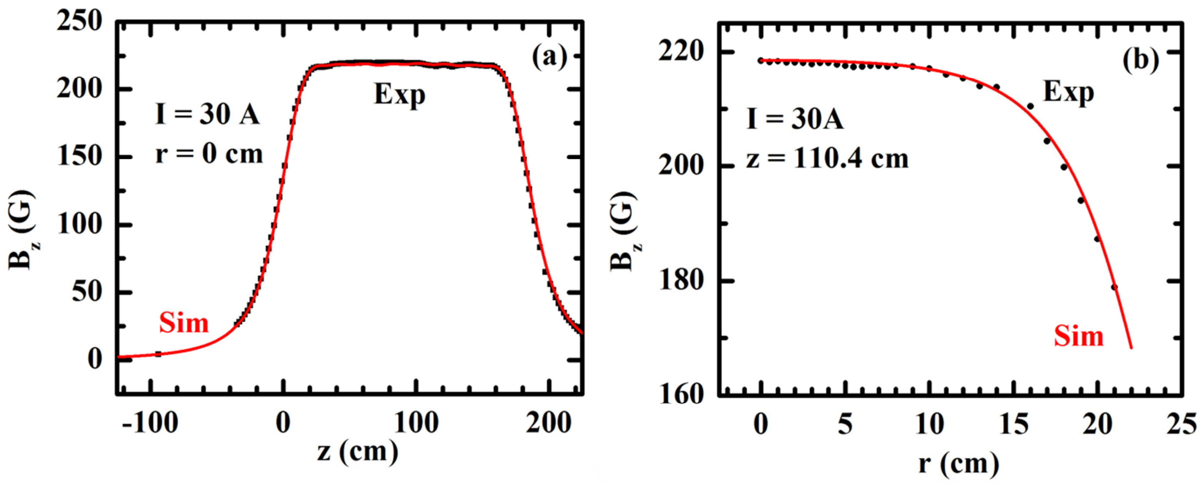

Figure 3.9: Comparison of the simulated and experimentally measured data (a) Variation of the axial magnetic field along the axis. (b) Variation of the axial magnetic field along the radius

3.2.3.4 Magnet support structure and final assembly

The support structure is designed with emphasis given to make it simple, quite flexible in placing the coils, making all the diagnostics ports very much accessible and, most importantly, economical. The magnets are mounted on a stainless steel stand that can be placed on the aluminium stand used for holding the vacuum system. Unlike the hylam support used for magnets in MLPD, this stainless steel stand allows for greater spacing between the magnets. Figure 3.10 shows a completed regular magnet coil consisting of five double pancakes resting on the stainless steel magnet holding stand. The smooth bottomed magnet holding (MH) stand can easily be slid on the aluminium stand thus enabling the user to easily change the position of the magnets if necessary. The slots at the bottom of the MH stand are used for bolting it to the aluminium stand thus locking the position of the magnets. The two rectangular blocks with holes on either side of the MH stand is used to pass guiding rods which is helpful in arranging the magnets coaxially. It must be emphasized that no magnetic material has been used in the magnet assembly or in the assembly of the vacuum vessel.

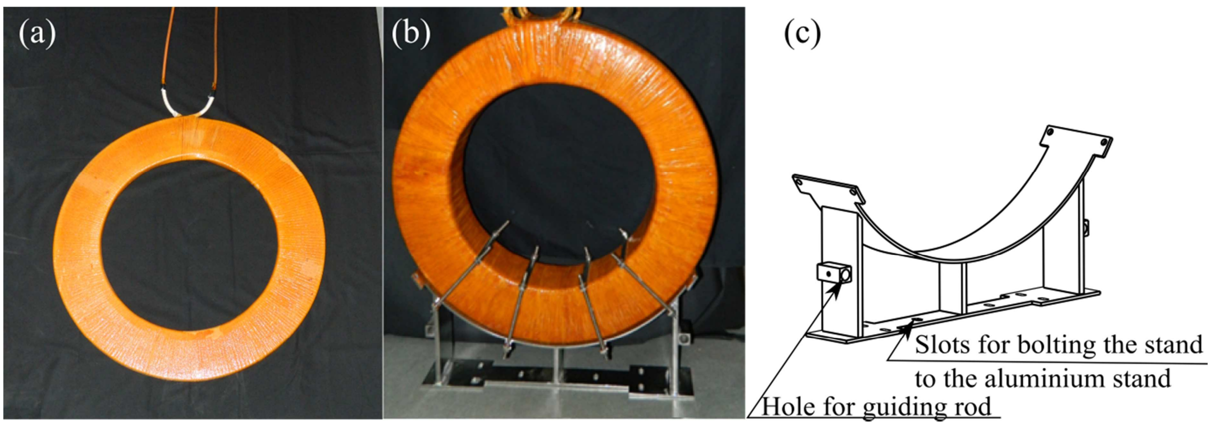

Figure 3.10 : (a) Picture of a double pancake after application of varnish. (b) Picture of a finished regular magnet made by joining five pancakes together. (c) Magnet holding structure.

A picture of the fully assembled experimental device is shown in Figure 3.11.

Table 1 : Magnet system description

	Regular magnet	**Extension magnet**	**Compensation magnet**
Location	Coaxially around main chamber	Coaxially around source chamber extension	Coaxially around source chamber
Inner Diameter	$42\ cm$	$64.5\ cm$	$64.5\ cm$
Outer diameter	$64.5\ cm$	$74.8\ cm$	$72.4\ cm$
Length along the axis	$10.5\ cm$	$4.5\ cm$	$4.5\ cm$
No. of turns	$120\ turns$	$20\ turns$	$16\ turns$
Resistance	$114\ m\Omega$	$24.8\ m\Omega$	$19.6\ m\Omega$
Total number of magnets	10	2	2
Power supply	Magnets are powered by four power supplies 1. 40V/250 A (2 magnets) 2. 60V/167 A (3 magnets) 3. 60V/167 A (3 magnets) 4. 40V/250 A (2 magnets)	Each magnet separately powered by 32A / 30 V power supply	20 V / 250 A power supply is used to power both magnets connected in series. For independent operation 32V/60A power supply is used.

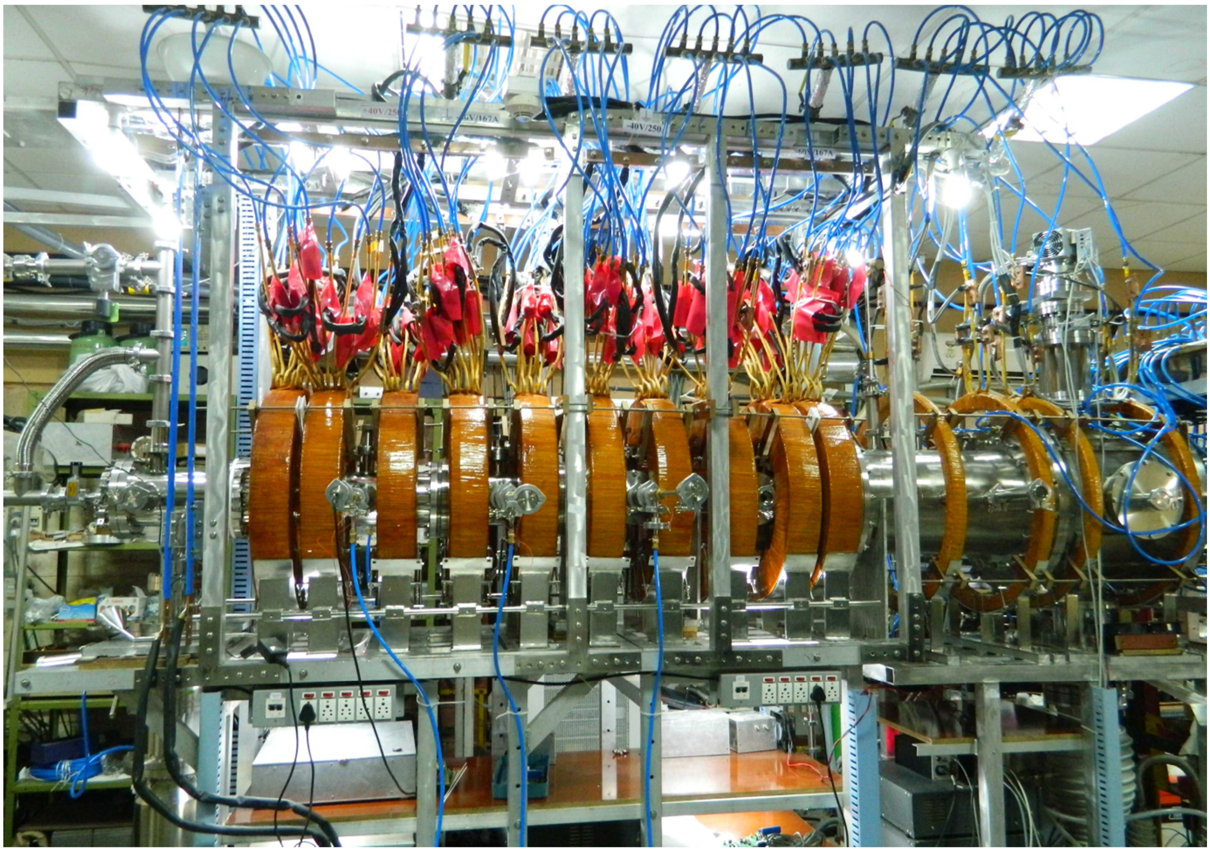

Figure 3.11: Picture of Inverse Mirror Plasma Experimental Device (IMPED).

3.3 Plasma Diagnostics

3.3.1 Langmuir probe

A Langmuir probe [83] is one of the oldest and most widely used diagnostic tools for measuring plasma parameters. A Langmuir probe in its simple form consists of a bare wire that is inserted in the plasma. The wire is biased with respect to a reference electrode or a grounded vessel and the current collected by the probe corresponding to each biasing voltage is measured. The variation of the probe current with respect to the biasing voltage is termed as the I-V characteristics.

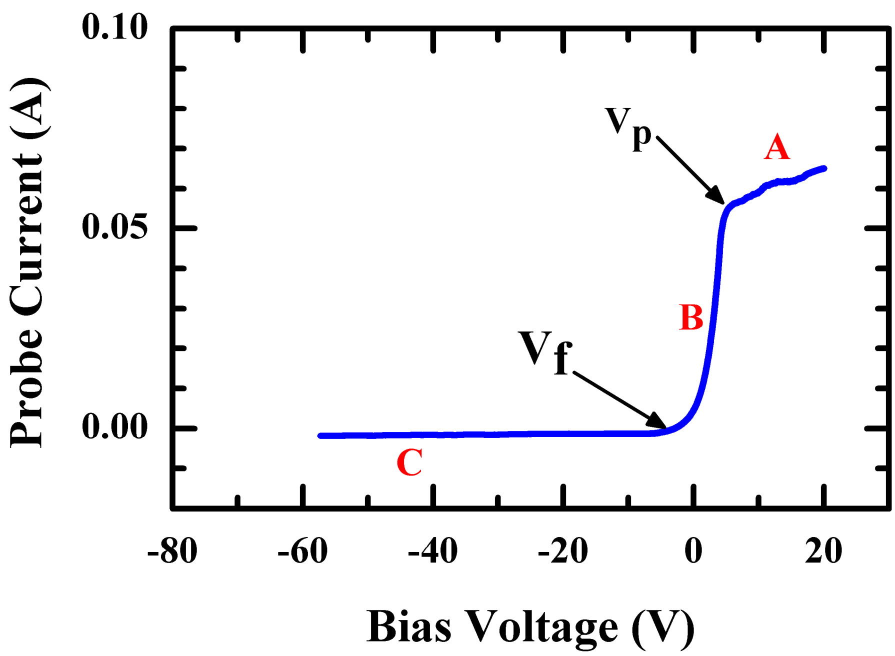

Figure 3.12: Typical I-V characteristics obtained in IMPED at high density.

Figure 3.12 shows a typical I-V characteristics. The electron current collected by the probe has been considered to be positive and the ion current negative. V_S is the potential of the plasma with respect to the probe reference which in this case is the grounded vessel. When the probe is biased at plasma potential, there is no electric field between the probe and the plasma. Electrons and ions impinge on the probe surface with their thermal velocities. The electron flux to the probe is much higher than the ions owing to the lower mass of the electrons $(m_e \ll m_i)$ and higher electron temperature $(T_e > T_i)$. As a result the current collected by the probe is predominantly electron current. If the probe voltage is increased above the plasma potential a sheath is formed around the probe and the sheath electric field attracts the plasma electrons entering the sheath to the probe. The probe current slowly increases on increasing the probe potential above the plasma potential as shown in the region A of Figure 3.12. This is because of the sheath expansion of the around the probe resulting in an increase in the collecting area.

Decreasing the probe potential, $V_{pr} < V_p$, the probe is now negative with respect to the surrounding plasma and increasing fraction of the impinging electrons is reflected from the negative potential (Region B). Eventually the potential is sufficiently small to reduce the collected electron current to small fraction of its saturation value. The total probe current is zero when the electron current is equal to the ion current $(I_e = I_i)$ at the floating potential V_f. Decreasing the potential further, entering the region C, eventually all the electrons are repelled and only ion current is collected by the probe. The ion current varies very slowly with the probe potential and this region is termed as the ion saturation region.

Over the years different Langmuir probe theories have been developed to interpret the I-V trace of the Langmuir probe for determination of the plasma parameters under a wide variety of operating conditions. The various ranges of λ_D/r_p, λ/r_p and λ/λ_D determine the well-known domains of operation, where r_p is the probe radius, λ_D is the debye length which is a measure of the sheath thickness and λ is the mean free path. These limits are illustrated in the three dimensional diagram $r_p - \lambda_D - \lambda$ diagram shown in Figure 3.13.

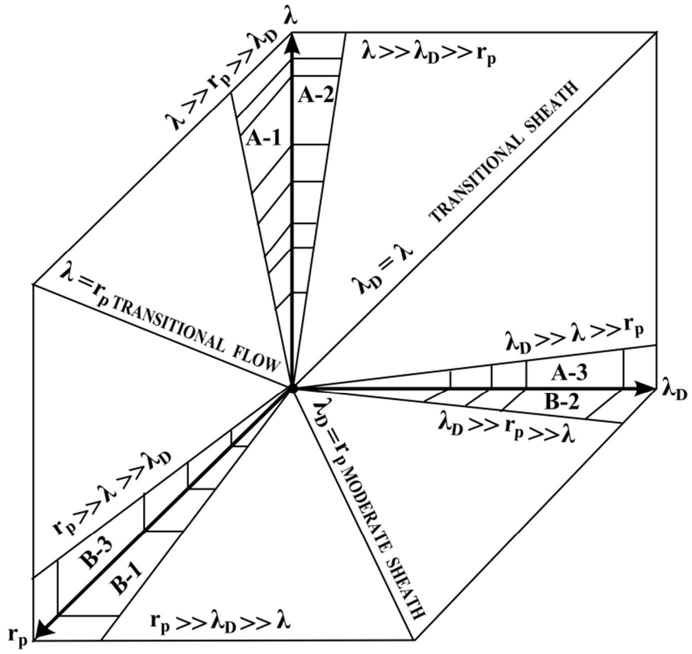

Figure 3.13 Three dimensional diagram illustrating various probe-operation regimes, probe radius *(r_p)*, Debye length (λ_D) and mean free path (λ) [84]

From the Figure 3.13 one can identify six different probe regimes that could be divided into two domains depending on the magnitude of Knudsen number, $K_n = \lambda/r_p$.

A. $K_n \gg 1$: Classical Langmuir probe

   a. $\lambda \gg r_p \gg \lambda_D$: thin sheath limit

   b. $\lambda \gg \lambda_D \gg r_p$: orbital limit thick sheath

   c. $\lambda_D \gg \lambda \gg r_p$: collisional thick sheath

B. $K_n \ll 1$: Continuum Electrostatic probe

   a. $r_p \gg \lambda_D \gg \lambda$: collisional thin sheath

   b. $\lambda_D \gg r_p \gg \lambda$: collisional thick sheath

   c. $r_p \gg \lambda \gg \lambda_D$: collisionless thin sheath

Most of the probe theories are asymptotic in one of the three parameters, λ, λ_D and r_p, and the domains of the applicability reside inside in one of the shaded areas of Figure 3.13 .

Condition $K_n \gg 1$ represents the classical Langmuir probe regime, The sheath may be collisionless (A- 1, A-2) or collisional (A-3) depending on the relative magnitudes of λ and λ_D. The $K_n \ll 1$ represents the condition where probes are always collisional relative to the gas (continuum flow) but for which the sheath may or may not be collisional depending on the relative magnitudes of λ and λ_D. In addition there are transitional domains represented by the diagonals.

Several Langmuir probe theories have been developed to extract plasma parameters like plasma density from the I-V curve in different domains operation. For example in the collisional thin sheath regime (B - 1) density can be determined from the ion current collected by the probe using the theory of C.H. Su and Kiel [85]. In the collisionless thin sheath regime (A-1) density can be determined from ion saturation current using the Bohm velocity. Similarly there are theories for operation in in continuum collisional thick sheath regime [86] (B – 2), collisionless orbital thick sheath limit [83] (A – 2) etc. In addition to the domains of operation described above there are number of other regimes of operation where Langmuir probe is used, notably magnetized plasmas [87, 88], turbulent plasmas [89, 90] etc. There are a number of monographs and review articles on Langmuir probe some of which are given in ref [91, 92, 93, 94, 95, 96]. There is no general theory for interpreting I-V characteristics for all operating conditions. Actually, the probe theory by which the plasma parameters are estimated depends on the shape of the probe, collision mean free path of the species, dimensions of the probe, Debye length, Larmor radius etc.

3.3.1.1 *Single Langmuir probe in quiescent collisionless plasma*

The usage of single Langmuir probe for measurement of plasma parameters in IMPED and MLPD is limited to quiescent collisionless quasineutral plasma. The earliest probe theory for determination of plasma parameters in a quiescent collisionless plasma using a Langmuir probe was proposed by Mott-Smith and Langmuir in 1926 [83]. They considered particle orbits within the space charge sheath surrounding a spherical or cylindrical probe in the collisionless regime; the probe current is limited only by the angular momentum of the orbiting ions. For this theory to be applicable the probe sheath must be much larger than the probe radius. The potential variation $V(r)$ inside the sheath has to be gentle enough that there is no “absorption radius” and the particles hit the probe at grazing incidence. This may not be the case in laboratory plasmas. An “absorption radius” might exist, outside the probe, such that the particles which cross it are destined to hit the probe [97].

In 1957 Allen, Boyd, and Reynolds (ABR) [98] derived a relatively simple differential equation which could be solved to give $V(r)$, for all r without division into sheath, presheath and plasma regions. However, this theory was only for spherical probes and only for $T_i = 0$, so that ions moved radially into the probe and there was no orbital motion and the absorption radius was at infinity. Chen [99] later extended the $T_i = 0$ calculation to cylindrical probes. The first probe theory which accounted for both sheath formation and orbital motions was worked out by Bernstein and Rabinowitz [100] , who assumed an isotropic distribution of monoenergetic ions. The theory is further refined by Laframboise [101], who extended the calculations to a Maxwellian ion distribution at temperature T_i. He presented the results as a tabulation of parameter ‘i’ such that

$$I_p = eA_p n_0 (k_B T_e/2\pi m_i)^{1/2} i\left(V_p/k_B T_e\ , r_p/\lambda_D\ , T_i/T_e\right) \tag{3.1}$$

where V_p the probe is potential with respect to the plasma, I_p is the probe current, A_p is the probe area, n_0 is the plasma density, m_i is the mass of the ion, T_e is the electron temperature, T_i is the ion temperature and k_B is the Boltzmann constant. Laframboise theory is applicable for a wide range of ratios of probe radius to Debye length (r_p/λ_{De}), a complete range of ion to electron temperature ratios (T_i/T_e), and have been experimentally verified in a variety of conditions [102, 103, 104].

3.3.1.1.1 Density determination

Since Laframboise theory is the most complete theory for cylindrical Langmuir probes and has a wide range of validity, we shall use Laframboise theory for density determination. However, use of Laframboise theory involves a lot of delicate computations and is not easily applied to experimental measurements. Several approximate fits to Laframboise's results have been made. Most notably by Kiel [105], Peterson and Talbot [106], Steinbr$\ddot{u}$chel et. al. [107, 108, 109], Mausbach [110] and Chen [111]. The fitting formulas of Kiel and Peterson–Talbot are not accurate for $r_p/\lambda_D < 5$, hence they are not used to determine the density in our case. The analytical expression used by Steinbrüchel et. al. and Mausbach to fit the numerical results of Laframboise is not accurate for large values for r_p/λ_D , say $r_p/\lambda_D = 80$. Hence not used for density determination. The fitted formula of Chen has a wide range of validity from 0 < $r_p\backslash\lambda_D < 100$. Hence has been used for density determination.

The fitting formulas as suggested by Chen are as follows

$$\frac{1}{I^*} = \frac{1}{(A\eta^B)^4} + \frac{1}{(C\eta^D)^4} \tag{3.2}$$

Where $\eta \equiv \eta_p \equiv -\frac{e(V_{pr}-V_s)}{k_B T_e}$ and $I^* = \frac{I_i}{I_0} = \frac{I_i}{en_0A_p}\left(\frac{k_BT_e}{2\pi m_i}\right)^{-1/2}$, V_{pr} and V_s are the probe potential and the plasma (space) potential with respect to the reference electrode.

The parameters A, B, C and D in (3.2) are given by the following expression.

$$A = a + \frac{1}{\frac{1}{b\xi^c} - \frac{1}{d \ln\left(\frac{\xi}{f}\right)}}$$

$$B, D = a + b\xi^c \exp(-d\xi^f) \qquad (3.3)$$

$$C = a + b\xi^{-c}$$

where $\xi = r_p/\lambda_D$. The coefficients $a, b, c\ and\ d$ in (3.3) are given in Table 2,

Table 2 : Coefficient for calculating ABCD($\boldsymbol{\xi}$) for all $\boldsymbol{\xi}$

	a	b	C	D	f
A	1.12	0.00034	6.87	0.145	110
B	0.50	0.008	1.50	0.180	0.80
C	1.07	0.95	1.01	-	-
D	0.05	1.54	0.30	1.135	0.370

In addition to cylindrical Langmuir probe plasma density has also been measured with planar probe. In case of planar probe the thin sheath condition $r_p/\lambda_D \gg 1$ gets more easily satisfied, in such a case one can assume that the probe collecting area is equal to the physical probe area. When $T_e \gg T_i$, the velocity of the ions in the sheath is given by Bohm velocity $v_B = \sqrt{k_B T_e/m_i}$. For a probe biased in the ion saturation region such that all the electrons are repelled and the probe only collects ions, the ion saturation current is given by

$$I_{ionsat} = 0.61 e n_0 A_p \sqrt{\frac{k_B T_e}{m_i}} \qquad (3.4)$$

For densities where the thin sheath assumption is no longer valid, one will have to consider the increase in the effective collecting area (A_{eff}) of the probe at large negative voltages due to sheath expansion for density determination. Sheridan [112] derived from his numerical simulation that of the ratio of the effective collecting area to the physical probe area (A_p) can be expressed as

$$\frac{A_{eff}}{A_p} = 1 + a\eta^b \tag{3.5}$$

The fitting parameters 'a' and 'b' in (3.5) are given $a = 2.28(\xi)^{-0.749}$ and $b = 0.806(\xi)^{-0.0692}$.

Other symbols have their usual meaning. The expression given in (3.5) is valid for $10 < \xi < 45$ and $5 < \eta < 30$.

Since the ion current is proportional to the collection area, the 'corrected' ion current ($I_{i\,corr}$) in which the sheath effect is removed, can be calculated from the 'measured' ion current ($I_{i\,meas}$).

$$\frac{I_{i\,corr}}{I_{i\,meas}} = \frac{A_p}{A_{eff}}$$

$$I_{i\,corr} = \frac{I_{i\,meas}}{1 + a\eta^b} \tag{3.6}$$

The density has been estimated from $I_{i\,corr}$ using $I_{i\,corr} = 0.61en_0A_p\sqrt{k_bT_e/m_i}$.

3.3.1.1.2 Electron Temperature

The plasma temperature is determined from the exponential electron repelling region of the I-V characteristics. In a Maxwellian plasma the electron current collected by the probe for probe potential less than the plasma (space) potential is given by

$$I_e = I_{e0} exp\left[-\frac{e(V_s - V_{pr})}{k_B T_e}\right] \qquad\qquad V_{pr} \leq V_s \qquad (3.7)$$

Where I_{e0} is called the electron saturation current. It is given by $I_{e0} = \frac{1}{4} e n_0 v_{the} A_p$. Other symbols have their usual meaning.

Taking logarithm on both sides of expression (3.7) one gets

$$lnI_e = lnI_{e0} - \frac{eV_s}{k_B T_e} + \frac{eV_{pr}}{k_B T_e}$$

$$lnI_e = \frac{eV_{pr}}{k_B T_e} + \left(lnI_{e0} - \frac{eV_s}{k_B T_e}\right)$$

Thus one gets an equation of a straight line with the magnitude slope given by $e/K_B T_e$ when lnI_e is the dependent axis and V_{pr} is the independent axis. Hence plasma temperature can be determined from the slope of the linear region of $lnI_e \; vs \; V_{pr}$ plot corresponding to the exponential region of the I-V characteristics.

3.3.1.1.3 Determination of EEDF

Knowledge of the electron distribution function is important for getting a better understanding of different phenomena. In particular $f(v)$ is important for kinetic theory and $f(\epsilon)$ is important in consideration of particle confinement by electrostatic potentials, where $\epsilon = \frac{1}{2} m v^2$. For a large planar probe the derivatives of the electron current with respect to the probe bias $\partial I_e / \partial V_{pr}$ and $\partial^2 I_e / \partial V_{pr}^2$ are proportional to $f(\epsilon)$. But when non–semi–infinite planar probes are used $\partial I_e / \partial V_{pr}$ is no longer proportional to $f(\epsilon)$. For any arbitrary convex probe geometry when the distribution function is isotropic and for anisotropic distribution functions with spherical probes, the distribution function is proportional to the second derivative of the probe current with respect to probe bias (V_{pr}).

$$\frac{\partial^2 I_e}{\partial V_{pr}^2} = \frac{2\pi e^3 A_p}{m_e^2} f(\epsilon)|_{\epsilon=e(V_p-V_{pr})}$$

$$= \frac{1}{4} A_p e^2 \left\{\frac{2e}{m_e(V_p - V_{pr})}\right\}^{1/2} f_E(\epsilon)|_{\epsilon=e(V_p-V_{pr})} \tag{3.8}$$

In our experiments we have determined distribution function from the second derivative of the electron current at lower values of magnetic field when the probe radius $r_p \lesssim r_{Le}$.

3.3.1.1.4 Additional species of electrons in a filament plasma

In low pressure filament discharges the electron distribution function is a sum of two Maxwellian distributions, a cold distribution which correspond to the temperature of the bulk plasma T_e and a hot electron distribution corresponding to temperature T_{ek}. The electron current collected by the probe in the electron retarding region can be written as shown in (3.9).

$$I_e = \underbrace{I_{ke}\, exp\left\{-\frac{e(V_s-V_{pr})}{k_B T_{ek}}\right\}}_{\text{(Kinetic e)}} + \underbrace{I_{e0} \exp\left\{-\frac{e(V_s-V_{pr})}{k_B T_e}\right\}}_{\text{(bulk e)}} \qquad V_{pr} \le V_s \tag{3.9}$$

At very low pressures at $\le 10^{-5}\, mbar$ in multidipole devices the primary electrons confined by the surface magnetic field and bounce many times before they ionize the neutral gas. Due to several bounces the primary electrons becomes isotropic with energy E_p. The primary electrons form a shell in velocity space at a speed $v_p = \sqrt{2E_p/m_e}$. The three dimensional distribution function can be approximated as $f(v) = n_p \frac{\delta(v-v_p)}{4\pi v_p^2}$.

The probe current due to primary electrons is then given by

$$I_{pe} = \frac{n_p e A v_p}{4}\ I_{peo} \qquad\qquad V_{pr} > V_s$$

$$I_{pe} = I_{peo}\left\{1 - \frac{2e\left(V_s - V_{pr}\right)}{m_e v_p^2}\right\}, \qquad\qquad V_s - \frac{1}{2}\ \frac{m_e v_p^2}{e} \leq V_{pr} < V_{pr} \tag{3.10}$$

$$I_{pe} = 0 \qquad\qquad V_{pr} \leq V_s - \frac{1}{2}\frac{m_e v_p^2}{e}$$

3.3.1.1.1 Floating potential

The floating potential is defined as the bias voltage at which a probe draws no current. The floating potential of a conductor is determined by the balance of the electron and ion current to and from the probe. For a Langmuir probe inserted in the quasineutral Maxwellian plasma with $T_e > T_i$, where planar approximation of the probe is valid i.e. $r_p \gg \lambda_D$, the condition for no net current collection is

$$I_{e0} exp\left[-\frac{e\left(V_s - V_f\right)}{k_B T_e}\right] = I_{ionsat} \tag{3.11}$$

$$ln\left(\frac{I_{ionsat}}{I_{e0}}\right) = \frac{e\left(V_s - V_f\right)}{k_B T_e}$$

Since $I_{ionsat} = 0.6 e n_0 A_p \sqrt{\frac{k_B T_e}{m_i}}$ and $I_{e0} = 0.25 e n_0 A_p \sqrt{\frac{8 k_B T_e}{\pi m_e}}$

$$\therefore \qquad \ln\left[\frac{6.1 e n_0 A_p \sqrt{\frac{k_B T_e}{m_i}}}{0.25 e n_0 A_p \sqrt{\frac{8 k_B T_e}{\pi m_e}}}\right] = \frac{e V_f}{k_B T_e} - \frac{e V_s}{k_B T_e}$$

After a little algebra one gets

$$V_f = V_s + \left(\frac{k_B T_e}{e}\right) ln\left(0.6\sqrt{\frac{2\pi m_e}{m_i}}\right) \tag{3.12}$$

For Argon plasma the relationship between V_f and V_s

$$V_f = V_s + 5.2T_e \tag{3.13}$$

Where T_e is in eV.

In case of cylindrical probes, when the thin sheath approximation is not valid, the ion current collected by the probe at floating potential is no longer given by $I_{ionsat} = 0.61en_0A_p\sqrt{\frac{k_BT_e}{m_i}}$. Thus expression (3.12) is no longer applicable. The floating potential of a cylindrical Langmuir probe was computed numerically by Chen [113], by considering the ion current to be given by the ABR theory, and the results were fitted to analytic functions. As per the fitting formulas of Chen, $V_f - V_s$ is 3.7 – 4.6 times the temperature for Argon when r_p/λ_D is varied from 1 – 10. This is significantly less than the usual value of 5.2 for Argon. The reason is that the sheath thickness at V_f causes a cylindrical probe of a given area to collect more ion current and thus the sheath drop has to be lowered to permit more electron flow to satisfy the zero current condition.

Presence of energetic electrons, e.g., primary electrons can make the floating potential of a probe more negative and the fitting formulas of Chen or expression (3.12) no longer holds. This is because in the presence of energetic electrons at floating potential the ion current has to balance the current due to energetic electrons in addition to the current due to bulk plasma electrons [93]. Thus the floating potential gets lowered such that the total electron current collected by the probe decreases sufficiently such that the ion current can balance it.

During our experiments in IMPED and MLPD we have monitored the difference between the plasma potential and floating potential and compared it with (3.12) and fitting formulas of FF Chen [113] to a first-hand information on the presence of faster electrons in the plasma.

3.3.1.2 Effect of magnetic field on probe characteristics

The presence of magnetic field alters the motion of electrons and ions in plasma. In the absence of magnetic field the electrons and ions particles move randomly in the plasma but in the presence magnetic field ions and electrons spiral around the magnetic field line with a radius, in the plane perpendicular to the field line, of $r_L = mv/qB$. The motion of the charged particles (electrons and ions) across the field is greatly restricted although motion along the field lines is similar to the magnetic field free case.

The effect on magnetic field on the current collected by the probe is determined by the ratio of Larmor radius (r_L) to typical probe dimension (r_p). If this Larmor radius for both ions and electrons is much greater than the probe dimension, then the previous zero magnetic field results are recovered.

The presence of magnetic field affects the motion of electrons more than ions because the Larmor radius of electrons is lower than that of the ions, owing the lower mass of electrons $\left(r_{Le}/r_{Li} = \sqrt{T_e m_e/T_i m_i}\right)$. As a result the electron saturation current collected by the probe decreases on increasing the magnetic field because the electron motion is impeded. This is evident from the reduction in the ratio of electron to ion saturation current with increase in magnetic field. In case of unmagnetized plasma the ratio of electron to ion saturation for a planar probe in Argon plasma is 180, however in the presence of high magnetic field it can decrease to ~ 25.

Often during experiments one encounters a moderately magnetized plasma where $r_{Le} < r_p$ but $r_{Li} > r_p$. In this case although the electron current is impeded by the magnetic field but the electron current collected by the probe is governed by the thermal Boltzmann factor $(n = n_0 \exp(eV/k_B T_e)$ in the region of the I-V curve away from the plasma potential and towards floating potential. The plasma temperature can be determined from the slope of the linear region of $\ln(I_e\ vs\ V_{pr})$ for $r_{Le} < r_p$. This has been experimentally verified by many authors, for example Pierre et al. [80] in a magnetized plasma acquired I-V characteristics using a plane probe of collecting area greater than gyro radius. The measured the electron temperature from the semilogarthmic plot of electron current versus probe bias was found to be in good agreement with the velocity measurement of ion acoustic waves propagating along magnetized plasma column. Brown et al. [114] in a magnetized plasma obtained the electron temperature from the probe characteristics by a measurement of the logarithmic slope in the transition region on the I-V curve. They compared probe temperature measurements with temperature measured using a three gridded energy analyser and found that both results agreed within experimental uncertainty.

For the case $r_{Le} < r_p$ but $r_{Li} >> r_p$ the density can be determined from the ion current using the unmagnetized collisionless plasma theory. But for the case of strongly magnetized plasmas ($r_{Le} \ll r_p$ and $r_{Li} < r_p$) the ions moves along the field lines and the probe area is reduced to its projection along the magnetic field. Our experiments are confined to magnetized and moderately magnetized plasma. The Langmuir probe is always oriented perpendicular to the magnetic field. The temperature is measured from the linear region of the $lnI_{electron}\ vs\ V_{pr}$ curve and the density is obtained from the ion saturation region ($r_{Li} > r_p$).

3.3.1.3 Construction of Langmuir probe

Langmuir probes are fundamentally of three types according to its shape, spherical, cylindrical and planar probes. For measurements in IMPED and MLPD we have used cylindrical and planar probes, spherical probes were not used because of difficulty in construction. The dimensions of the probe tip were decided on the basis of heat load on the probe due to the plasma, availability of theory for interpreting the probe characteristics, a good signal to noise ratio, minimization of the perturbation caused by the probe and required spatial resolution. Damage to the probes due to heat flux is avoided by making the probes from refractory materials like Tungsten and Molybdenum. Cylindrical probes of diameter $0.25\ mm$, $0.5\ mm$ and $1\ mm$ and length 3 to $6\ mm$ are used to measurements. The radius of the planar probe used is $3\ mm$. Probes of the above mentioned dimensions can easily withstand the plasma heat load in our operating range. Planar probe is used only for measurements in the low magnetic field region where the Larmor radius of the ions is greater than the probe dimensions. The presence of probe in the plasma perturbs the plasma locally thus to minimize the disturbance a small probe is preferred. A small probe also improves the spatial resolution. But a small probe reduces the probe signal which increases the signal to noise ratio. Hence the selection of probe dimension is trade-off between localized probe perturbation, spatial resolution and signal to noise ratio. For this reason cylindrical Langmuir probe of the above mentioned dimensions has been used for most measurements presented in this thesis.

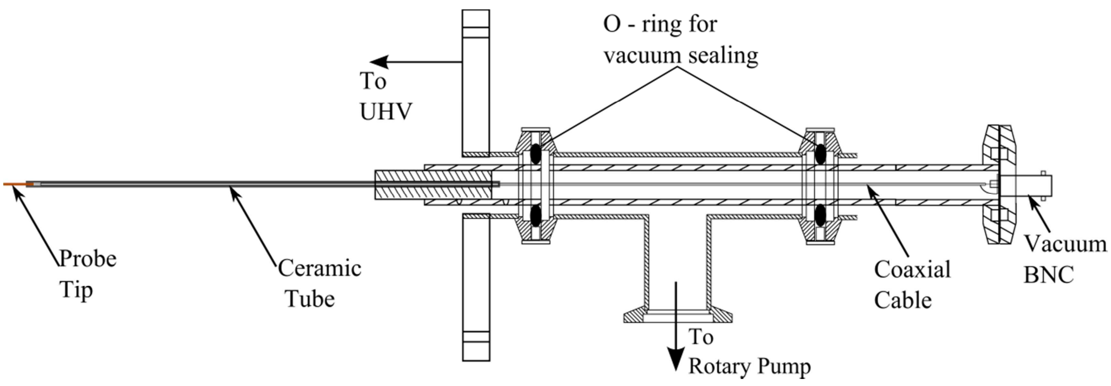

Figure 3.14: Langmuir probe assembly using differentially pumped feedthrough. All electric probes are introduced in the vacuum system through a differentially pumped feedthrough like the above.

Figure 3.14 shows the assembly of a single Langmuir probe. One end of the probe tip is brazed with copper wire for making electrical connections. The copper wire is soldered to a miniature coaxial cable and the other end of the coaxial cable is connected to a vacuum compatible BNC. The probe tip is held in position in the plasma by an ultrahigh vacuum (UHV) compatible ceramic tube which is connected to a metallic shaft. UHV grade ceramic is used to avoid local outgassing from altering the plasma parameters near the probe. Since the ceramic tube is an insulator, the disturbance caused by it is very small compared to the disturbance caused by a metallic tube of similar dimension. In IMPED and MLPD for radial radial probes only the ceramic tube and the probe tip is exposed to the plasma the metallic shaft is never exposed to the plasma. As far as the axial probes are concerned, the probe tip is separated from the metallic probe shaft by a $0.5\,m$ long ceramic tube. The diameter of the metallic radial probe shaft is dictated by the requirement to prevent sagging of the probe shaft. As far as axial probe is concerned a dogleg shape structure is used to hold the probe in position while the probe shaft rests on the surface of the vacuum vessel. The vacuum sealing is carried out using a differentially pumped feedthrough, this is used to prevent local rise in pressure inside the vacuum vessel during movement of the probe.

Figure 3.15 shows some of the Langmuir probes that are used in IMPED and that have been used in MLPD.

Figure 3.15: Different Langmuir probes that were made for measuring plasma parameters. (a) Radial cylindrical single probe *5 mm* length and *0.5 mm* radius, (b) Radial planar single Langmuir probe having radius *3 mm*, (c) Axial cylindrical Langmuir probe with the holding ceramic structure in dog leg shape configuration, probe radius 1mm and length *5 mm*, and (d) Axial planar single Langmuir probe having radius *3 mm*.

3.3.1.4 Langmuir probe measurement circuit

The Langmuir probe measurement circuit in its basic form consists of a voltage source for biasing the Langmuir probe and a shunt resistance in series with the probe and the biasing power supply for measuring the probe current for different biasing voltage. The biasing power supply and the measuring resistance can be connected in two ways. In one case, one connects the Langmuir probe directly to a floating power supply which is connected to the vessel reference (ground) through a shunt resistance as shown in the Figure 3.16a. The disadvantage of this method is that the capacitance between the floating power supply and the ground will be so large that ac signals will be short circuited to the ground and the probe cannot be expected to have a good frequency response. The bias supply can also act as an antenna to pick up spurious signals. The spurious pick up can be avoided by housing the floating power supply and the measuring resistance in a single grounded metallic box. But this solution aggravates the capacitance between the floating supply and the ground. To avoid this one can ground the bias supply and place the measuring resistance on the hot side as shown in the Figure 3.16b. We have used this scheme in our Langmuir probe circuits.

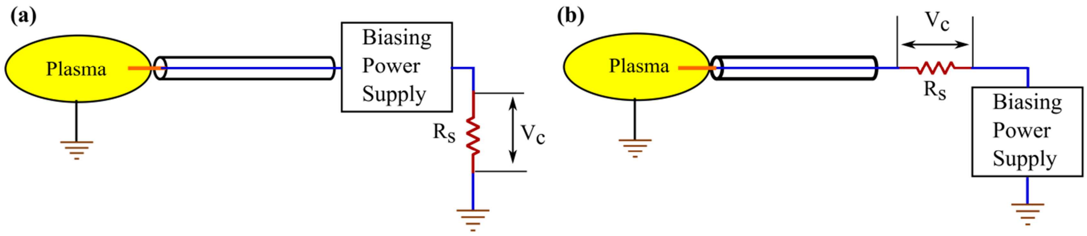

Figure 3.16: Two ways in which a probe, current sensing resistor and biasing power supply can be connected.

The Langmuir probe is biased by a triangular voltage waveform which is varied from $-90\,V$ to $+\,10\,V$. This high voltage bias is generated by a high voltage amplifier PA 85 with a function generator (Max 038/XR 2206) at its input. The probe current is measured by measuring the voltage drop across a resistance using an isolation amplifier. In some of our circuits we have used a galvanic isolation amplifier (AD215) and in the other circuits the current signal is optoelectronically transmitted (HCPL253) to the grounded data acquisition system. The current measuring resistance is varied from $50\ \Omega$ to $470\ \Omega$. The wiring is carried out using coaxial cable with a grounded outer shield to reduce noise pick up. The Langmuir probe bias voltage is swept at a low frequency $\sim 2.2\,Hz$. This is done to ensure that the displacement current between the central conductor and the outer shield of the coaxial cable is much less than the ion saturation current. This however reduces the temporal resolution of the measurement. But for measuring steady state plasma parameters high time resolution is not a necessary.

For time resolved measurements at high frequency a specially designed Langmuir probe has been made using a triaxial cable with a driven shield. The effectiveness of the method has been illustrated below.

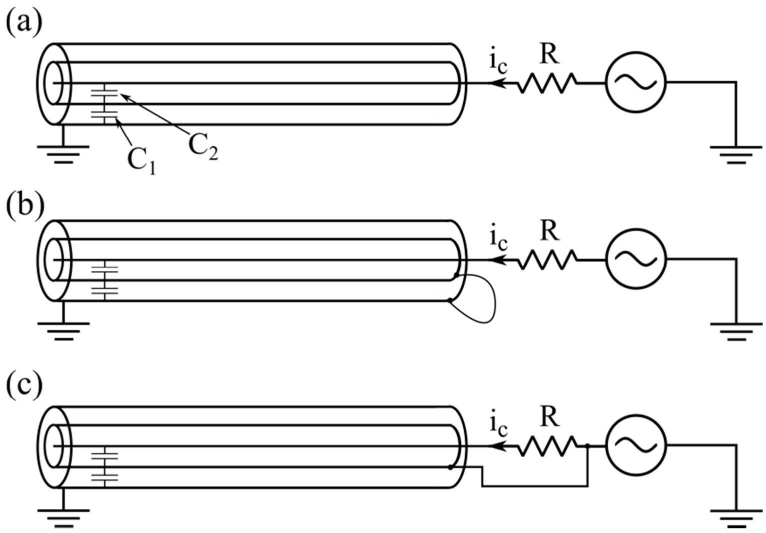

Figure 3.17: Three configuration in which a triaxial cable can be wired. A Belden make triaxial cable of length *1.2 m* is used this experiment.

A triaxial cable typically comprises of a central conductor and two coaxially placed outer shields isolated from each other. Figure 3.17a shows a triaxial cable and the capacitance associated with it. The effective capacitance between the inner and outer shield is given $C_1C_2/(C_1+C_2)$. The capacitive current between the inner conductor and the outer shield can be reduced if the voltage drop across one of the capacitors can be reduced. By driving the inner shield(guard) with the same voltage as the inner conductor, the capacitive current between the inner conductor and the outer shield can be drastically reduced. We demonstrate this experimentally using a current measuring resistance and a function generator connected in series. Figure 3.17 shows three configurations in which the triaxial cable can possibly be used experimentally. In Figure 3.17a the inner conductor is driven while the outer shield is grounded and the middle shield floating. In Figure 3.17b the inner conductor is driven while the outer and the middle shield grounded. In Figure 3.17c both the inner and the middle conductor is driven while outer is grounded. The inner conductor is driven by a 6Vpp 1 MHz sinusoidal signal to determine the capacitive current in all three configurations. In case (a) the effective capacitance between the inner conductor and the outer shield is a series combination of the capacitance between the inner conductor and the inner shield and the inner shield and the outer shield. In the second case the capacitance between the inner conductor and the inner shield is the effective capacitance as the outer and the inner shield is shorted $\left(C_{eq}{\sim}C_1\right)$. In the third case, since the inner shield is driven by the same potential as the inner conductor, the ΔV between inner conductor and the inner shield tends to zero hence the capacitive current from the inner conductor to the driven guard (inner shield) tends to zero. Thus it may be expected that the capacitive current for the case (b) will be maximum followed by case (a). The capacitive current in case (c) is expected to be minimum. Our experimental results shows that capacitive current for case (a) is $2.5\ mA$, case (b) is $4.57\ mA$ and case (c) is $10\mu A$ which agrees with the prediction.

The Langmuir probe system for high frequency measurements uses a driven shield to reduce the capacitive current between the central conductor and the outer grounded shield. The circuit used is shown in the Figure 3.18.

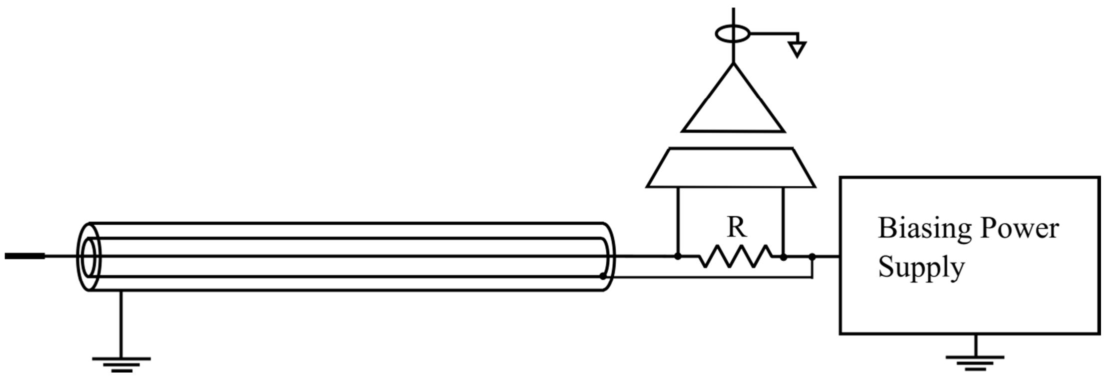

Figure 3.18: High frequency Langmuir probe circuit.

3.3.1.5 Analysis of I-V trace of MLPD and IMPED plasma

A code has been written in MATLAB for quick determination of the plasma parameters from a single Langmuir probe I-V trace. The electron temperature has been measured from the slope of the logarithmic the of electron current in the electron-retarding region, whereas the plasma density has been determined from the attractive-field probe current in the ion saturation region where the current is theoretically well defined. Measurements have been carried out iteratively. The code can be operated both in the automatic and semi-automatic mode. But considering the large density variation $10^9 - 10^{12}\ cm^{-3}$ that can be attained in IMPED, most of the measurements were carried out in the semi-automatic mode. The difference between the automatic mode and semi-automatic mode lies in the identification of the linear region of the $\ln(I_{electron}\ vs\ V_{pr})$, which is done manually in the semi-automatic mode.

The I-V trace evaluation procedure is described below:

A. Step 1: The Langmuir probe data is loaded and smoothed to remove the digital noise. The smoothing procedure includes fitting a straight line in the sampled ramp voltage and generating the voltage data point from the equation of the fitted straight line. The acquired probe current was smoothed by using the Savitzy Golay technique. The first numerical value obtained from the probe characteristics is the floating potential $V_f = V_{pr}\ (I_p = 0)$. This is followed by the determination of the plasma potential (V_s) from the maximum of the first derivative of the probe current.

B. Step 2: Removal of the ion current from the electron current. For that, first the ion current which varies weakly with the probe potential is subtracted from the probe current. This is done by making use of the linear dependence of the square of the probe current on the probe potential [115]. $I_i^2 - V$ tend to be linear over a large range of density [111]. The ion saturation part of I-V characteristics at sufficiently negative probe potential is fitted with the equation [116] $I_i = C\left(V_s - V_{pr}\right)^{1/2}$ and extrapolated to $I_i = 0$, where V_s is the plasma potential and C is a constant. The fitted curve is then subtracted from the total probe current to obtain electron current. In addition to fitting $I_i = C\left(V_s - V_{pr}\right)^{1/2}$, the code also has the facility to fit a straight line [117] in the ion saturation region of the I-V characteristics and then extrapolate it plasma potential for obtaining ion current. The method of determination of ion current is user selectable.

C. Step 3: The electron temperature is determined form the semi logarithmic plot of the electron current versus probe potential. The $\ln I_e\ vs\ V_{pr}$ plot has two distinct linear regions. A straight line is fitted in the region corresponding to the kinetic electrons to determine the temperature of the faster electron component. After subtracting [118] the contribution from the faster electron component from the electron current, a straight line is fitted in the linear region of $In\ I_e\ vs\ V_{pr}$ corresponding to the bulk electrons to determine the bulk electron temperature.

D. Step 4: Initially a rough estimate of the density is made from the ion current in the ion saturation region using the Bohm formula.

$$I_{ionsat} = 0.61 n_{iBhom} e A_p \sqrt{k_B T_e / m_i}$$

The ion current in the most negative probe potential is used to determine the density.

E. Step 5: The total current to a cylindrical probe may be written as a summation of the current collected by the curved surface of the cylindrical probe I_{curved} and the flat

I_{flat} end surface of the probe. The current collected by the curved surface is estimated by multiplying the total current collected by the probe with the aspect ratio factor 'A_r'.

$$I_{curved} = I_p A_r = I_p \frac{2\pi r_p l}{2\pi r_p l + \pi r_p^2} = I_p A_r \tag{3.14}$$

F. Step 6: Having a guess density from the Bohm formula in step 4, estimation of temperature from step 3, plasma potential from step 1. We evaluate the ion current collected by the curve surface of the probe for every probe potential in the ion saturation region using (3.3) and Table 2. For every experimentally measured probe potential in the ion saturation region, the probe current collected by the curved surface at that probe potential was determined for a range of densities spanning from $n_{Bohm}/20$ to $5n_{Bohm}$. The density corresponding to the estimated probe current that had the closest match to the measured probe current collected by the curved surface was determined. In this fashion values of density corresponding to each probe potential and measured probe current in the saturation region were determined. For each of this density value the theoretical ion current is calculated as a function of probe potential from equation (3.3). The density corresponding to the ion current curve that has the closest match with the experimentally obtained ion current in the ion saturation region is determined by the method of least squares.

G. Step 7: This is an additional step, it is carried out only when r_p/λ_D > 10 based on the values of density determined from step 6. In this step the current collected by the flat end part of the cylindrical probe is estimated. For values of r_p/λ_D lying between 10 and 45, the ion current collected by the flat probe is determined using Bohm formula but the physical collecting area of the probe is replaced by the effective collecting due to sheath expansion as per equation (3.5). Method described in step 6 is followed to determine the density but instead of comparing the theoretical ion current collected by the curved surface of the probe with the experimentally measured ion current (I_{curved}) collected by the curved surface the total probe current is compared.

H. Step 8: Using the value of density estimated in Step 7, the theoretical ion current is determined for different probe potentials and subtracted from the measured probe current to get the electron current. The steps 3,5,6,7 and 8 are repeated till the values of density and temperature converge.

I. Step 9: With successful determination of density and temperature, the second derivative of the electron current is calculated to determine the EEDF. The usual two point differentiation formula has not been used here to minimize noise. The derivative of the probe current is estimated by sliding a second order polynomial of the form $I = aV^2 + bV + c$ in the IV trace covering 21 data points in each fit. The differentiated value dI/dV at the 11$^{\text{th}}$ data point is determined by $dI/dV|_{11^{th}} = 2a\,V|_{11^{th}} + bV|_{11^{th}}$. Total number of data points in a single I-V trace is generally 2100 points. The code allows the user to change the number of data points used to fit the second order polynomial. This method allows us to differentiate the data and also has a smoothing effect.

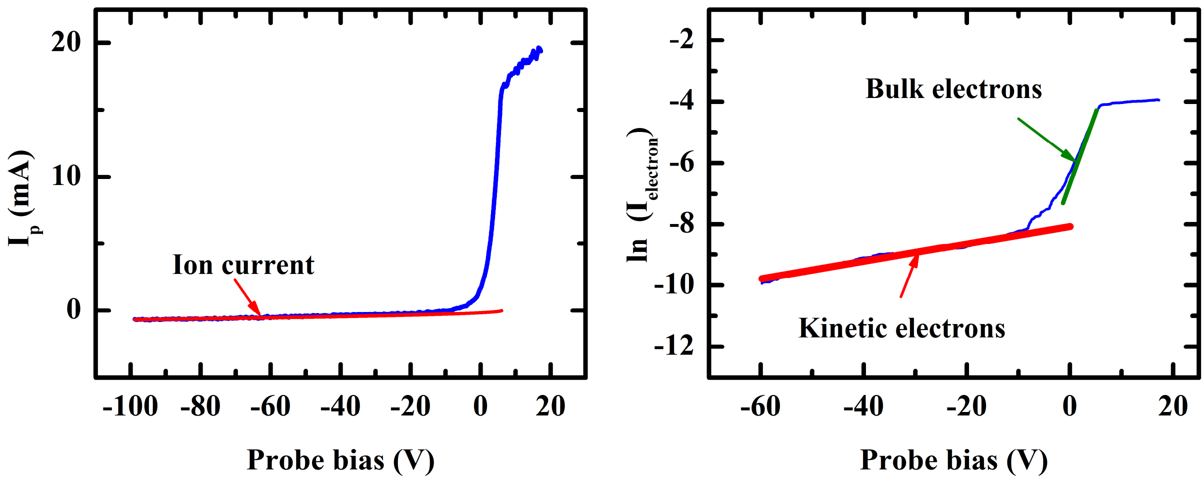

Figure 3.19 : (a) The blue line represents a typical IV characteristic obtained in IMPED and the red line represents the fitted ion current. The ion saturation part of I-V characteristics at sufficiently negative probe potential is fitted with the equation $I_i = C(V_s - V_{pr})^{1/2}$ and extrapolated to $I_i = 0$, where V_s is the plasma potential and C is a constant. (b) Shows the variation of $\ln(I_{electron})$ with probe bias. The red line represents the contribution due to kinetic electrons and the olive line represents the contribution by electrons.

3.3.2 Emissive probe

The concept of electron emitting probe was proposed by Langmuir [119] in 1923. Electron emission from the probe provides an opportunity for direct measurement of plasma potential. Emissive is particularly useful for measurement spatial gradient in the plasma potential for determining electric field. The operation of emissive probe is based on one principle. When a probe is biased more positive than the local plasma potential, electrons emitted from the probe are reflected back to the probe. When the probe is biased negative with respect to the plasma potential, electrons from the emitting probe escape to the plasma and appear as an effective ion current. Emissive probe measurements are not sensitive to plasma flow and beams because it directly depends on the plasma potential rather than electron kinetic energy.

3.3.2.1 Working Principle

The emissive probe I-V curve has two components, the collected current and the emitted current. Neglecting the space charge effects, the emission current from a hot wire can be written as

$$
\begin{aligned}
I_e &= I_{e0} exp\left[\frac{e(V_{pr} - V_p)}{T_W}\right] g(V_{pr} - V_p), && V_{pr} > V_p \\
&= I_{e0}, && V_{pr} < V_p
\end{aligned}
\tag{3.15}
$$

Where V_{pr} is the probe bias, V_p is the plasma potential, I_{e0} is the temperature limited electron emission saturation current and T_W is the hot wire temperature in energy units. The quantity $g(V_{pr} - V_p)$ accounts for the orbital momentum and depends on the hot wire radius and the sheath radius. The temperature limited emission current I_{e0} is given by Richardson Dushman equation.

$$
I_{e0} = AT_w^2 S \ exp\left(\frac{e\phi_W}{T_w}\right) \tag{3.16}
$$

Where 'A' is the Richardson's constant, 'ϕ_W' is the work function of the wire and 'S' is the area of the wire. In case of emission from the filament inside the plasma, the emitted current is constant for bias less than the plasma potential because the emitted electrons do not see any retarding potential (neglecting space charge effects). The emission current appears as an apparent ion collection current. When the bias is above the plasma potential, the electrons feel a retarding force, as the plasma acts like a cathode and the emission current decreases rapidly.

Neglecting space charge effects, electrons collected from the Maxwellian plasma with temperature T_e

$$I_c = I_{c0} exp\left[\frac{-e\left(V_{pr} - V_p\right)}{T_e}\right] \qquad V_{pr} \leq V_p$$

$$= I_{c0} g'\left(V_{pr} - V_p\right) \qquad V_{pr} \geq V_p \tag{3.17}$$

Where, $I_{c0}$is the electron saturation current, $T_e$is the temperature of the electron and $g'(V_{pr} - V_p)$ accounts for the orbital angular momentum of collected electrons. The collected current of an emissive probe is just the same as that a cold Langmuir probe.

3.3.2.2 Methods of emissive probe

There are three methods for determining plasma potential using emissive probe.

3.3.2.2.1 Floating potential method

The floating potential of a sufficiently heated emissive probe is close to local plasma potential, and this is the most widely used method for plasma potential determination using emissive probe. When an emitting probe is immersed in the plasma, the floating potential of the probe is that potential at which the incoming electron current from the plasma is balanced by the outgoing emitted current and the incoming ion current. As the emission of the probe is increased lesser amount of coming ion current is necessary to balance the incoming electron current due to compensation by emitted current. Thus as the emission increases, the floating potential of the probe approaches the plasma potential.

When measuring the plasma potential using the floating point method as the emissive probe heating current is increased from no emission, the floating potential rapidly rises at first, but plateaus at the plasma potential. After this point, increasing the emission only slightly changes the floating potential due to space charge effects. Figure 3.23 shows the variation of floating potential with of a heated emissive with increasing in heating current.

3.3.2.2.2 Inflection point method [120]

Equations (3.16) and (3.17) describing the I-V characteristics of emissive probe shows that when the space charge effects are neglected, the inflection point corresponds to the plasma potential. For an emitting probe the inflection point is shifted by space charge effects due to emission and this shift is linear as shown in Figure 3.20. Therefore, the inflection point is measured for a number of low emission levels to minimize the space charge effects and these points are linearly extrapolated to zeros emission to get the plasma potential without the space charge effects.

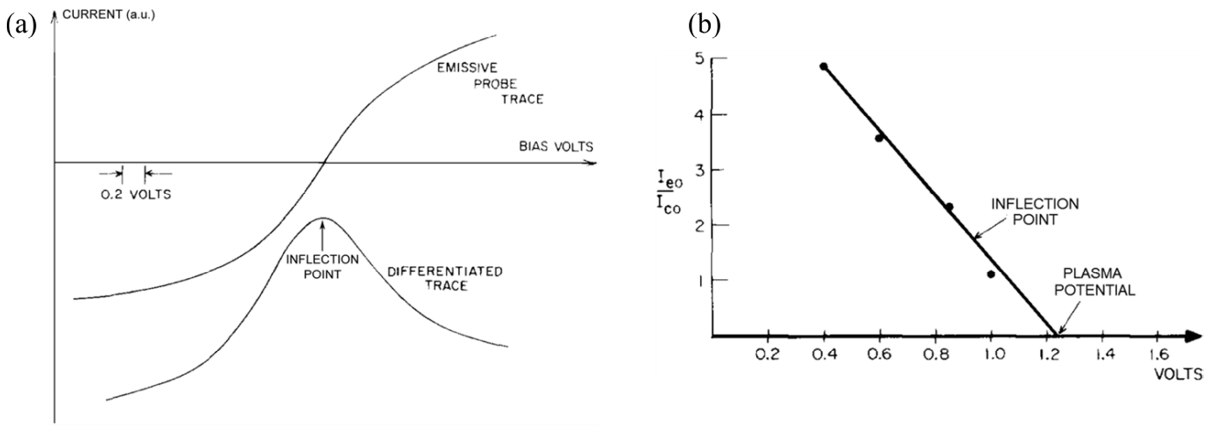

Figure 3.20: (a) An experiment emissive probe I-V trace and its derivative, which is used to determine the inflection point. (b) The vertical axis is temperature limited emission normalized to electron saturation current. The line fit to the inflection point is extrapolated to yield the plasma potential. [121] [120]

3.3.2.2.1 Separation point method

This method is based on the fact that the I-V characteristics of a hot probe and cold probe tend to separate from each other near the plasma potential. The bias voltage corresponding to the separation can be taken as the plasma potential. The accuracy of this method theoretically is on the order of T_w/e, though the uncertainty in determining the precisely where the curves separate can be much larger. [121]

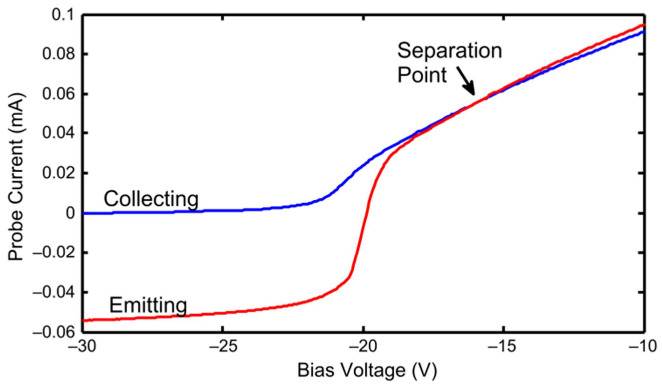

Figure 3.21 : The I-V characteristics of an emitting and a collecting probe. The separating is identified as the plasma potential. [121]

3.3.2.3 Effect of magnetic field on emissive probe

An emissive probe in a magnetic field [121] has a modified effective probe area since the electrons emitted perpendicularly to the field will be trapped in gyro-motion and won't be able to escape and be emitted. This effect is significant if the probe wire oriented along the magnetic field line in which case almost none of the emitted electrons could escape. This problem can be avoided by orienting the emissive probe perpendicular to the magnetic field. A joule heated filament experiences Lorentz force $\left[d\vec{F} = I\left(d\vec{l} \times \vec{B}\right)\right]$ in the presence of an external magnetic field. If the magnetic field is strong enough it can deform a filament with current passing through it. The Lorentz force may reduce the life time of the filament also. Use of Laser heated emissive probe avoids this problem.

The presence of a magnetic field affects the inflection point/emission current relationship [120]. For a given emission current the inflection point will be more negative when a magnetic field is present than when magnetic field is absent. In our experiment we have measured the plasma potential using the floating potential method. The length of the emissive probe was held perpendicular to the magnetic field. A 0.125 mm diameter tungsten wire was used to make the emissive probe; we did not observe bending of the tungsten filament of the above mentioned diameter during operation.

3.3.2.4 Construction and operation of emissive probe

A 0.125 mm tungsten wire has been used to make the emissive probe. The wire was bent in the form a hairpin and inserted in a miniature double bore ceramic. Contact between the leads of the wires connected to the power supply and the tungsten filament is made by squeezing the filament and the connecting wire into the bore of the ceramic tube as shown in Figure 3.22 (a). Plasma potential has been measured using the floating potential method as is not affected by magnetic field and large number of measurements can be carried out using this method very quickly.

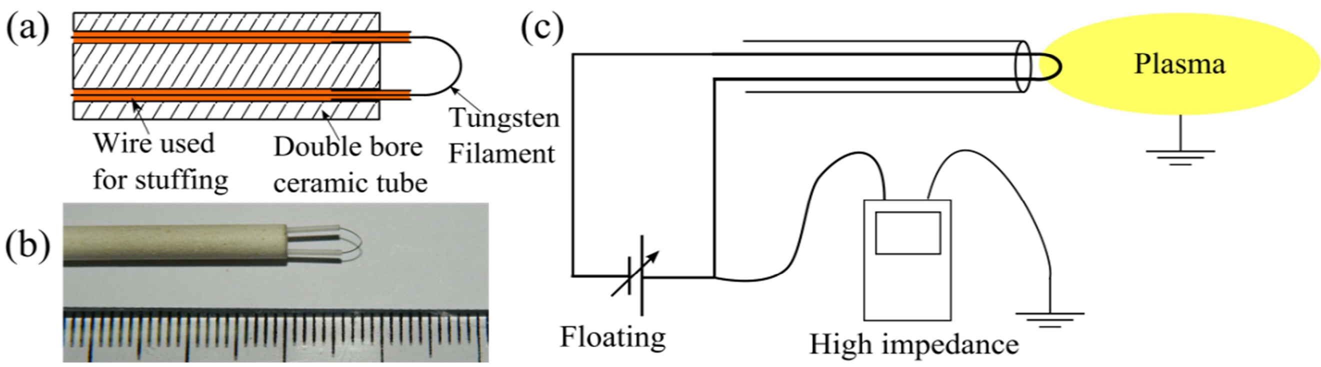

Figure 3.22: (a) Emissive probe construction, (b) Picture of emissive probe, (c) Emissive probe circuit

The filament is heated by passing current through it using a floating power supply with a very good isolation. The potential between the floating hot emissive probe and the grounded vessel is measured using a high impedance ($10M\Omega$) voltmeter. The emissive probe circuit is shown in Figure 3.22c. The length of the emissive probe was held perpendicular to the magnetic field lines to minimize magnetic field effects on electron emission from the probe. The variation of the floating potential of the emissive probe with increase in filament heating current is shown in Figure 3.23.

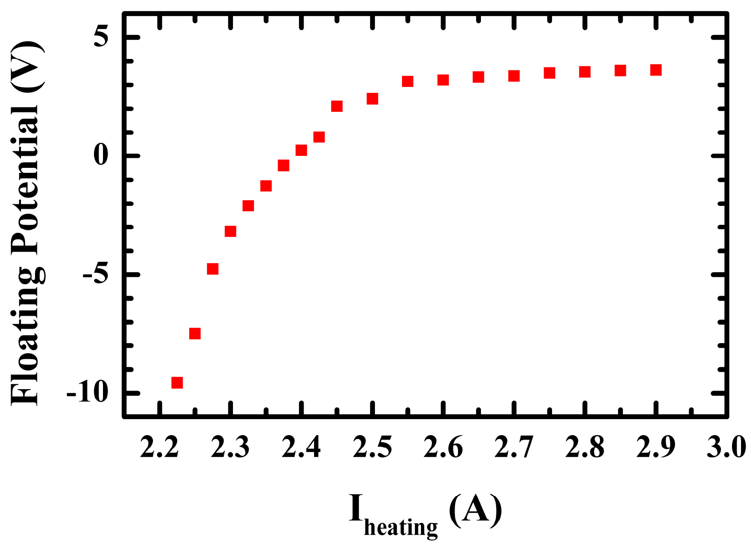

Figure 3.23: Variation of floating potential of a joule heated filament with increase in heating current

3.3.3 Rack probe for fluctuation measurement

The production of quiescent magnetized plasma is one the primary requirements to be satisfied experimentally for the proposed wave studies. The determination of the degree of quiescence of plasma involves measurement of density fluctuations at different operating regimes. It involves a survey of the stability (or instability) of numerous possible modes of oscillation. A magnetized plasma may have a number of intrinsic instabilities and before embarking on the proposed wave experiments a survey of the different modes present in the plasma is desired. For this purpose a set of probes have been designed and made for characterising the different modes present in the system. These probes are used for sampling fluctuations in ion saturation current and floating potential for examining the fluctuation spectra of density and plasma potential. The data (times series) is acquired at a sampling rate of $10\, mega\ samples\ per\ second$ and the record length is $10\, million\, points$. The time series is Fourier analysed to get the power spectrum which shows the power at different frequencies constituting the fluctuations. Linear spectral analysis is, however, of limited use when various spectral components interact with one another due to some nonlinear or parametric processes. In such a case, higher order spectral techniques, like the bispectrum (third – order spectrum) analysis, are useful in completely characterizing the fluctuating signals. Digital bispectral analysis technique for investigating nonlinear wave-wave interaction in plasmas as described by Kim and Powers [122] has been used in the spectral analysis of the fluctuation data.

Three probes placed in the poloidal plane of the main chamber are used for measuring the mode number. Axial wave number k_z is measured using three probes placed at three axial locations; these three probes can be moved radially. The wavelengths are determined from the wave number spectra using a pair of probes [123] by analysing the time series simultaneously acquired by the two probes.

3.3.4 Ion wave exciter and detection

Experiments on phase mixing of plasma oscillations will involve the study of the evolution of plasma oscillation in a non-uniform background plasma density. An inhomogeneity in the back ground density can be easily introduced by exiting an ion wave in the background. The advantage of this method is that by changing the amplitude and wavelength of the ion wave, the density gradient as seen by the plasma oscillation can be changed and the evolution of plasma oscillation at different density gradients can be studied. Over the years several experimental techniques have been devised for excitation and detection of Ion waves, some of the techniques have been mentioned in the section below.

3.3.4.1 Transmitting Antenna

Ion waves are usually excited by applying a pulsed voltage to a negatively grid immersed in the plasma. The grid is made of fine wire to intercept as little plasma as possible, and the wire spacing is several Debye lengths. As an example Wong et al. used a grid spanning their plasma column made from $0.0025\ cm$ wire with $0.075\ cm$ spacing in a plasma with a 0.001 cm Debye length. A 5 V modulation of the $-20\ V$ bias produced a 10% density perturbation. In addition to a single gridded exciter, a double grid [124] or plate exciter can also be used for excitation of ion wave.

3.3.4.2 Detection of ion wave

Many techniques have been used to detect ion waves. In some experiments, the receiver and the transmitter are identical, and the ion current drawn by the biased receiver grid is observed. Alexeff and Jones [125] discuss the use of emissive probes biased negatively and of cold probes biased positively. They reported increased sensitivity with such probes, although care must be taken to ensure that the electron current drawn by the probe is not sufficient to perturb the plasma. When using electric probes to excite and detect ion density perturbation it is essential to separate the directly coupled signal from the plasma coupled signal at the receiver probe. The separation of the capacitive and the wave signal is often accomplished by time-of-arrival measurement. The directly coupled signal appears immediately in the receiver on application of the wave exciting voltage on the exciter while the signal of the slow moving ($\sim 10^{-5}\ cms^{-1}$) ion acoustic wave usually appears after many microseconds. So if a single sine burst is applied on the exciter, first a directly coupled signal will appear on the receiver, this will be followed by the wave signal many microseconds later which can be easily observed in the oscilloscope.

There is another way to completely eliminate the capacitive coupled between the exciter and the detector and that is by using a microwave interferometer [126] as detector. A microwave beam narrower than the acoustic wavelength crosses the plasma perpendicular to the direction of propagation. It is combined with a reference signal from the same source, and the sum is detected. The density variations of the acoustic wave modulate the index of refraction for the electromagnetic wave. The consequent phase modulation of the microwave beam appears as an amplitude modulation of the sum of beam plus reference. Although this method is more complex, it is only sensitive to the density of the plasma in the microwave beam and is free from the difficulty associated with electric probes.

3.3.4.3 Our wave excitation and detection system

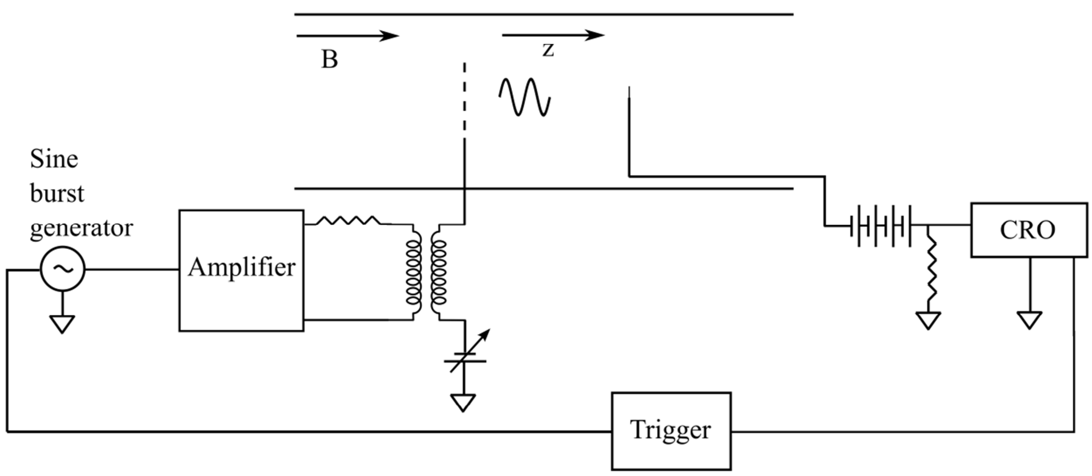

Figure 3.24: Schematic of the wave exciting and detecting circuit.

Disturbance in the ion time scale is excited by applying a oscillating voltage to a 30mm diameter stainless steel (SS304) mesh having a wire of diameter 0.26mm and 0.9mm aperture. The ion wave is detected by using a Langmuir probe biased in the ion saturation region. The separation between the capacitive and wave signal is accomplished by time-of-arrival measurement. The circuit being used for exciting and detecting ion wave is shown in Figure 3.24. The wave propagation data are shown in Figure 3.25, which depicts Langmuir probe receiver signals at four axial locations when the exciter is energized with a single burst voltage pulse. The data is acquired at $1 \times 10^{-4}\ mbar$, $-70\ V$ discharge voltage, R_m = 49.5 ($R_m = B_{main}/B_{source}$) and 327G magnetic field in the main chamber. The propagation speed of the observed peak is found to be $2.6 \times 10^{5}\ cms^{-1}$ which is close to the ion acoustic speed estimated from the temperature measurement using Langmuir probe.

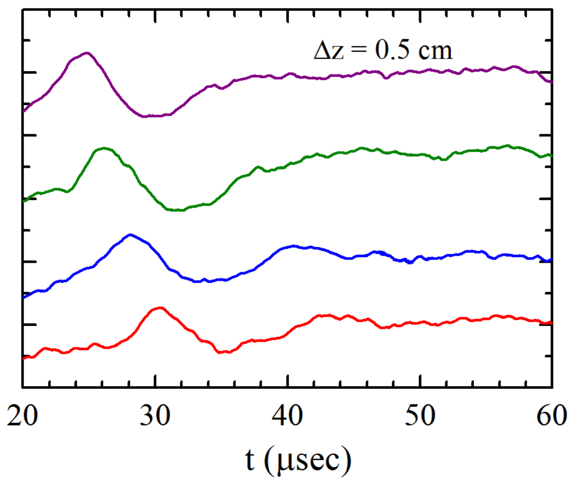

Figure 3.25: Propagation of the disturbance in ion time scale

3.3.5 Excitation of plasma oscillations

Plasma oscillations and wave associated with are high frequency oscillations and waves. For a density range of 10^9 to 10^{11} cm^{-3} , the plasma oscillation frequency varies from $284\ MHz$ to $2.8\ GHz$. At electron plasma frequency, the vacuum electromagnetic wavelength is comparable to the apparatus size hence conventional circuit theory as in the case of ion acoustic waves can no longer be applied but rather one has to resort to microwave techniques. The speed of the electron plasma wave is much higher compared to the ion acoustic speeds hence the time of arrival technique used for ion acoustic waves fail here.

For exciting and detecting plasma oscillation/electron plasma wave three schemes are available. The first scheme employs three gridded exciters [127] for exciting and detecting signals in the electron time scale. The central grid is the power grid it is connected to the central conductor of a matched coaxial transmission line and the outer two outer grids are at rf ground. Grounding the facing element of the exciter and receiving pair minimized direct coupling. For carrying out the wave experiments it is essential to reduce the signal due to direct coupling to value much less than plasma wave signal detected by the receiver. Figure 3.26a shows a three gridded exciter developed for exciting plasma oscillations. In order to minimize plasma loses to the grid experiments were also carried out using a three gridded exciter for excitation of the wave but a probe attached to a 50 ohm semi rigid coaxial cable is used as receiver as shown in Figure 3.26c.

In the second scheme as shown in Figure 3.26b, a tungsten wire fed directly from a 50 Ω semi rigid coaxial line is to be used for exciting Langmuir wave [68] and another tungsten wire is to be used for detection. To reduce the direct pick up between the exciter and receiver a stainless steel cylinder of continuous length 1 m are placed in the main chamber and both the exciting and receiving probes are inside the cylinder. The cylinder act as high pass filter and the experiment will be conducted below the cut off frequency. Both the above mentioned techniques are to be used for exciting waves for plasma densities below and around $10^9\ cm^{-3}$.

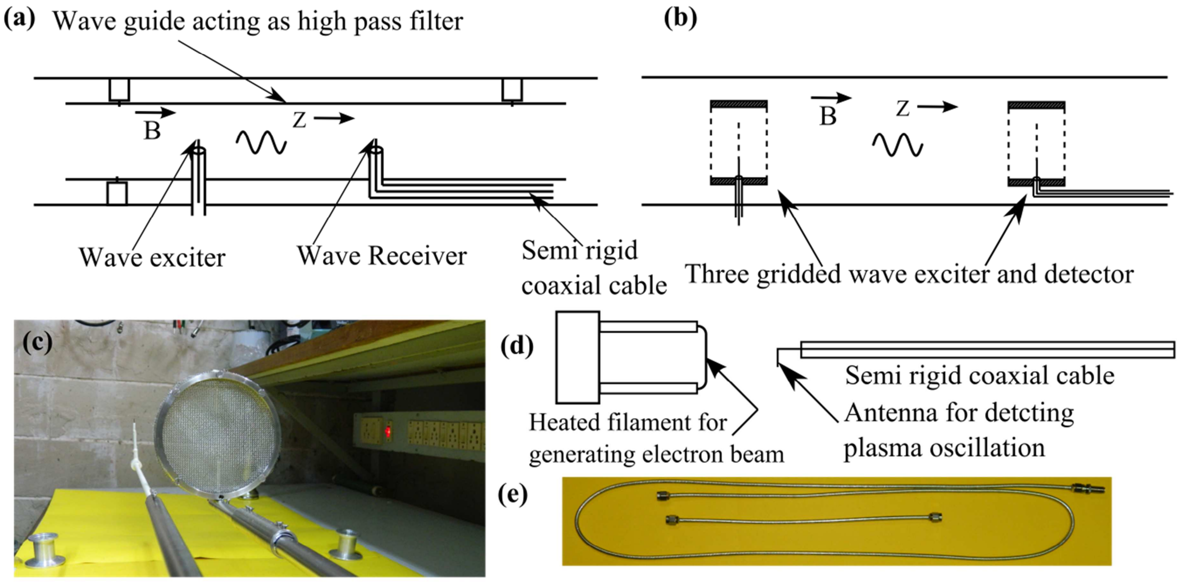

Figure 3.26: (a) Excitation and detection of Langmuir waves using a probe connected to a *50 ohm* semi-rigid coaxial cable. The probes are placed inside a cylinder of smaller diameter which acts as a high pass filter. (b) Three gridded exciters for exciting and detecting plasma oscillation. (c) Picture of the three gridded exciter. (d) Scheme for exciting and detecting plasma oscillation using an electron beam, (e) Picture of a connecterized semi-rigid cable used for making the high frequency circuits.

The third scheme involves excitation of electron plasma wave by making use of two-stream instability. Introduction of an electron beam of density n_{ob} and velocity v_{ob} in cold plasma gives rise to electrostatic waves of frequency ω and wave number k beyond a threshold. Let the beam density n_{ob} be much smaller than the plasma density. Using the fluid equations and linear perturbation theory the dispersion relation can be written as

$$\frac{\omega_{pi}^2}{\omega^2} + \frac{\omega_{pe}^2}{\omega^2} + \frac{\omega_{pb}^2}{(\omega - kv_{ob})^2} = 1 \tag{3.18}$$

If the ions are assumed to be infinitely massive (3.18) becomes

$$1 = \frac{\omega_{pe}^2}{\omega^2} + \frac{\omega_{pb}^2}{(\omega - kv_{ob})^2} \tag{3.19}$$

Equation (3.19) is a quartic equation. It will have four roots. Depending upon the situation, it may have four real roots, or two real roots and two complex roots. The complex roots will be complex conjugate of each other. Equation (3.19) is numerically solved and the results are plotted for different ratio's of beam density (n_{ob}) and plasma density (n_o). The ratio of beam and plasma density is given by $\eta = n_{ob}/n_o$.

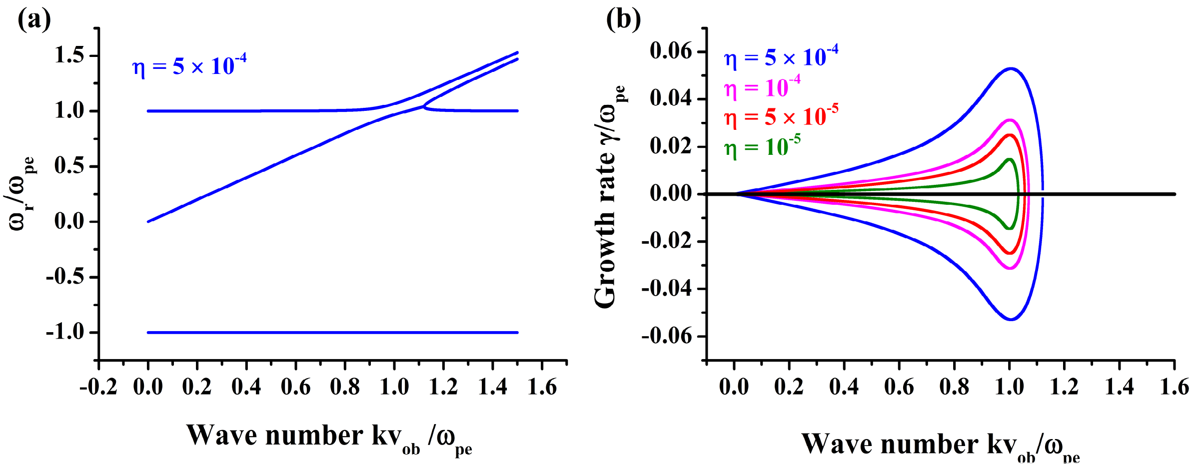

Figure 3.27: Linear dispersion relation of beam plasma instability

The solution of (3.19) is graphically shown in Figure 3.27 which shows that complex conjugate unstable solutions [128] for ω exists when $|k| < \left(\frac{\omega_{pe}}{u}\right)\left(1 + \eta^{\frac{1}{3}}\right)^{3/2}$. The figure also shows that the unstable solutions occur when ω is close to kv_{ob} and also close to ω_{pe} and kv_{ob} is equal to ω_{pe}. Using this information an analytical expression for growth rate can be obtained by substituting $\omega = \omega_{pe} + \delta \approx \mathrm{kv_{ob}} + \delta$ in (3.19), and carrying out a bit of algebra, where$\delta \ll \omega_{pe}$.

$$\omega_{max} \approx \omega_{pe}\left[1 - \frac{1}{2}\left(\frac{1}{2}\eta\right)^{\frac{1}{3}}\right]$$
$$\gamma_{max} \approx \omega_{pe}\left[\frac{1}{2}\sqrt{3}\left(\frac{1}{2}\eta\right)^{1/3}\right] \tag{3.20}$$

Thus it is observed for a weak beam $\eta \ll 1$ one gets $\omega_{max} \approx \omega_{pe}$. Thus from the experimental point of view it is observed that it is possible to excite plasma oscillation using a weak beam. In the presence of magnetic field the electrons are expected to gyrate around the magnetic field lines. But the equation of motion of the electron along magnetic field bears the same form as without the magnetic field $(\vec{B})$ case. Hence two-stream instability appears at $\omega{\sim}\omega_{pe}$ as if magnetic field is absent if motion along $(\vec{B})$ is only considered.

An electron beam generated by an electrically biased heated tungsten filament is used to excite plasma oscillations in IMPED over a wide range of frequencies during the wave experiments. The plasma oscillation is detected by a floating probe connected directly to spectrum analyser. A connected semi-rigid cable and high frequency vacuum feedthroughs have been used to make the receiver probe. Plasma oscillation is excited by introducing an energetic electron beam $\sim 103\ eV$ in the plasma along the magnetic field with low beam density ($\eta \ll 1$) and it is detected by a high frequency receiver probe placed at a distance of $3\ cm$ away from the heated filament. The spectrum analyser connected to the receiver probe shows a single peak centred on the plasma oscillation frequency as shown in Figure 3.28.

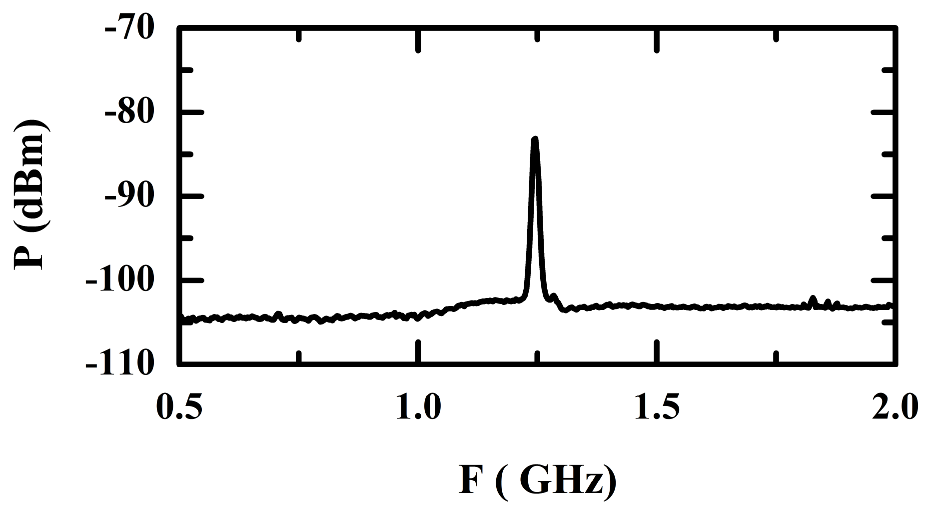

Figure 3.28: Frequency spectra of the detector signal measured at *3 cm* away from the heated filament biased at *-100 V*. Location of the heated filament $z = 152.5$ *cm* and $r = 0$ *cm*. Pressure, magnetic field and discharge voltage is held constant at 10^{-4} *mbar*, *1090 G* and - *90V* respectively.

The method of excitation and detection of plasma oscillation using the two stream instability is described in much greater detail in chapter 6 of this thesis. Excitation of plasma oscillation using a weak electron beam and detection of oscillation frequency also serves as a diagnostics to cross verify the density measurement of Langmuir probe.

3.4 Summary

A linear magnetized plasma device has been designed and fabricated in-house at the Institute for Plasma Research for carrying out extensive experimentation on plasma waves and instabilities. The device is built in two stages initially a prototype has been developed and this has been followed by the fabrication and installation of the final version of the device. The device consists of a multi-filament plasma source placed in the low magnetic field region connected to a main chamber having uniform magnetic field through a transition magnetic field region. The multifilament can produce plasma of a number of ion species like helium, argon, neon, krypton, and xenon and their different combinations. The axial profile of the magnetic field can be tailored to obtain many different configurations by feeding current to the coils independently. These independent variations of magnetic fields in the source, extension, and main chamber enable the machine operation with different mirror ($R_m = B_{main}/B_{source}$) ratio configurations. Furthermore, this machine is designed for accommodating many plasma sources and the present plasma source can easily be replaced by other sources such as duoplasmatron [53], microwave source [61], and oxide coated cathode [76], it can also be converted into a Q-machine if the need arises. A number of diagnostics have been developed for the characterizing the plasma and carrying out the wave experiments. A low noise Langmuir probe system has been developed for measuring time resolved density and temperature. A code has been written in MATLAB® for efficiently processing the single Langmuir probe I-V trace over a wide operating range for determining the plasma parameters. A set of rack probes for measuring density and potential fluctuations in the plasma has been developed. Excitation and detection system for ion acoustic wave and plasma oscillation have been developed and tested for the proposed wave experiments. Thus it can be concluded that a versatile linear magnetized plasma device along with a wide array of diagnostics have been developed for experimental study of waves and instabilities in a magnetized plasma.

Chapter 4 Plasma Characteristics

The versatility of a linear plasma device especially designed for plasma wave studies lies in its ability to produce various plasmas over a wide parameter range in order to accommodate several experiments. For example, availability of a wide range of plasma density over a wide range of pressure and external magnetic field facilitates several different experimental studies by having different collision frequencies, cyclotron frequencies, etc. In this chapter the variation of plasma density and temperature with controlling features is presented. In section 4.1 the plasma characteristics of Magnetized Linear Plasma Device (MLPD) is presented and the importance of results of MLPD in the design of Inverse Mirror Plasma Experimental Device (IMPED) has been stressed. The plasma characteristics of IMPED is described in section 4.2. A four order density variation and temperature variation of 6 times have been achieved in IMPED using different control features. All these control features and their effectiveness has been discussed in detail in in section 4.2.1. The pulsed discharge option of IMPED has been described in section 4.2.2. This is followed by summary in section 4.3.

4.1 MLPD Plasma

The variation of plasma density with different control parameters is studied with Langmuir probe. A planar probe of radius 3 mm and a cylindrical probe of radius 0.5 mm and length 5 mm have been used to make the measurements. The probes were always oriented perpendicular to the magnetic field. The base pressure of the system is $1 \times 10^{-5}\ mbar$ and system is purged with argon gas a number of times before striking the discharge. Steady state argon plasmas were produced in MLPD and its characteristics are presented below.

Figure 4.1 shows the variation of density with pressure in MLPD measured at z = 32 cm and r = 0 cm. The axial magnetic field in the main chamber is maintained at 95 G, the discharge voltage is fixed – 80 V and filament heating current is $\sim 2\,A$. The density varied from $1.1 \times 10^{11}\ cm^{-3}$ to $1.8 \times 10^{10}\ cm^{-3}$ on decreasing pressure from $9 \times 10^{-4}\ mbar$ to $5 \times 10^{-5}\ mbar$.

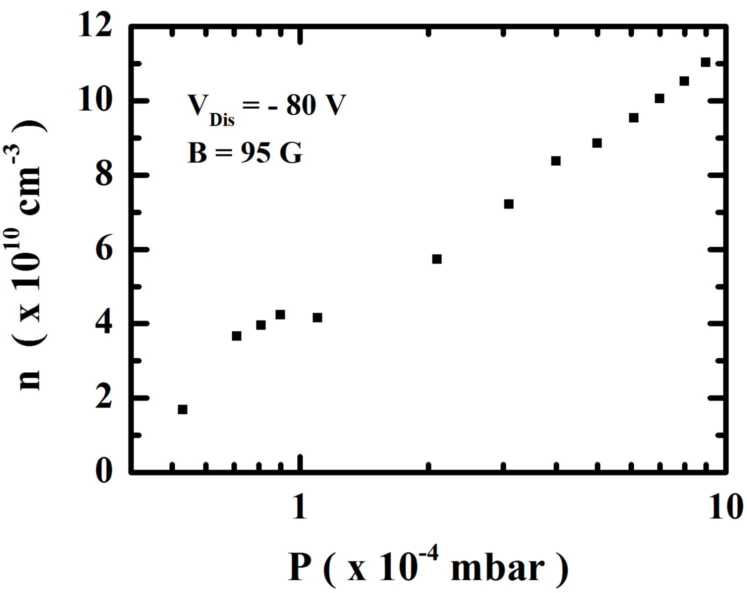

Figure 4.1 : Variation of Plasma density with pressure in the main chamber of MLPD at *z = 32 cm* and *r = 0 cm*. V_{Dis} and B_{main} are held constant at *-80 V* and *95 G* magnetic field.

The experimental study of the variation of plasma density with pressure shows that the lowest of operating pressure of MLPD is $\sim 5 \times 10^{-5}\ mbar$. This gives an insight on the motion of charge particles in the source and the main chamber. The ionization length [129] of an 85 eV electron at $5 \times 10^{-5}\ mbar$ is $20.6\ m$ which is much larger than the system length. Thus in order to ionize the gas the primary electrons emerging from the heated filaments will have to suffer multiple reflections between the end flange of the source chamber and the magnetic mirror at the interface of the source and the main chamber, such that the path traversed by the electrons is greater than or equal to the ionization length before finally escaping into the wall of the source or the main chamber. Figure 4.1 is also an important result from the design point of view of IMPED. One of the differences between MLPD and other linear plasma devices [40, 80] is that, in other devices cusp confinement in the source chamber is present both curved surface and on the flat surface parallel to the axial source flange while in MLPD cusp confinement is only limited to the axial source flange. There is no cusp confinement on the curved surface. Successful production of plasma at low operating pressures in MLPD shows that cusp confinement on the curved surface is not necessary for production of plasma at low operating pressures using multifilament plasma source. The axial magnetic field near the filament due to solenoid magnets surrounding the main chamber is enough to confine the ionizing electrons radially in the source chamber for plasma production in the device at low operating pressures. This is an important result as it leads to significant reduction in production costs and also enables the user to access a greater density range experimentally as will be shown later in section 4.2.1.4.

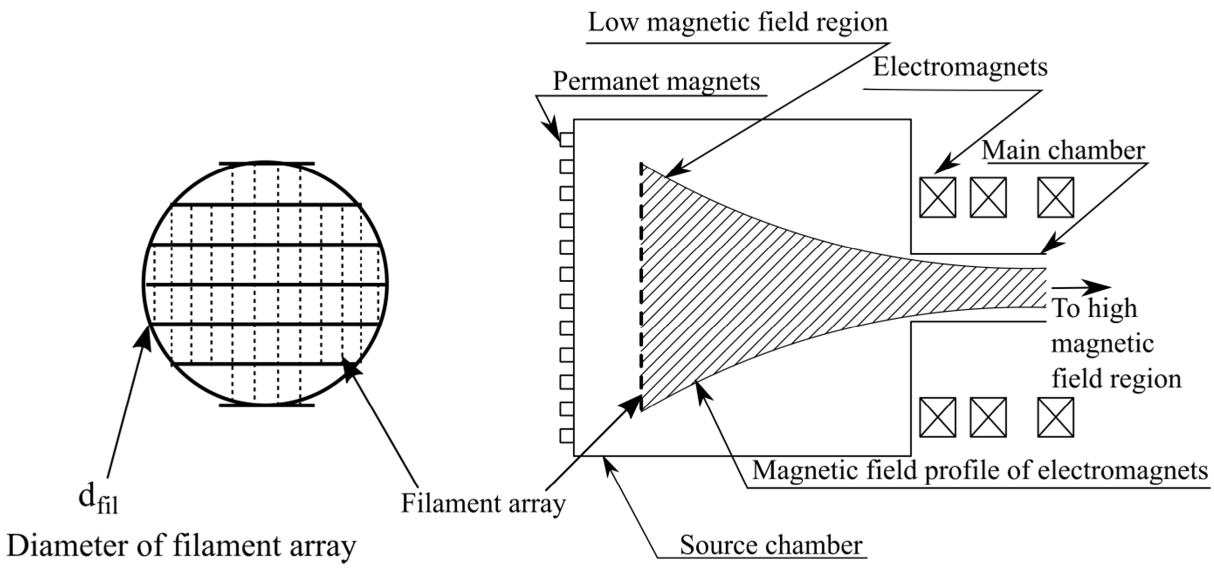

Figure 4.2 : Schematic of the multifilament cathode on the left and its location in the source chamber in the fringing field of the solenoid magnet surrounding the main chamber.

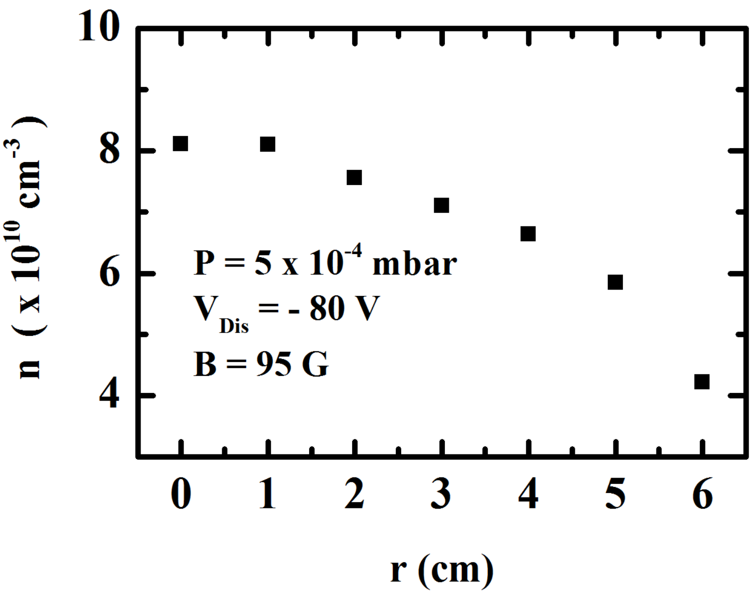

Figure 4.3: Radial variation of density at $z = 32\ cm$. $B_{main} = 95\ G$, $V_{Dis} = -\ 80\ V$ and $P = 5 \times 10^{-4}\ mbar$

The plasma produced is radially uniform. Figure 4.3 shows the radial variation of density in the main chamber at z = 32 cm at $5 \times 10^{-4}\ mbar$, V_{Dis} = -80 V and 96 G magnetic field. The plasma density decreases to 80% of its peaks value at r ~ 4 cm. The diameter of the uniform plasma in the main chamber may be related to the diameter of the filament area by the conservation of particles along flux lines, as the plasma is expected to diffuse along the magnetic field lines from the source to main chamber (refer Figure 4.2).

From the conservation of particles along magnetic flux lines one may write,

$$B_{source} \times A_{source} \approx B_{main} \times A_{main} \tag{4.1}$$

$$\therefore\ d_{main} \approx \sqrt{\frac{B_{source} \times d_{fil}^2}{B_{main}}}$$

$$d_{main} \approx \sqrt{\frac{26 \times 15.6 \times 15.6}{95}} = 8.2\ cm \tag{4.2}$$

The estimated value of the uniform diameter using the conservation of particles along flux lines principle, matches very well with the experimental result as shown in Figure 4.3. From this it can be concluded that the net motion of the electrons and ions are primarily in the axial direction along the magnetic field lines.

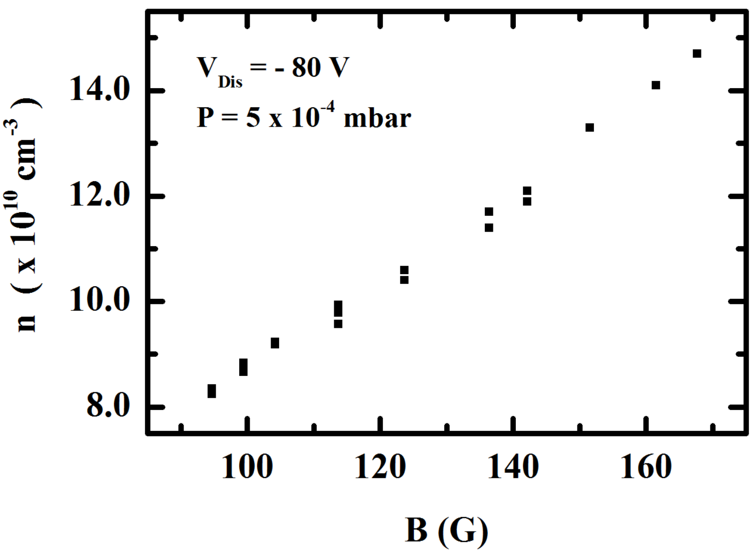

Figure 4.4 : Variation of density with magnetic field in the main chamber at $z = 32\ cm$ and $r = 0\ cm$. Pressure and discharge voltage are held constant at $5{\times}10^{-4}$ *mbar* and *-80 V* respectively.

Considering that magnetic field is one of the controlling parameters for varying density in a magnetized plasma device. The variation of density with magnetic field is studied as shown in Figure 4.4. The magnetic field is changed from 95 G to 168 G in main chamber and the density was found to increase from $8 \times 10^{10}\ cm^{-3}$ to ~ $1.5 \times 10^{11}\ cm^{-3}$ at – 80 V discharge voltage and $5 \times 10^{-4}\ mbar$ operating pressure.

With the experience gained in the experiments conducted in MLPD, the designs of IMPED was finalized. In section below the plasma characteristics of IMPED is presented.

4.2 IMPED Plasma

Both steady state and afterglow plasma can be produced in the IMPED. The variations of plasma density and temperature with different control parameters such as pressure, magnetic field magnitude and profiles, and bias voltages have been characterized to explore the suitability of IMPED for wave studies. The base pressure of the system is $2 \times 10^{-6}\ mbar$, the system was purged with dry argon a number of times before commencing argon plasma production. Cylindrical Langmuir probes of dimensions $l_p = 6\ mm$ and $r_p = 0.5\ mm$, and $l_p = 4\ mm$ and $r_p = 0.25\ mm$ have been used to measure the plasma density and temperature. The Langmuir probe is oriented perpendicular to the magnetic field. All measurements are carried out in the main chamber unless otherwise stated specifically.

4.2.1 Steady State Plasma

4.2.1.1 Variation of density and temperature with pressure and magnetic field

The plasma density in IMPED can be varied by varying the operating pressure, discharge voltage, magnitude of axial magnetic field. In the first set of experiments, the plasma densities in the range of $\sim 10^{10} - 10^{11}\ cm^{-3}$ has been obtained by varying the argon fill-pressure from $\sim 8 \times 10^{-4}$ to $1.7 \times 10^{-5}\ mbar$, keeping the discharge voltage at −90 V, the mirror ratio, R_m = 49.5 with B_{main} = 1090 G, and filament current 2 A. As shown in Figure 4.5, a variation of plasma density ∼20 times is observed in the above mentioned pressure range. The plasma density did not vary substantially when the discharge voltage is varied from −50 V to −90 V, keeping the fill-pressure, B_{main}, and R_m constant at 1×10^{-4} mbar, 1090 G, and 49.5, respectively.

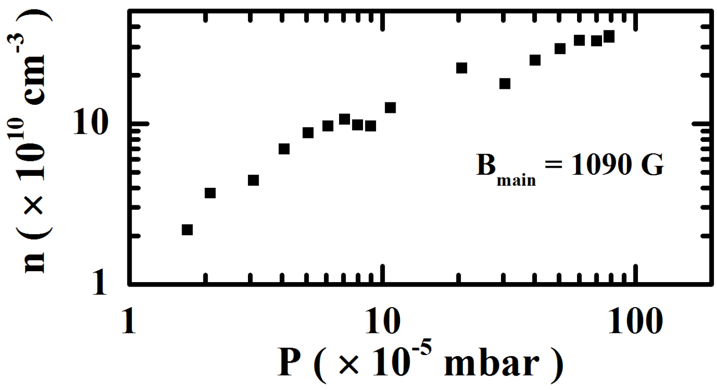

Figure 4.5 : Variation of density with pressure at constant magnetic field. Measurements were made at V_{Dis} = *- 90 V*, R_m = *49.5*, *z = 32 cm* and *r = 0 cm*

The plasma density in IMPED can also be varied at fixed fill-pressure by varying the source and main chamber magnetic fields keeping mirror ratio, R_m, constant at 49.5 and discharge voltage fixed at −90 V. The plasma density decreases by a factor of ~20 with decreasing the axial magnetic field strength in the main chamber from 1090 G to 109 G and proportionally decreasing B_{source} to keep R_m constant as shown in the Figure 4.6. The decrease in magnetic field strength in both source and main chamber reduces the confinement in both the chambers which cause the density to decrease in both main and source chambers.

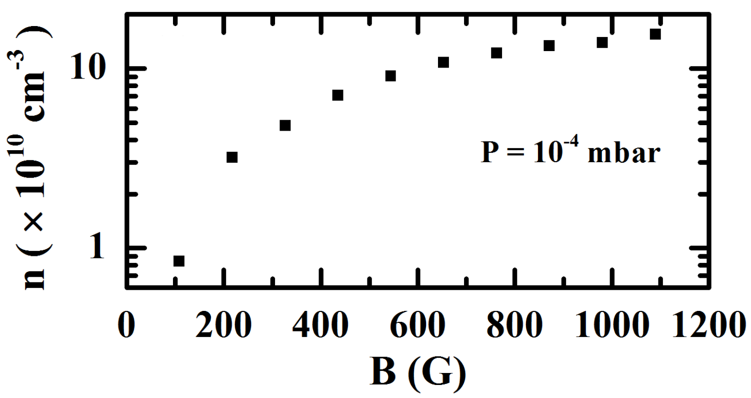

Figure 4.6 : Variation of density with magnetic field at constant pressure. Measurements were made at V_{Dis} = *- 90 V*, R_m = *49.5*, *z = 32 cm* and *r = 0 cm*.

Unlike density, the minimal temperature variations in the main chamber are observed, varying only from 4.5 to 2 eV, over the entire filling pressure range of $2 \times 10^{-5}\ mbar - 8 \times 10^{-4}\ mbar$ as shown in Figure 4.7(a). The decrease in temperature with increase in pressure may be attributed to the increase in collisions with pressure. Marginal decrease in temperatures has been observed from 3 to 2 eV with decrease in B_{main} from 1090 G to 218 G, keeping R_m and fill-pressure constant at 49.5 and 10^{-4} mbar respectively, as shown in Figure 4.7(b).

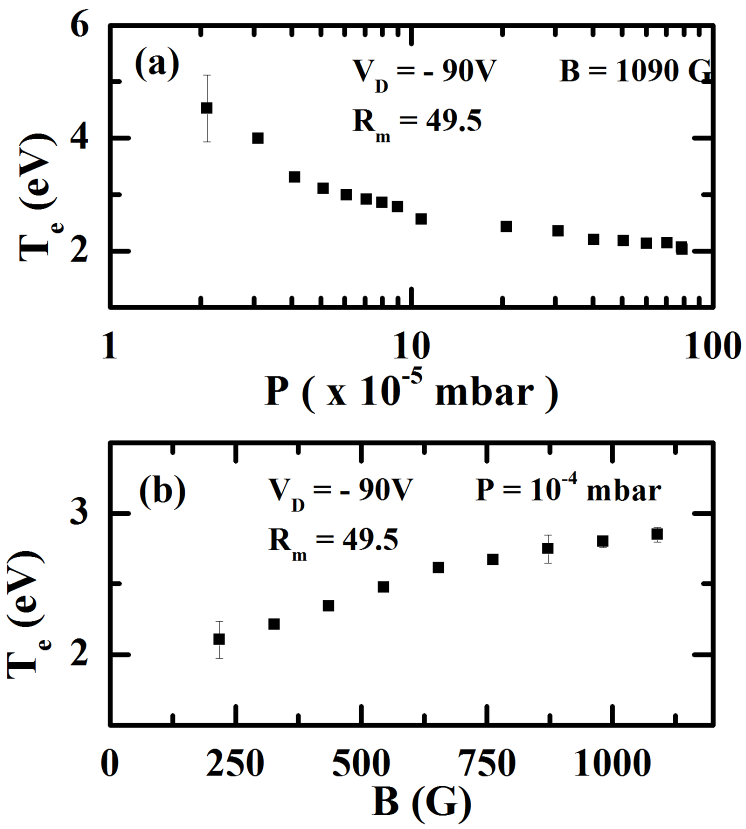

Figure 4.7: (a) Variation of temperature with pressure at constant magnetic field (b) Variation of temperature with magnetic field at constant pressure. Both measurements were made at V_{Dis} = - 90 V, R_m = 49.5, *z = 32 cm* and *r = 0 cm.*

4.2.1.2 *Variation of plasma parameters using a unique transition magnetic field*

IMPED provides another interesting option to vary the plasma density and temperature in the main chamber without altering the operating pressure and the magnitude of the magnetic field in the main chamber. The option involves changing plasma parameters by changing the mirror ratio, i.e., the ratio of magnetic field in the main chamber, (B_{main}), and the magnetic field in the source chamber (B_{source}). This can be done by changing current in the compensation and extension coils. This is the precisely the reason for which we designed to introduce these coils in the transition region. The mirror ratio can be changed by varying B_{source} keeping B_{main} constant or varying B_{main} keeping B_{source} constant or by varying both B_{source} and B_{main}. In first case we vary B_{source} keeping B_{main} constant and study its effect on plasma. Figure 4.8(a) shows the variation density on the axis of the main chamber at z = 32 cm on changing B_{source} from ~30 G to 2 G keeping B_{main}, fill-pressure, and V_{Dis} constant at 1090 G, 10^{-4} mbar, and −90 V respectively. The density is found to change by a factor of ~ 10. The cause of the reduction in density in the main chamber is investigated by considering the different effects associated with the decrease in B_{source} when B_{main} is held constant.

Decrease in B_{source} enhances the cross field diffusion in the source chamber as there is no cusp magnetic field confinement on the periphery of the source chamber, hence, decreasing the density in the source chamber. Furthermore, decreasing B_{source} and keeping the B_{main} constant lead to increase in the mirror ratio (R_m), which should in principle increase the confinement in the source extension chamber and the incremental reduction in density in the main chamber should be more than that in the source chamber extension. However, measurement of the density in the source chamber extension along with that in the main chamber revealed that density decreases in similar fashion in both the source and main chamber as shown in Figure 4.8(b). Therefore, in this case, the cross-field confinement plays an important role in controlling the density in the main chamber as compared to mirror effect [42, 39].

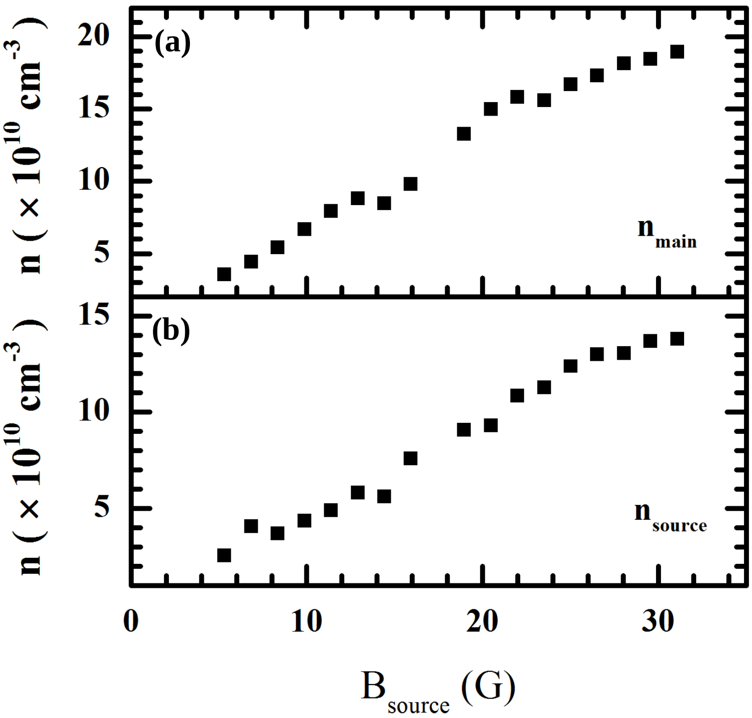

Figure 4.8: Variation of density with source magnetic field. (a) Measured at z = *32 cm* and r = *0 cm*. (b) Measured at z = *- 47.5 cm* and r = *0 cm*. Other parameters for both measurements are $P = 10^{-4}$ *mbar*, V_{Dis} = *- 90 V and* B_{main} = *1090 G*

In second case the magnetic field near the filaments is held constant while the magnetic field in the main chamber is reduced. This implies that on decreasing the magnetic field in the main chamber the mirror ratio will decrease as a result more particles will enter the main chamber easily along the field lines from the source. Also at the same time, the cross field diffusion will increase in the main chamber. The former process will increase the density in the main chamber while the later will decrease the density in the main chamber. Hence depending on which process is dominant the density in the main chamber will change.

With reference to Figure 4.9 the magnetic field in the source was held constant at 22G while the magnetic field in the main chamber was decreased from 1090G to ~ 200 G. The ion saturation current initially increased in the main chamber with decrease in magnetic field till 872G, indicating mirror effect is dominant. But as the magnetic field is reduced below 872G, the loss due to cross field diffusion in the main chamber dominates. As a result the ion saturation current in the main chamber decreases. The langmuir probe used in the measurement is located at z = 152.5 cm and r = 0 cm. Thus it may be concluded the density observed in the main chamber is a cumulative of the two effects, the mirror effect and cross-field diffusion in the main chamber.

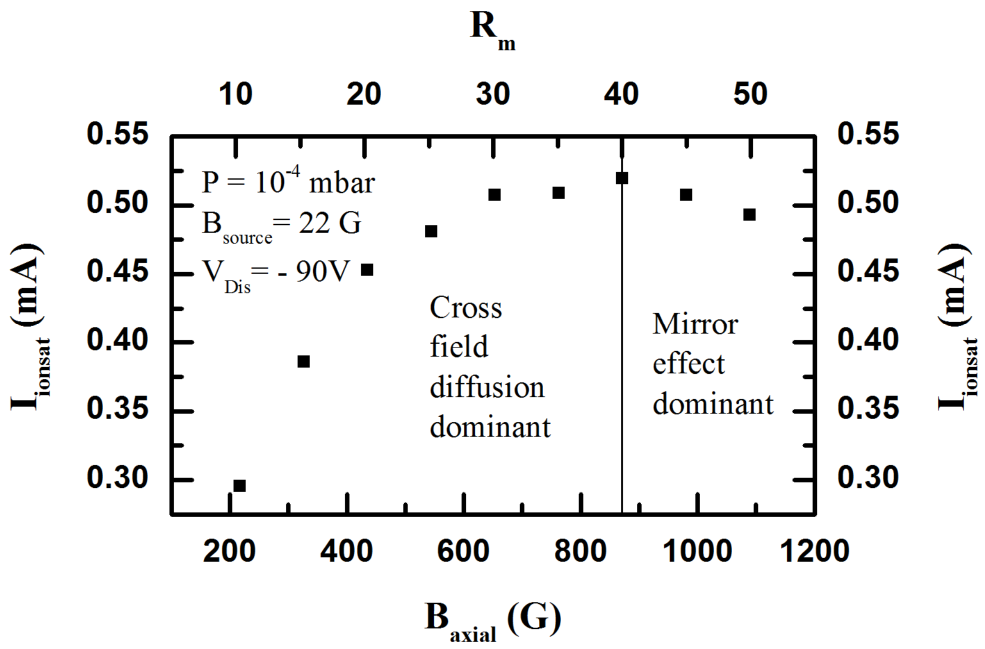

Figure 4.9: Variation of density in the main chamber with mirror ratio. Mirror ratio is changed by varying B_{main} holding B_{source} constant at *22 G*. Measurements carried out at V_{Dis} = *-90V*, $P = 10^{-4}$ *mbar, z = 152.5 cm* and *r = 0 cm.*

Thus it is observed that changing the magnetic field in the source chamber and holding the magnetic field in the main chamber is an effective tool for variation of density in the main chamber. A density variation of one order is observed. But unlike density, temperature shows small variation with mirror ratio. Variations within a factor of 2 are observed when B_{source} is reduced from 31 G to 5 G keeping B_{main} and pressure constant at 1090 G and 10^{-4} $mbar$

respectively (Figure 4.10). Similar variation of temperature on decreasing B_{source} and holding B_{main} constant at $1090\,G$ is also observed at other operating pressures $6 \times 10^{-4}\ mbar$ and $6 \times 10^{-5}\ mbar$ as shown in Figure 4.10b.

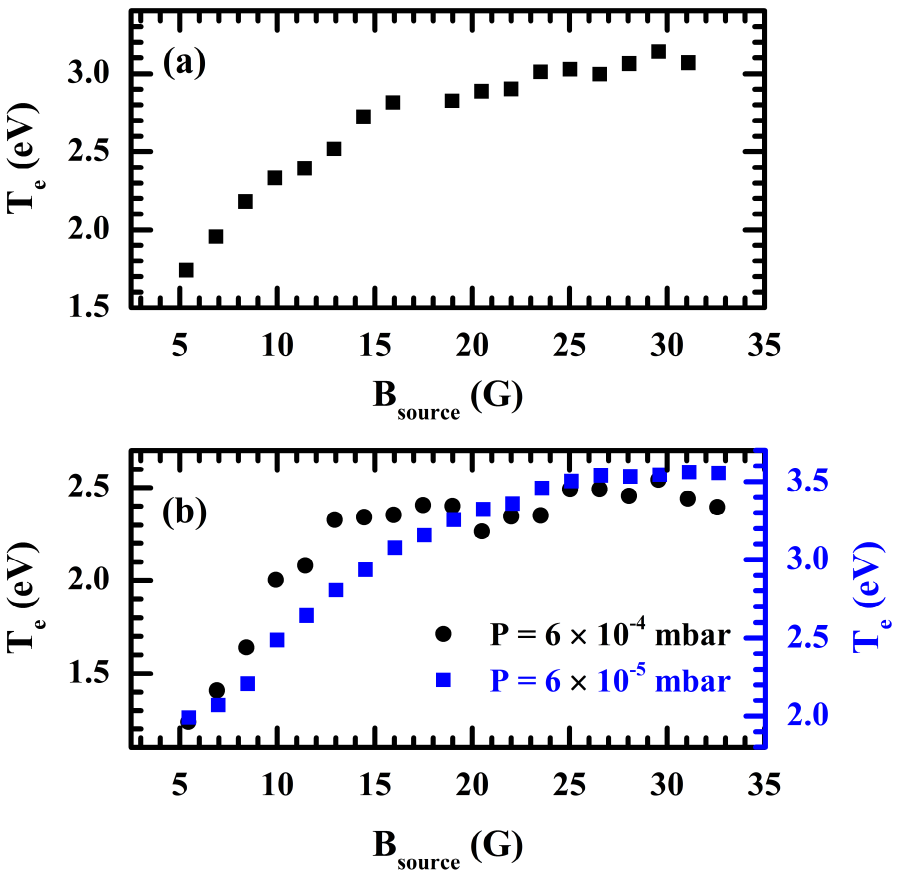

Figure 4.10: Variation of temperature on the axis of the main chamber at $z = 32\ cm$ when B_{source} is decreased holding B_{main} constant at *1090 G*. (a) Pressure held constant at $10^{-4}\ mbar$ (b) Pressure held constant at $6{\times}10^{-4}\ mbar$ and $6{\times}10^{-5}\ mbar$. For both measurement V_{Dis} is fixed at – *90 V*.

Thus it can be concluded that the variable transition magnetic field between the plasma source and main chamber along with no cusp confinement on the curved surface of the source chamber increases the range of densities and temperature that can be accessed for experimental purpose for a given operating pressure and magnetic field in the main chamber.

Density as low as $4 \times 10^9\ cm^{-3}$ is obtained in the main chamber under the condition of fill-pressures $5 \times 10^{-5}\ mbar$, $V_{Dis} = -60\ V$, $B_{main} = 1090\ G$, and keeping magnetic field near the source to a minimum (~1 G) by feeding compensation with currents in the opposite direction. On the other hand, a high density of $\sim 2 \times 10^{12}\ cm^{-3}$ is obtained at $9 \times 10^{-4}\ mbar$ fill-pressures, $-90\ V$ discharge voltage, and 1090 G magnetic field in the main chamber by increasing the filament heating current.

4.2.1.3 Axial and radial variation of plasma parameters

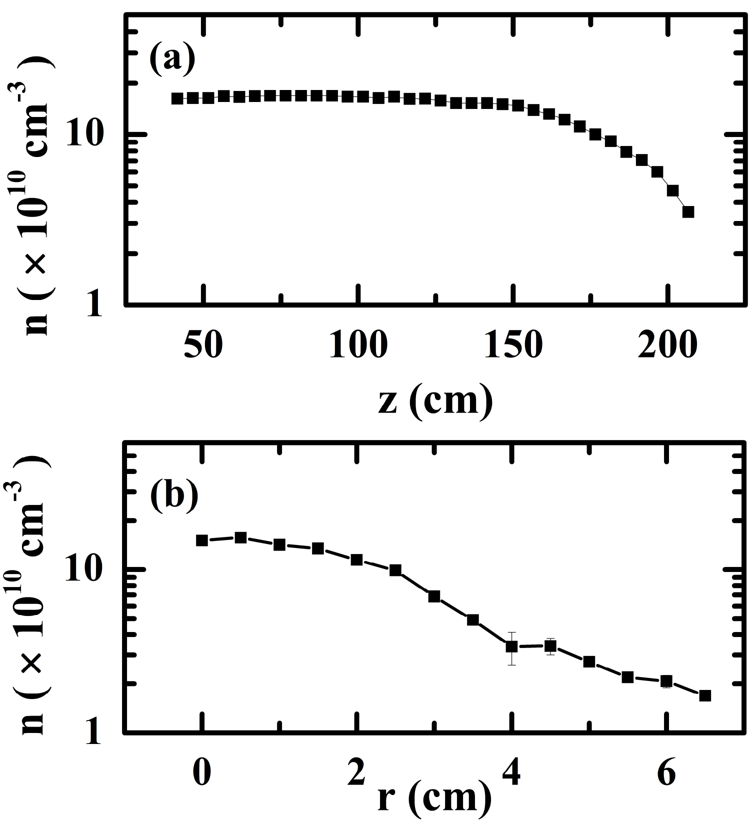

Figure 4.11: (a) Axial variation of density (b) Radial variation of density at *z =32 cm*. Both measurements were made at $P = 10^{-4}\ mbar$, $V_{Dis} = -90\ V$, $B_m = 1090\ G$ and $R_m = 49.5$.

The plasma produced is axially uniform. Figure 4.11 (a) shows the axial variation of plasma density at 10^{-4} mbar pressure, - 90V discharge voltage, 1090 G magnetic field in the main chamber and R_m = 49.5 . The uniform density region is seen to correspond to the flat top magnetic field region in the main chamber. The plasma in the main chamber is also radially uniform. The radial variation of plasma density at z = 32 cm is shown Figure 4.11(b). Thus it can be concluded that the uniform plasma required for the wave experiments as per design requirements has been achieved experimentally in IMPED.

4.2.1.4 Variation of plasma parameters using a mesh

Experiments with a mesh in between two chambers have been a common feature of double plasma devices [74] designed for wave studies. A time varying potential can be applied to the grid to excite waves or one may introduce a beam in the target chamber by biasing the grid. A mesh may also be used to alter the plasma parameters in a plasma device. For example Mackenzie et al. [130] observed that a positively biased grid consisting of $0.025\,mm$ diameter tungsten wires separated by $3\,mm$ raised the temperature of an argon plasma from $T_e = 0.5\,eV$ to almost $4\,eV$. The reason for the increase in temperature was ascribed to the selective absorption of low-energy electrons by the biased grid. The biased grid acted as an angular momentum trap from which the higher energy electrons escape but low energy electrons are absorbed. Considering the obvious advantages of a grid, facilities were made in IMPED for attaching an isolated grid that can used to alter the plasma parameters.

In order to study the effect of mesh on plasma parameters in IMPED an isolated mesh is attached between the source and source extension chamber in the IMPED as shown in the Figure 4.12. The mesh can be grounded or biased externally as per requirement of the experiment. The mesh used is of plane weave type; it has 61 lines per inch and is made of $0.15\,mm$ diameter stainless steel (SS 316) wire.

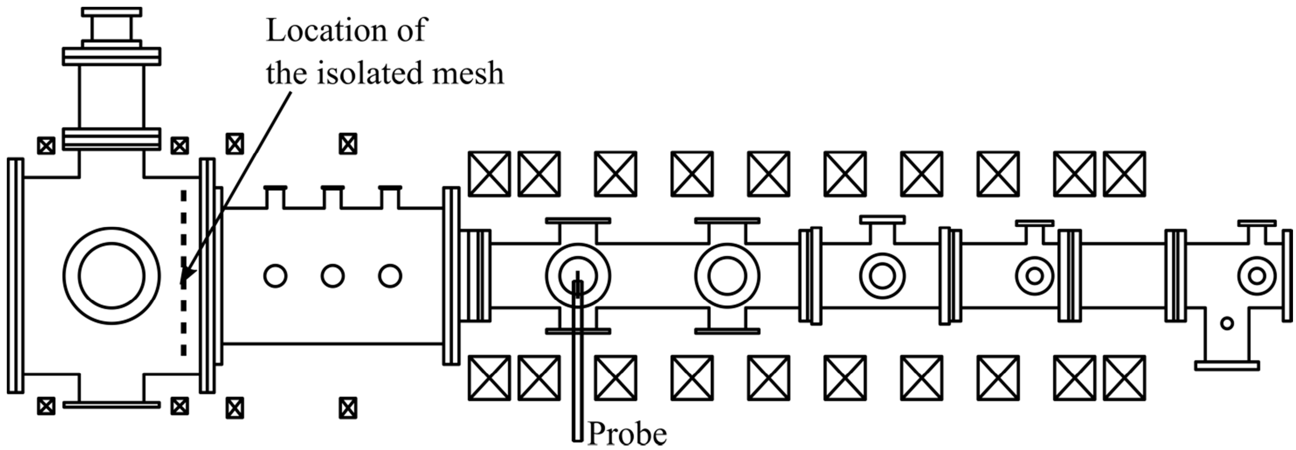

Figure 4.12: Schematic of IMPED showing the location of the isolated mesh and the probe used to make the measurements in the main chamber.

In the first set of experiments the mesh is electrically connected to the ground and variation of plasma parameters with different control features have been studied. A variation of plasma densities in the range of $\sim 1.2 \times 10^{11}$ to $3 \times 10^{9}\ cm^{-3}$ has been obtained by varying the argon fill-pressure from $\sim 7.3 \times 10^{-4}$ to $3 \times 10^{-5}\ mbar$, keeping the discharge voltage at − 90 V, the mirror ratio, R_m = 49.5 with $B_{main} = 1090\ G$, and filament current ~ 2 A. As shown in Figure 4.13a, a variation of plasma density ~ 40 times is observed in the above mentioned pressure. A comparison without mesh (refer Figure 4.5) case shows that the presence of mesh decreases the density in the main chamber by a factor of ~ 10. This is because the grounded mesh acts as a sink for the plasma as a result it reduces the plasma density.

The variation of plasma density in IMPED with magnetic field is studied by changing the source and main chamber magnetic fields keeping mirror ratio (R_m) constant at 49.5 at fixed fill-pressure and discharge voltage fixed at − 90 V. The plasma density decreases by ~ 6 times with decreasing the axial magnetic field strength in the main chamber from 1090 G to 109 G and proportionally decreasing B_{source} to keep R_m constant as shown in the Figure 4.13(b). On comparing the density in the main chamber in the presence of mesh to case when the mesh was not attached between the source and the source chamber extension, a decrease in density by one order at 1090 G is observed.

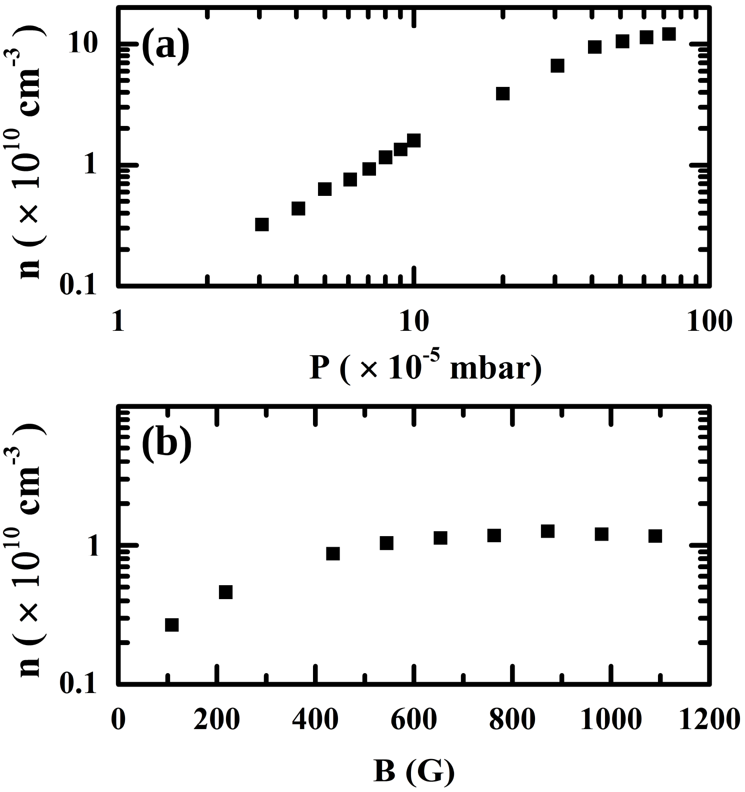

Figure 4.13(a) Variation of plasma density with pressure when B_{main} = *1090 G* (b) Variation of plasma density with values of axial magnetic field in the main chamber at 10^{-4} *mbar* . Both measurements are made at *r = 0 cm, z = 32 cm,* V_{Dis} = *- 90V* and R_m = *49.5*.

As observed in the experiments without mesh the temperature variation with pressure and magnetic field is minimal. The temperature changed by a factor of 2 from $\sim 1.2\ eV$ to $2.6\ eV$ when the pressure is decreased from $7.3 \times 10^{-4}\ mbar$ to $3 \times 10^{-5}\ mbar$ at fixed $B_{main} = 1090\ G$, $R_m = 49.5$ and $V_{Dis} = -90\ V$. The temperature variation with pressure is shown in Figure 4.14a. Similar change in temperature by a factor of 2 from $1.7\ eV$ to $0.8\ eV$ is observed when the magnetic field is decreased at a constant $R_m(= 49.5)$ from $1090\ G$ to $109\ G$ as shown in Figure 4.14b. The pressure is held constant at $10^{-4}\ mbar$ and discharge voltage is fixed at $-90\ V$ during the temperature measurement.

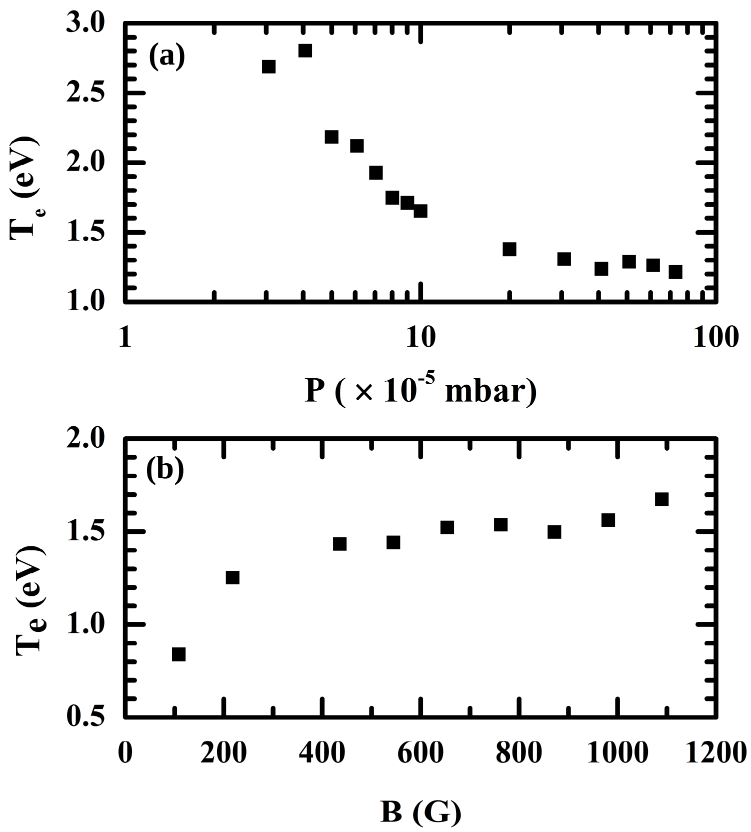

Figure 4.14: (a) Variation of plasma temperature with pressure when B_{main} = *1090 G* (b) Variation of plasma temperature with values of axial magnetic field in the main chamber at 10^{-4} *mbar*. Both measurements are made at *r = 0 cm*, *z = 32 cm*, V_{Dis} = *- 90 V* and R_m = *49.5*.

A comparison of the plasma temperature in the main chamber in the absence and the presence of mesh show that the temperature in the main chamber is consistently less in the presence of mesh. The reason for the reduction in temperature of the electrons may be due to loss of confinement in the presence of the grounded mesh. In order to confirm this reason, an experiment is conducted to improve the confinement of electrons using the mesh and observe its effect on the temperature. This is done by biasing the mesh negatively at $-\ 22\ V$ to ensure that it repels the plasma electrons impinging on it. Thus a negatively biased mesh is expected to improve the electrostatic confinement of electrons. The experimental results are shown in Figure 4.15. The plasma electron temperature increases from $1.2\ eV$ (mesh grounded) to $2.1\ eV$ when the mesh is given a $-22\ V$ negative bias supporting our argument that decrease in confinement is the cause of temperature reduction in the presence of grounded mesh. It may also be noted that the plasma temperature when mesh is biased negatively to $-22\ V$ is nearly equal to the plasma temperature measured at the same location without any mesh at the same operating pressure discharge voltage and magnetic field.

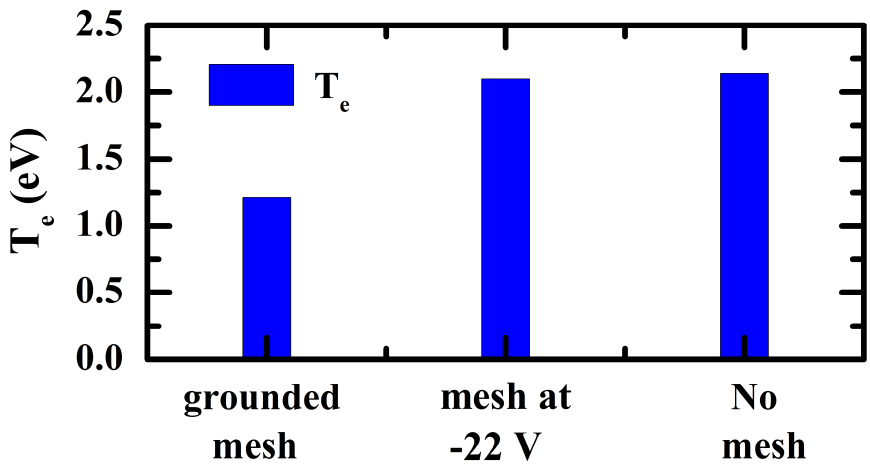

Figure 4.15: Plasma temperature in the presence of grounded mesh, mesh held at - *22 V* and without any mesh at $z = 32\ cm$, $r = 0\ cm$, $P = 7.3\times10^{-4}\ mbar$, $V_{Dis} = -90\ V$, $B_{main} = 1090\ G$ and $R_m = 49.5$.

4.2.2 After glow plasma

Inverse Mirror Plasma Experimental Device has the option for pulsed discharge to study waves in afterglow plasma. The option of afterglow plasma is particularly desirable as it enables the production of Maxwellian plasma. Within few tens of microseconds [40] of switching of the plasma source, the primary electrons are expected to be lost to the vessel wall leaving only the bulk plasma electrons. The characteristics of afterglow plasma are also of interest because it yields a measure for the particle confinement time [80], energy relaxation time and provides quiescent plasma. This is why we have implemented the option of afterglow plasma production in IMPED.

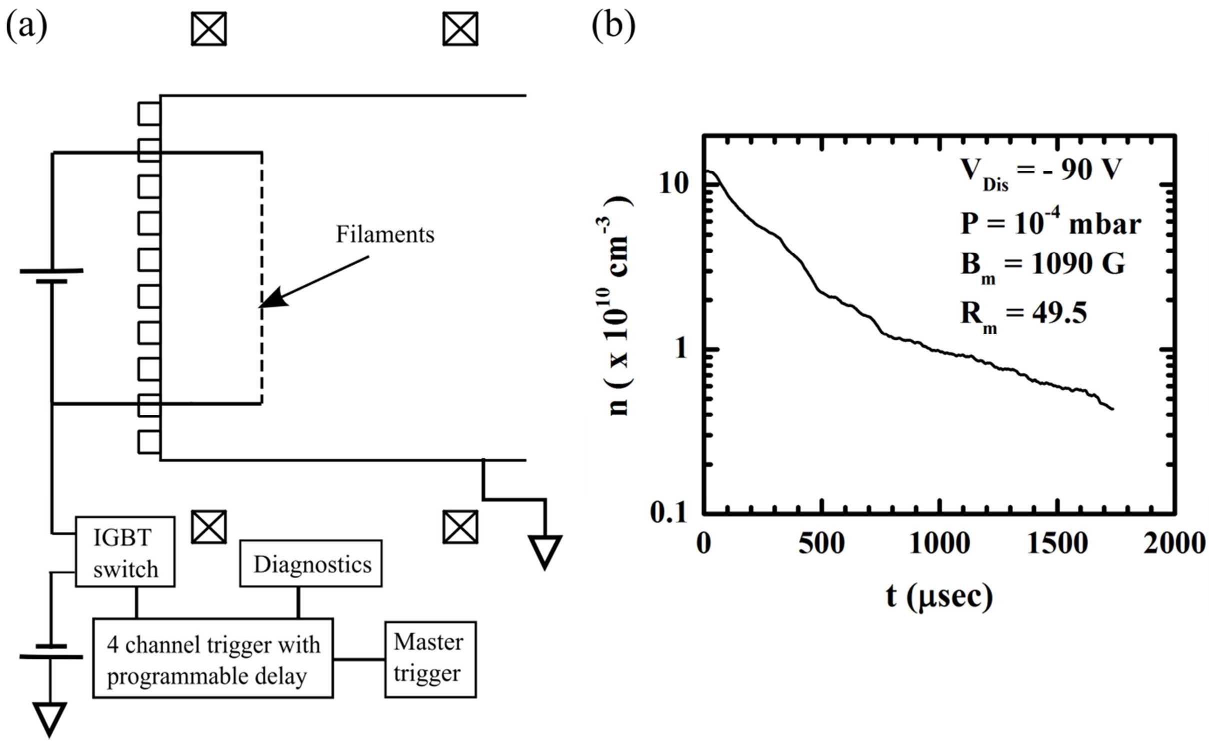

Figure 4.16: (a) Schematic of the afterglow circuit. (b) Density decay in afterglow at $z = 32$ cm, $r = 0$ cm. $V_{Dis} = -90$ V, $P = 10^{-4}$ $mbar$, $B_{main} = 1090$ G and $R_m = 49.5$.

The IMPED is operated in pulsed mode also by switching off the acceleration or discharge voltage of the multi-filamentary discharge. The circuit layout for the afterglow plasma experiment is shown in the Figure 4.16a. A master trigger is used to trigger a four channel trigger generator with programmable time delay. The output from the programmable trigger generator is used to switch off the IGBT and also to trigger the diagnostics. A Langmuir probe located in the main chamber at $r = 0$ cm and $z = 32$ cm is used for making the plasma density measurement. The variation of the plasma density with time is shown in the Figure 4.16b, discharge voltage is maintained at – 90V, magnetic field in the main chamber is maintained at 1090 G, $R_m = 49.5$ and the operating pressure is 10^{-4} $mbar$. The density decreases with time with an e-folding time of $336\,\mu sec$. This time is more than enough to carry out the planned phase mixing of nonlinear plasma oscillations experiment, as the phenomenon is expected to occur within $1\,\mu sec$.

4.3 Summary

The experimental results of MLPD and its contribution in designing of upgraded device IMPED have been described in this chapter, followed by plasma characterisation data of IMPED. A density variation of four orders $(10^9 - 10^{12}\ cm^{-3})$ has been experimentally achieved in IMPED using different control parameters, notably pressure, axial magnetic field, mirror ratio, mesh and filament heating current. Hence the initial target of realizing four order density variations for parametric wave studies has been met experimentally. The plasma temperature is varied from 0.8 eV to 5 eV using the above mentioned control features of IMPED. Thus the required range of temperature $(\,2 - 5\ eV)$ for the phase mixing experiment is satisfied. Out of all the controlling features used for varying the plasma parameters usage of the flexible transition magnetic field (mirror ratio) in the absence of cusp confinement in the curved surface of the source chamber is unique to IMPED. Its effectiveness in varying both density and temperature has been substantiated with experimental data and the cause of the variations of plasma parameters has also been experimentally established. The effectiveness of a mesh in altering plasma parameters in the downstream magnetized plasma has been experimentally explored. Probe measurements show that the plasma is radially and axially uniform. The axial uniformity extends $1.2\ m$ in the main chamber thus satisfying the uniform plasma requirement. In addition to producing argon plasmas, plasmas of other ion species like helium, neon, krypton, and xenon and their different combinations can also be produced in this device. Thus, it can be concluded that the entire requirement for wave studies in IMPED except quiescence have been experimentally satisfied.

Chapter 5 Production of quiescent plasma

This chapter describes the method used for production of quiescent plasma in Inverse Mirror Plasma Experimental Device (IMPED). The effectiveness of the method over a large operating range has been substantiated with experimental data. Considering that wave studies is the primary motivation for constructing IMPED, a brief study of the intrinsic instabilities in IMPED plasma have been carried out to ensure that the inherent instabilities in the plasma do not interfere with the proposed wave studies.

5.1 Quiescent plasma production in IMPED

The novel feature of IMPED is its capability to produce plasma with very low density fluctuations. It is quite well known that a plasma with a high degree of quiescence is a basic requirement for most research involving basic plasma physics. Since the phase mixing experiments primarily require an excitation of a controlled perturbation for studying the background ion response [13], low ambient noise (density fluctuation) is absolutely desired to maintain a good signal to noise ratio. This is also true for any wave experiment involving excitation of a controlled density perturbation and study of its propagation characteristics.

The quiescence of the plasma is estimated by measuring the fluctuations in the ion saturation current. The ion saturation current and its fluctuating component are acquired simultaneously in a 1 GHz oscilloscope (Tektronix). One million points are stored at 5 mega samples per second in both the channels. The quiescence, i.e., $\delta n/n$, is estimated from the ratio of the root mean square (rms) value of the fluctuating component and the mean value of ion saturation current. For a given fill-pressure, the density fluctuations are controlled by varying the mirror ratio($R_m = B_{main}/B_{source}$). The mirror ratio is altered by either by varying B_{source} or by varying B_{main} or by a combination of both.

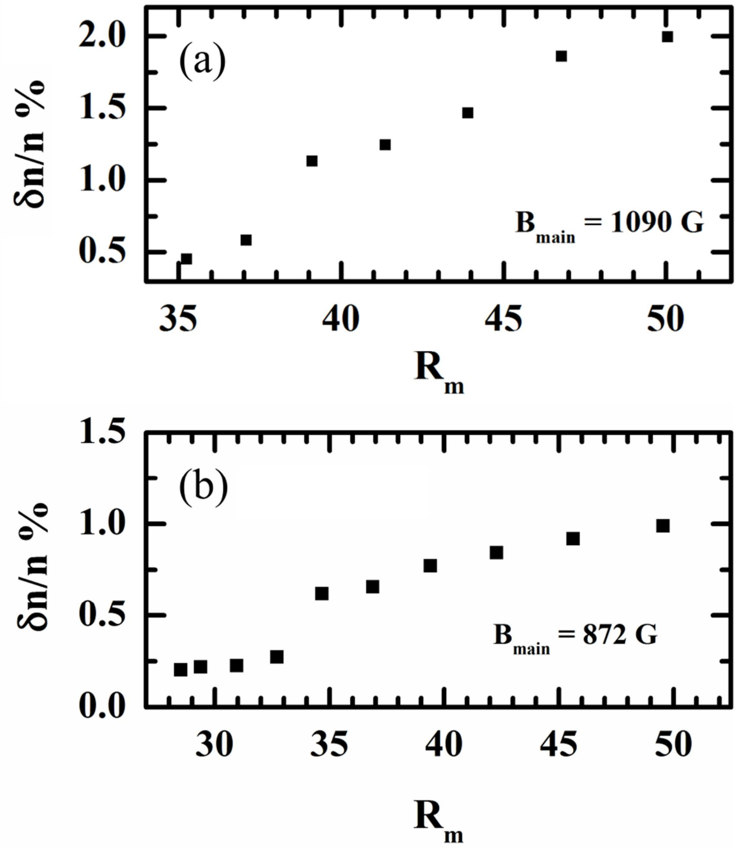

Figure 5.1: Variation of quiescence with mirror ratio in the uniform plasma region, (a) B_{main} held constant at *1090 G* while B_{source} is varied, fluctuations are measured at $r = 0\ cm$ and $z = 152.5\ cm$ (b) B_{main} held constant at *872 G* while B_{source} is varied, fluctuations are measured at $r = 0\ cm$ and $z = 110.4\ cm$. Discharge voltage and operating pressure are maintained at *– 90 V* and 10^{-4} *mbar* respectively.

The variation of quiescence with mirror ratio (R_m) is plotted in Figure 5.1a and Figure 5.1b at fill-pressure $10^{-4}\ mbar$ and $V_{Dis} = -90V$. In Figure 5.1a, the mirror ratio is varied by varying B_{source} from 22 G to 31 G keeping B_{main} constant at 1090 G, whereas in Figure 5.1b, the mirror ratio is varied by changing B_{source} from 17.6 G to 30 G keeping B_{main}

constant at $872\ G$. Plasma with very low density fluctuation, $\delta n/n \sim 0.2\%$ is observed at $B_{main} = 872\ G$ and $B_{source} = 30\ G$.

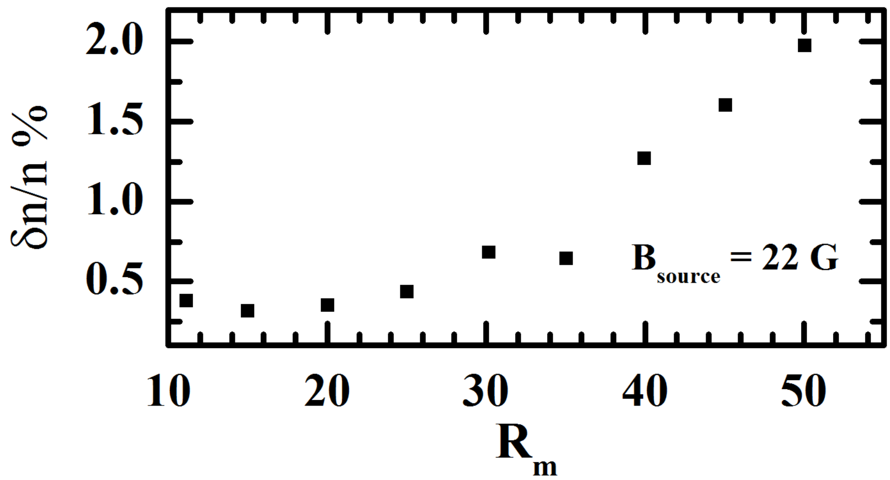

Figure 5.2: Variation of quiescence with mirror ratio at *r=0 cm* and *z=152.5 cm*. Mirror ratio is changed by varying B_{main} holding B_{source} constant at *22 G*. Discharge voltage is maintained at *– 90 V* and fill pressure of argon is maintained at 10^{-4} *mbar*.

The effectiveness of controlling plasma quiescence by varying B_{main} holding B_{source} constant is shown in Figure 5.2. B_{source} is kept constant at 22 G and B_{main} is varied. Quiescence values of as low as $\sim 0.3\%$ have been achieved at a mirror ratio, $R_m \sim 15$, keeping B_{source} constant at 22 G. Thus, it is observed that low mirror operation of IMPED leads to the maintenance of quiescence $\delta n/n\ \leq 1\%$ over a broad span of magnetic field values in the main chamber and hence over a wide range of density.

Considering that, along with magnetic field, the plasma density varies over a wide range with change in pressure, the effectiveness of low mirror ratio operation in producing quiescent plasma for different operating pressures is studied experimentally. The operating pressure is varied from $8 \times 10^{-4}\ mbar$ to $3 \times 10^{-5}\ mbar$ at $-\ 90\ V$ discharge voltage for two values of B_{main}. Figure 5.3a shows the variation of quiescence with pressure for $R_m = 49.5$ and

$R_m = 37$, when the magnetic field in the main chamber is held constant at $1090\ G$. Figure 5.3b shows the variation of quiescence with pressure for three mirror ratio's 49.5, 37 and 29.3 at a fixed $B_{main} = 872\ G$. The density fluctuations are found to decrease with increase in pressure as a whole and the level of density fluctuations for any given pressure is less at lower mirror ratios. However, the decrease in density fluctuation is not monotonic with pressure, there is a local increase in density fluctuation at $\sim 5 \times 10^{-4}\ mbar$ when the magnetic field in the main chamber is maintained at $872\ G$.

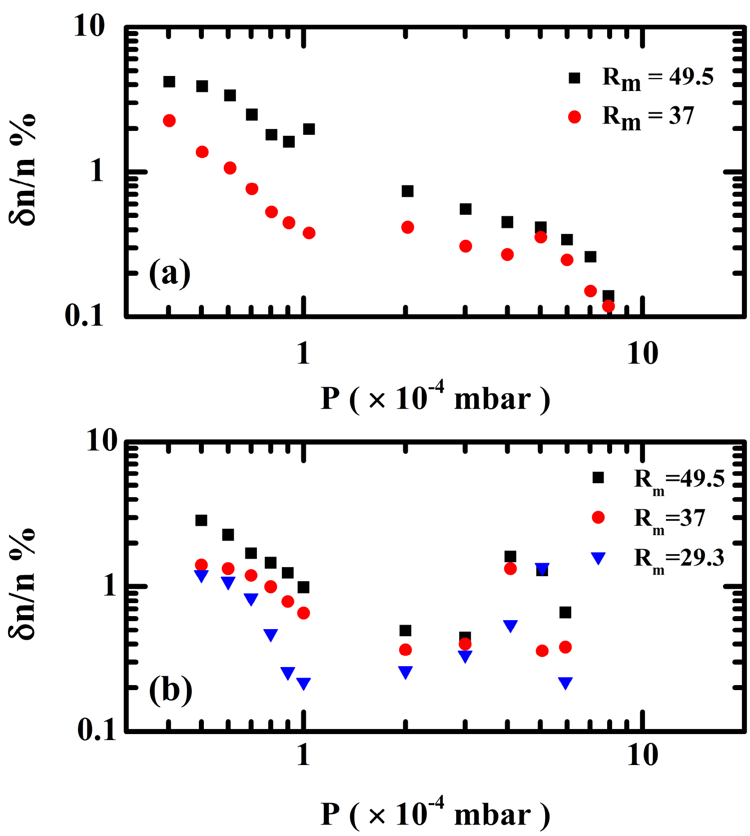

Figure 5.3: Variation of quiescence with pressure for different mirror ratios; (a) B_{main} is held constant at 1090 G and measurements are carried out at *r=0 cm* and *z=152.5 cm* (b) B_{main} is held constant at *872 G* and measurements are carried out at *r=0 cm* and *z=110.4 cm*. Discharge voltage for both measurements is maintained at - *90 V*.

Thus, it is observed that low mirror ratio operation of IMPED leads to the production of quiescent plasma with $\delta n/n \lesssim 1\%$ for wide range of pressure and magnetic field, satisfying the low density fluctuation criteria over a wide operating range required for wave studies. However, to get a glimpse of the intrinsic instabilities in IMPED a radial variation of the density fluctuation spectrum is studied.

5.2 Intrinsic instabilities in IMPED plasma

A magnetized plasma column may support a number of unstable modes which may give rise to fluctuations in density. A pressure gradient perpendicular to a magnetic field may give rise to drift waves. In a cylindrical magnetized plasma column where there is a radial density gradient transverse to the axial magnetic field, the propagation of the drift wave is mainly azimuthal with an axial component (finite $k_{||}$). In addition to drift wave (DW) instability, fluctuations in a magnetized plasma may also occur due to Rayleigh-Taylor instability and Kelvin-Helmholtz instability.

Rayleigh-Taylor or gravitational instability in hydrodynamics occurs when a heavy fluid is supported by a light fluid. The equilibrium here is unstable and any perturbation at the interface between both the fluids triggers the instability. The heavier fluid is displaced downward while the lighter fluid is displaced upward. In plasma device gravity may not be of major importance. However, in plasma devices with curved magnetic fields, the centrifugal force acting on the plasma due to particle motion along the curved magnetic lines of forces acts as an effective “gravitational” force. In a cylindrical linear magnetized plasma device, plasma rotation can be induced by a radial electric field, which may act as an effective gravity. This can trigger the instability when the central dense plasma column rotates at least as fast as the external less dense layer [131]. Unlike drift waves, Rayleigh-Taylor (RT) fluctuations are purely azimuthal and have $k_{||} = 0$. Fluctuations due to RT instability is characterized [131] by $max\left|\frac{e\tilde{\phi}}{k_B T_e}\right| \approx 1$ and $max\left|\frac{e\tilde{\phi}/k_B T_e}{\tilde{n}/n}\right| \geq 1$. Location of the maximum fluctuations due to RT instability is at $max\left|\frac{1}{n}\frac{dn}{dr}\right|$.

Kelvin-Helmholtz (KH) instability [132, 133] in hydrodynamics occurs when there is velocity shear between layers of fluid flowing relative to each other. In a linear cylindrical plasma column with a uniform axial magnetic field and non-uniform radial electric field, plasma rotates non-uniformly due to $\vec{E} \times \vec{B}$ rotation and may be subjected to KH instability [134]. The fluctuation amplitude is maximum inside the velocity shear layer. The above mentioned instabilities can be identified based on the criteria derived by Jassby [134], which is summarized in Table 3.

Table 3: Criteria for the characterization of DW, RT and KH instabilities [131]

Parameters	**Drift waves**	**Rayleigh-Taylor**	**Kelvin-Helmholtz**
$k_{\|\|}$	$\sim 1/L$	0	0
Radial Location	$\max(\omega_D)$	$max\left\|\frac{1}{n}\frac{dn}{dr}\right\|$	Maximum of the velocity shear
$max\left\|\frac{e\tilde{\phi}}{k_B T_e}\right\|$	1	1	$\gg 1$
$max\left\|\frac{e\tilde{\phi}/k_B T_e}{\tilde{n}/n}\right\|$	≤ 1	≥ 1	$\gg 1$
Local variation of phase for potential fluctuation	$\leq 45^0$	$40^0 - 90^0$	$90^0 - 180^0$

5.2.1 Radial variation of fluctuation spectra

The density fluctuations at various radial locations are measured at two mirror ratio's and its power spectrum is analysed to observe the fluctuation frequency that is being suppressed at lower mirror ratio operation of IMPED.

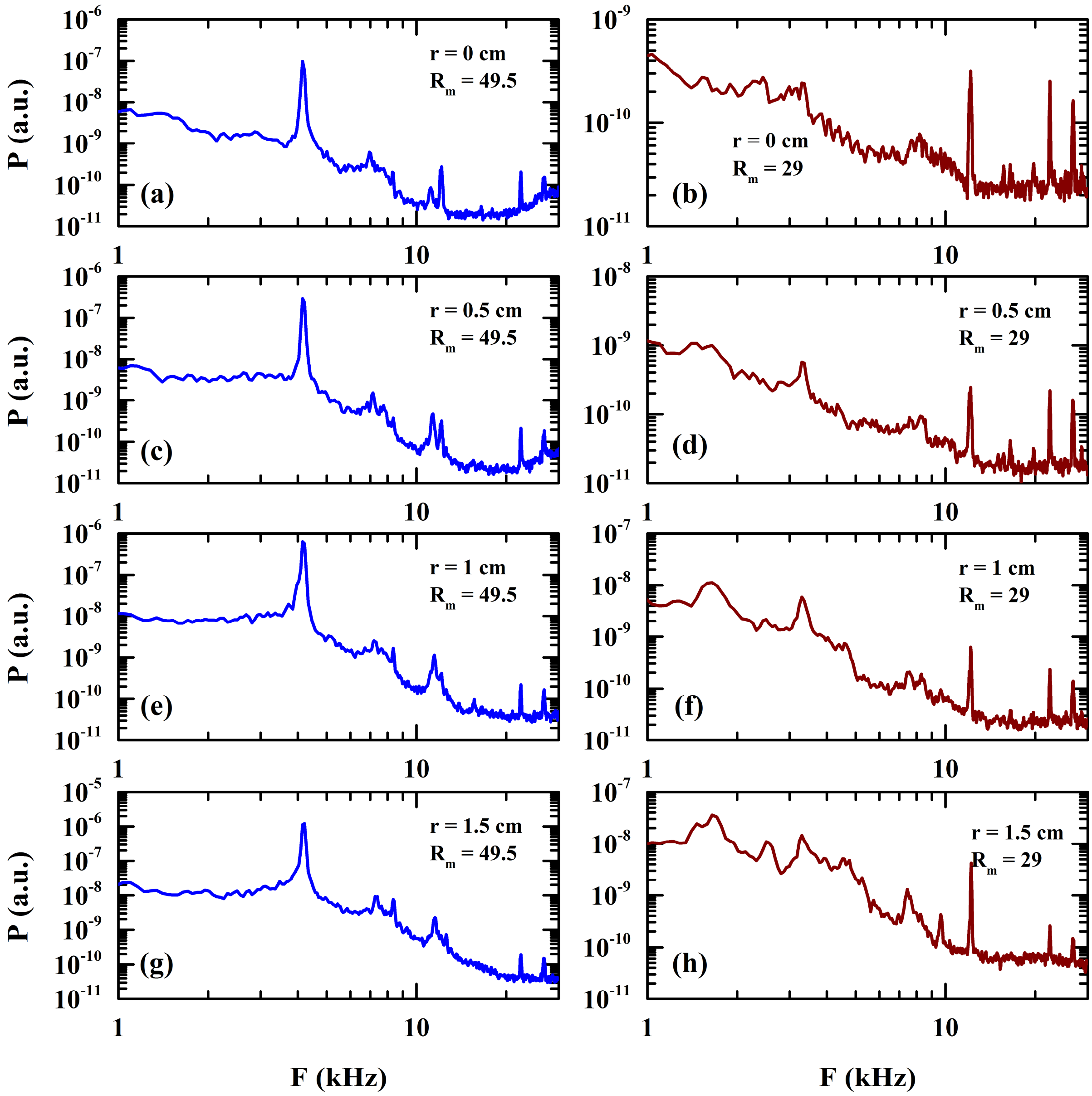

Figure 5.4 : Density fluctuation spectra at different radial locations for two different mirror ratio. B_{main} is held constant at *872 G* at $P = 10^{-4}$ *mbar* and $V_{dis} = -90\ V$. Measurements are made at *110.4 cm*

Form Figure 5.4 it is observed that a $\sim 4.2\ kHz$ low frequency fluctuation that exist at higher mirror ratio $R_m = 49.5$ is no longer visible at lower mirror ratio $R_m = 29$. Also the power in the fluctuations is much lower at $R_m = 29$ than at $R_m = 49.5$, which is in agreement with our $\delta n/n$ measurements at various mirror ratios presented in section 5.1. A radial density gradient perpendicular to the magnetic field is well-known for giving rise to instabilities [135] causing plasma density fluctuations. Exploring the possibility of density gradient causing the reduction in density fluctuation at low mirror ratios in IMPED, the radial density profile has been measured in the main chamber for two mirror ratios of 49.5 and 29.

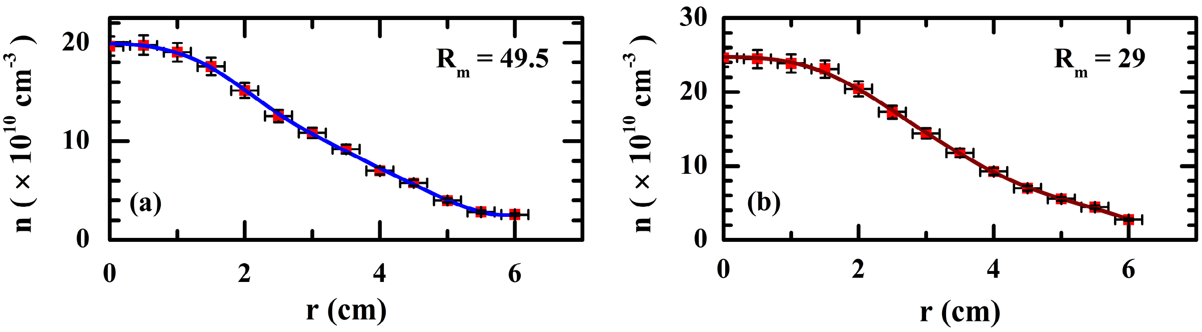

Figure 5.5: Radial density profiles at two mirror ratios. (a) $R_m = 49.5$ (b) $R_m = 29$. Both measurements are carried out at $z = 110.8\ cm$. $B_{main}=872\ G$, $V_{Dis}= -90\ V$ and $P=10^{-4}\ mbar$.

As shown in Figure 5.5, the radial plasma density profile becomes more flat on reducing the mirror ratio from $R_m = 49.5$ to $R_m = 29$. For $R_m = 29$, the plasma density falls to 80% of its peak value at $r \sim 2.1\ cm$, while f or $R_m = 49.5$, the density falls to 80% of its peak value $r \sim 1.9\ cm$. Flattening of radial density profile with reduction in mirror ratio may be understood as follows. The electrons and ions move from the source chamber to the main chamber along the magnetic field lines extending from the filament area to the main chamber, hence determining the plasma column diameter in the main chamber. At lower mirror ratios, the magnetic field lines intersecting the filament area occupies a greater diameter in the main chamber; thus, the radial uniformity of the plasma improves. Therefore, density fluctuations in IMPED can be effectively controlled by controlling the radial density profiles through the mirror ratio R_m. This feature also enables to control the radial uniformity of the plasma column in IMPED.

In low mirror ratio operation, a dominant high frequency $\sim 12.4\ kHz$ is observed away from the axis. The power spectrum of the fluctuations measured at $z = 110.8\ cm$ away from the axis of the device for different radial locations is shown in Figure 5.6.

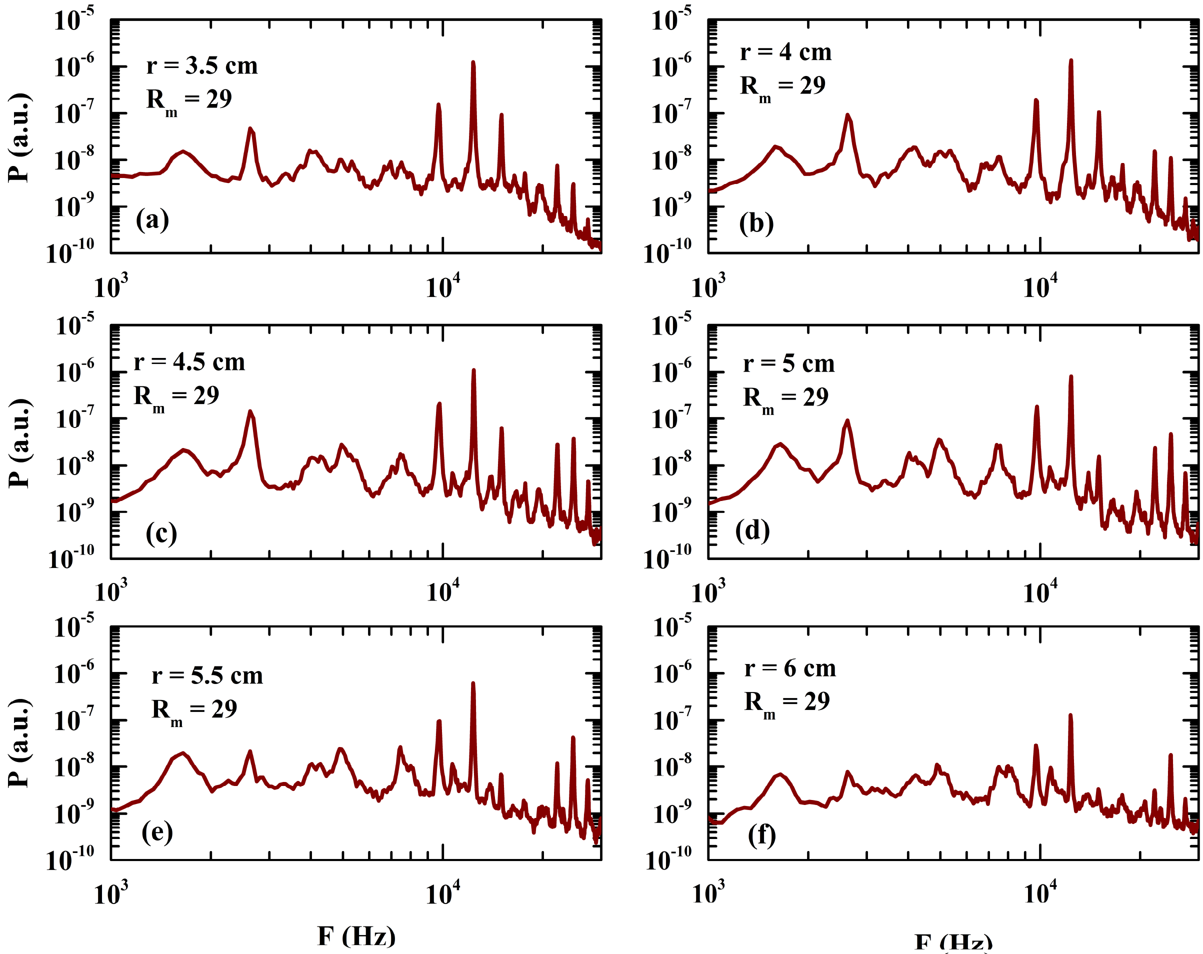

Figure 5.6: Power spectrum of the density fluctuations at different radial locations for R_m=29 when B_{main}=872 G. The pressure is maintained at 10^{-4} mbar, V_{Dis} is fixed at - 90 V.

In order to identify this high frequency fluctuation ($f \sim 12.4\ kHz$), the radial variation of the power in this frequency is plotted and is compared with the radial variation of plasma potential. The plot of the radial variation of power in the high frequency fluctuation is shown in Figure 5.7a and radial variation of plasma potential is shown in Figure 5.7b.

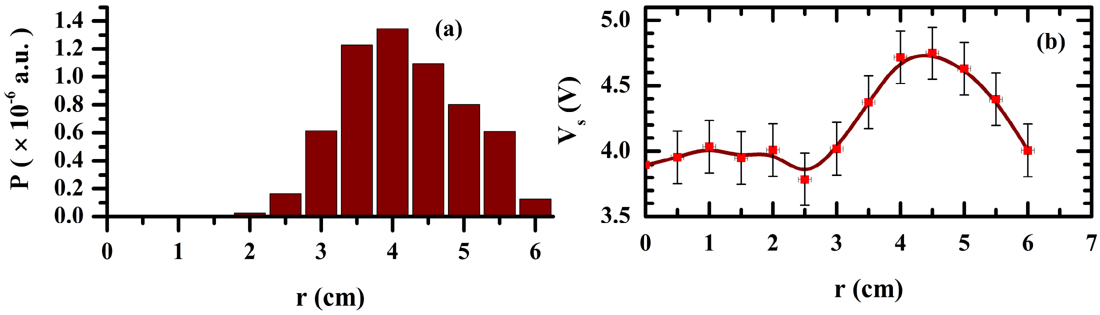

Figure 5.7: (a) Radial variation of power in the dominant high frequency fluctuation (b) Radial variation of plasma potential. Both the measurements have been made at *z = 110.8 cm*. Mirror ratio, operating pressure, magnetic field in the main chamber and discharge voltage is held constant at *29*, *10^{-4} mbar*, *1090 G* and - *90 V* respectively.

From Figure 5.7a it is observed that the maximum power in the dominant high frequency fluctuation is at $r \sim 4\ cm$. From the radial variation of plasma potential as shown Figure 5.7 b, it is observed that there is a strong shear in the electric field at $r \sim 4 - 4.5\ cm$. Thus, it can be conjectured that the dominant high frequency fluctuation observed away from the centre may be due to Kelvin-Helmholtz instability. The parallel wavenumber [136] of this dominant high frequency fluctuation $f \sim 12.4\ kHz$ is measured using three axially arranged probes at $r = 4\ cm$. $k_\parallel$ is found to be $0.0025\ cm^{-1}$, thus confirming that $f \sim 12.4\ kHz$ is an azimuthal mode. To gain further insight into the nature of this fluctuation, the ratio of $\left(e\hat{\phi}/T_e\right)/(\hat{n}/n)$ is calculated at three radial locations. At $r = 3.5, 4\ and\ 4.5\ cm$ the ratio

$\left(e\hat{\phi}/T_e\right)/(\hat{n}/n)$ is 4, 5.1 and 8.2, respectively. Thus, it is observed that $\left(e\hat{\phi}/T_e\right)/(\hat{n}/n) \gg 1$ for the high frequency fluctuation which also indicates that the fluctuations may be due to Kelvin-Helmholtz instability. Hence, from the above results it may be concluded that the high frequency fluctuation is due to KH instability.

The power spectrum of the density fluctuations away from the axis shows a number of interesting phenomena as shown in Figure 5.6. The high frequency Kelvin-Helmholtz mode $f \sim 12.4\ kHz$ seems to be coupling with low frequency modes having frequencies in the few $\sim kHz$ range and producing side bands. The asymmetries of the side bands are varying with radial location. At $r \sim 3.5\ cm$ (refer Figure 5.6a), the side bands are nearly symmetrical, but as one moves away from the centre say at $4.5\ cm$ (refer Figure 5.6c) the asymmetry increases. The frequency range of the low frequency modes are in the drift wave range for typical laboratory magnetized plasma. The observed side bands may be due to a nonlinear interaction between low frequency drift and the high frequency KH instability. To confirm this, auto bispectral analysis of the density fluctuation data is carried out.

5.2.2 Bispectral analysis

Bispectral analysis [137] is used for investigating nonlinear coupling among waves that satisfy the selection rules for frequency $(f_3 = f_2 \pm f_1)$ and the wave number $(k_3 = k_1 \pm k_2)$. This method is used particularly for analysing fluctuation spectrum associated with self-excited waves phenomena. As in such cases, spontaneously independent waves may get excited which may satisfy the selection rules but are not coupled nonlinearly. Nonlinear coupling results in new spectral components that are phase coherent, which is not true for independently excited waves. The detection of nonlinearly coupled waves may be carried out with higher order spectrum, which measures the degree of phase coherence between the waves.

The bispectrum $\hat{B}$ of density fluctuation is defined as

$$\hat{B}(f_3) = \langle \hat{n}(f_1)\hat{n}(f_2)\hat{n}(f_3) \rangle \tag{5.1}$$

Where $f_3 = f_1 + f_2$, $\hat{n}(f)$ is the Fourier transformed expression of density fluctuation $\hat{n}(t)$. Though the strength of three wave coupling may be represented by bispectrum, it is usually very difficult to use for describing the coupling state of the fluctuations. Therefore, we use bicoherence instead of bispectrum, which indicates the correlation of the frequency components between $\hat{n}(f_1)\hat{n}(f_2)$ and $\hat{n}(f_3)$. The bicoherence of density fluctuation is given by

$$\hat{b}^2(f_3) = \frac{\left|\hat{B}(f_3)\right|^2}{\langle |\hat{n}(f_1)\hat{n}(f_2)|^2 \rangle \langle |\hat{n}(f_3)|^2 \rangle} \tag{5.2}$$

The value of bicoherence is a measure of the strength of the interaction between frequency components, for example $\hat{b}^2(f_3) = 0.99$ implies that the power in f_3 is entirely due to interaction between f_1 and f_2.

The bicoherence of density fluctuation time series acquired at $r = 4.5\ cm$ and $z = 118.8\ cm$ at $10^{-4}\ mbar$ is shown in Figure 5.8. The magnetic field in the main chamber is maintained at $872\ G$ and R_m is fixed at 29. It shows that $\sim 12.4\ kHz$ fluctuation is coupling nonlinearly with $\sim 2.625\ kHz$ producing side bands, $f_3 = f_1 + f_2$. It also shows that $\sim 12.4\ kHz$ has a strong interaction with itself, resulting in harmonics generation.

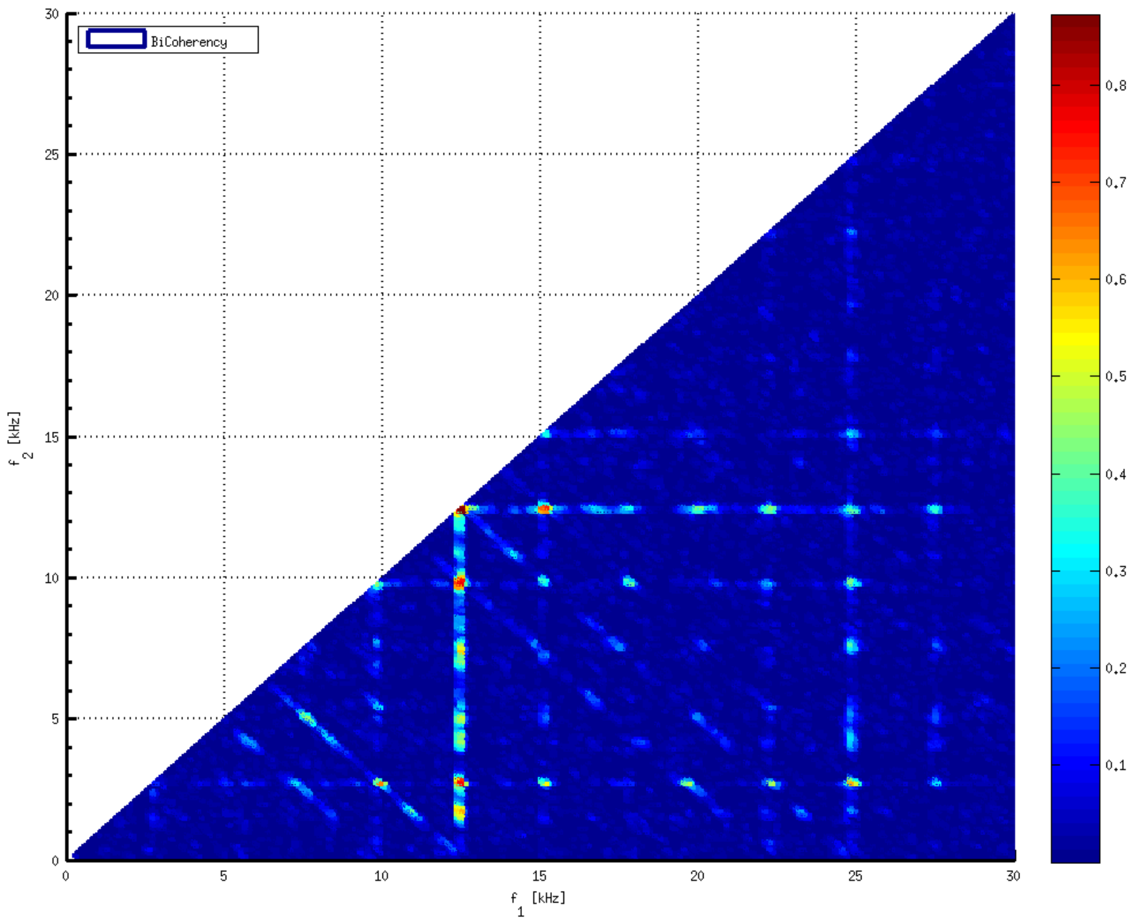

Figure 5.8: Bicoherence spectrum of density fluctuation measured at $r = 4.5\ cm$ and $z = 110.8\ cm$. Other parameters are $B_{main}=872\ G$, $R_m=29$, $P = 10^{-4}$ *mbar and* $V_{Dis}= -90\ V$.

Thus, from Figure 5.8 it may be concluded that IMPED provides a test bed for studying KH and DW instabilities. The experimental study of these instabilities is desirable to get a better understanding of transport in magnetically confined devices. However, it should be noted that the nonlinear interactions present in IMPED plasma are confined in a region away from the axis. The plasma near the axis is free from nonlinear interactions as can be seen from the bicoherence spectrum of the density fluctuations at $r = 0\ cm$ and $r = 0.5\ cm$.

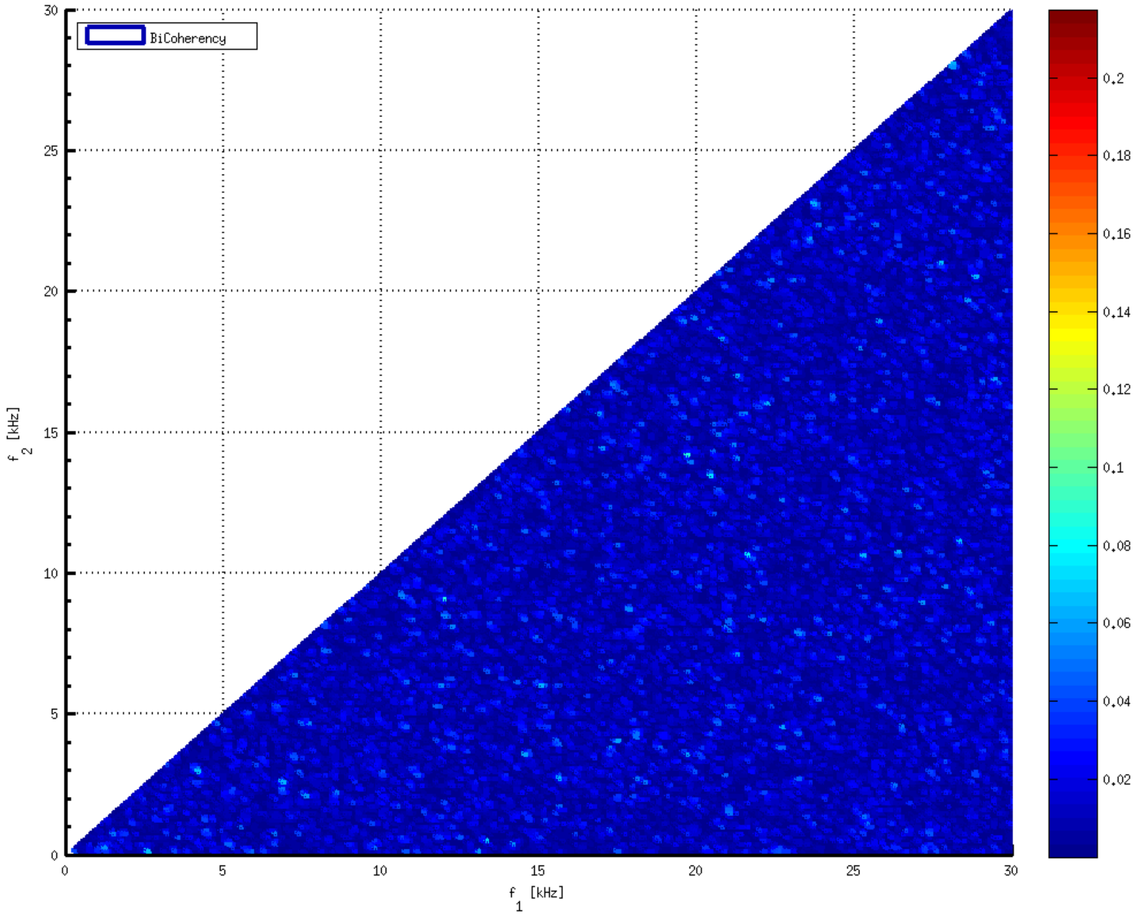

Figure 5.9: Bicoherence spectrum of density fluctuation measured at *$r = 0$ cm* and *$z = 110.8$ cm*. Other parameters are *B_{main}=872 G, R_m=29, $P = 10^{-4}$ mbar* and *V_{Dis}= -90 V*.

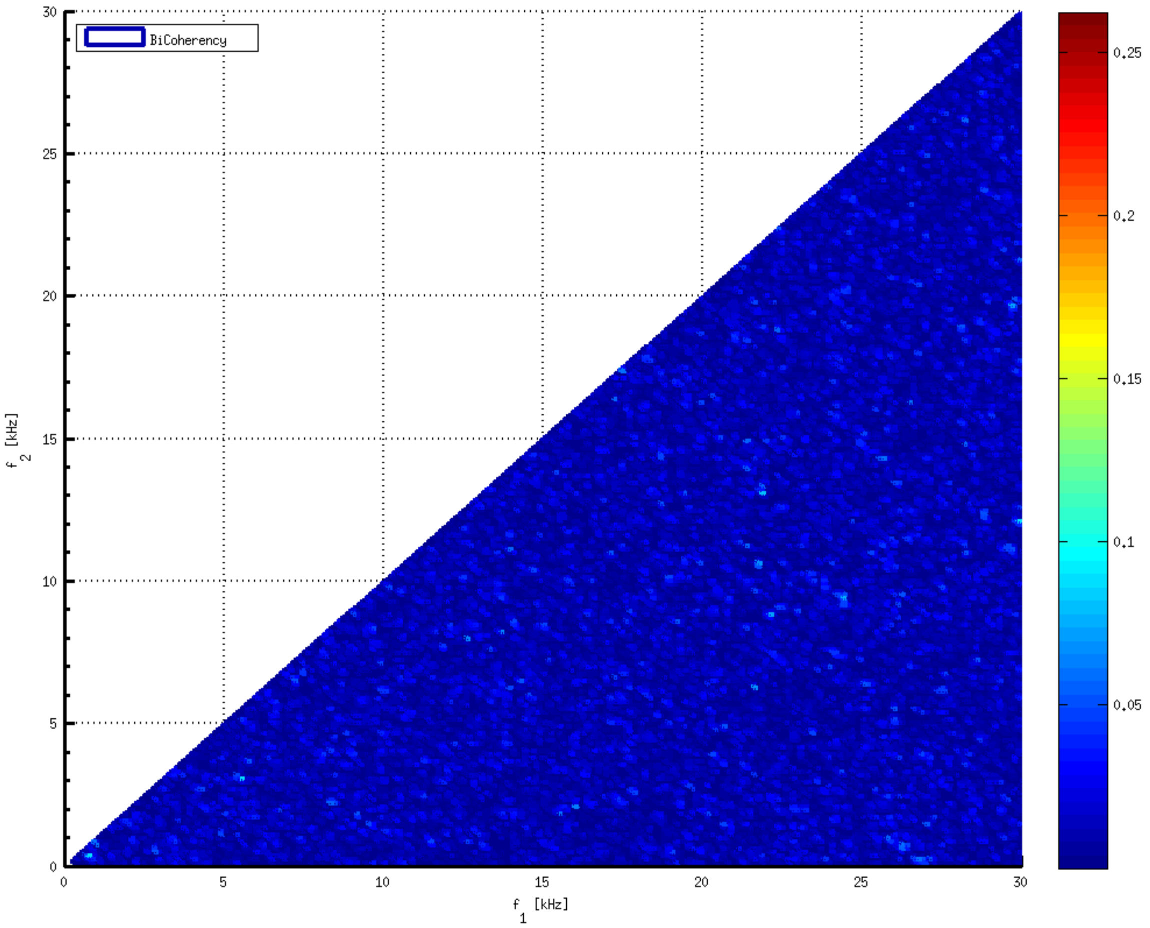

Figure 5.10: Bicoherence spectrum of density fluctuation measured at $r = 0.5\ cm$ and $z = 110.8\ cm$. Other parameters are $B_{main}=872\ G$, $R_m=29$, $P = 10^{-4}\ mbar$ and $V_{Dis}= -90\ V$.

5.3 Summary

A method for production of quiescent magnetized plasma has been proposed using the flexible transition magnetic field between the plasma source and the main chamber, that allows independent variation of magnetic field in the source (B_{source}) and the main chamber (B_{main}). Plasma with low density fluctuation is produced by operating the system in low mirror ratio (R_m) configuration. The effectiveness of this method is substantiated with experimental data. The plasma quiescence can be maintained around $\delta n/n \lesssim 1\%$ over a wide operating range spanning from 5×10^{-5} to 10^{-3} $mbar$ pressure and 109 G to 1090 G

magnetic field in the main chamber, by operating the system in low mirror ratio configuration. The effect of low mirror operation on the nature of fluctuations in IMPED is explored experimentally. Operation in low mirror ratio configuration gives rise to a sheared electric field at the edge of the plasma, which in turn induces a sheared $\vec{E} \times \vec{B}$ rotation. Kelvin-Helmholtz instability is observed due to the sheared rotation at the plasma edge. Bicoherence spectrum of density fluctuation revealed nonlinear coupling of KH with low frequency modes (may be DW) producing side bands. Strong interaction of the dominant spectral component of KH with itself is observed. These results may be interesting to the wider physics community because KH instability due to velocity shear layer is common in hydrodynamic systems. However, it must be noted that nonlinear interactions due to self-excited modes are limited to the region away from the centre of the plasma and density fluctuations near the axis are very less ($\delta n/n \lesssim 1\%$).

Chapter 6 Experiments on plasma oscillations

The present chapter describes the experimental study of plasma oscillations in the presence of a background plasma density perturbation. This chapter is divided into five sections; section 6.1 describes the excitation of plasma oscillations using two stream instability, section 6.2 gives an account of the experiments on interaction of plasma oscillations with a ion acoustic wave and an intuitive explanation of the observed phenomenon is given in section 6.3, followed by a brief summary in section 6.4.

6.1 Excitation of plasma oscillations

Plasma oscillation [1] is one of the fundamental modes of plasma. It can be excited by resonant coupling between a weak beam and the fundamental eigen mode of the plasma. If the beam density and energy exceeds the threshold value, the beam plasma interaction will give rise to excitation of plasma oscillation. This can be easily seen by considering a one dimensional two stream instability in cold plasma ($k_B T_e = k_B T_i = 0$) of density n_o where an electron beam of density n_{ob} streams with velocity v_{ob}. In the laboratory frame, the dispersion relation is given by

$$1 - \frac{\omega_{pe}^2}{\omega^2} - \frac{\eta\omega_{pe}^2}{(\omega - kv_{ob})^2} = 0 \tag{6.1}$$

where k is taken to be real, and $\omega(k)$ is the complex frequency $(\omega_r + i\gamma)$ which describes the complex behaviour of the k^{th} fourier mode and η is the ratio of the beam density (n_{ob}) and the plasma density $(n_{o)}$. Equation (6.1) gives complex unstable solutions when $|k| < (\omega_p v_{ob})(1 + \eta^{1/3})^{3/2}$ [138]

The frequency, wave number and growth rate of the most unstable linear waves are, respectively, [138],

$$\omega_{max} = \omega_{pe}\left[1 - \frac{1}{2}\left(\frac{1}{2}\eta\right)^{\frac{1}{3}} + \frac{3}{4}\left(\frac{1}{2}\eta\right)^{\frac{2}{3}} + \cdots\right] \tag{6.2}$$

$$k_{max} = \frac{\omega_{pe}}{v_{ob}}\left[1 + \frac{3}{2}\left(\frac{1}{2}\eta\right)^{\frac{2}{3}} + \cdots\right]$$

$$\gamma_{max} = \omega_{pe}\left[\frac{1}{2}\sqrt{3}\left(\frac{1}{2}\eta\right)^{\frac{1}{3}} - \frac{1}{4}\sqrt{3}\left(\frac{1}{2}\eta\right)^{\frac{2}{3}} + \cdots\right]$$

Thus, it is observed that in the presence of a weak beam ($\eta \ll 1$), the frequency of the most unstable mode is the plasma frequency (ω_{pe}) and the wavelength is given by $\sim v_{ob}/f_{pe} = 2\pi v_{ob}/\omega_{pe}$. However, a laboratory plasma has a finite temperature and collisionality, therefore, the collisionless cold plasma conditions are not strictly satisfied. Hence, for this purpose the dispersion relation of two stream instability due to a weak electron beam is deduced by taking into account the finite temperature and collisionality. Using the dispersion relation, the growth rate and frequency of the most unstable mode is theoretically calculated.

The governing equations for determining the beam plasma dispersion relation are the equation of motion of electrons fluids, continuity equation and Gauss' law. Let us consider a weak electron beam of initial density n_{ob} and velocity v_{ob} be introduced in the plasma with equilibrium density n_o and temperature T_e.

The equation of motion and continuity equation of the plasma electron fluid may be written as

$$m_e n_e \left[\frac{\partial \overrightarrow{v_e}}{\partial t} + (\overrightarrow{v_e}.\nabla)\overrightarrow{v_e}\right] \tag{6.3}$$

$$= \gamma k_B T_e \nabla n_e - e n_e \vec{E} - m_e \nu_{pen} n_e \overrightarrow{v_e} - m_e \nu_{pei} n_e \overrightarrow{v_e}$$

$$\frac{\partial n_e}{\partial t} + \nabla.(n_e \overrightarrow{v_e}) = 0 \tag{6.4}$$

where ν_{pen} and ν_{pei} are the electron-neutral collision frequency and the electron-ion collision frequency of plasma electrons, respectively. Other symbols have their usual meaning. Solving (6.3) by the process of linearization, where $n_e = n_o + n_1$, $\overrightarrow{v_e} = \overrightarrow{v_o} + \overrightarrow{v_1}$ and $\vec{E} = \overrightarrow{E_o} + \overrightarrow{E_1}$. Subscript zero represents the equilibrium quantities and the subscript one represents the first order perturbation. At equilibrium$\overrightarrow{v_o} = \overrightarrow{E_o} = \nabla n_o = \partial n_o/\partial t = 0$. Therefore equation (6.3) and (6.4) takes the form

$$m_e n_o \frac{\partial \overrightarrow{v_1}}{\partial t} = -e n_o \overrightarrow{E_1} - \gamma k_B T_e \nabla n_1 - m_e n_o \overrightarrow{v_1}(\nu_{pen} + \nu_{pei}) \tag{6.5}$$

$$\frac{\partial n_1}{\partial t} + \nabla.(n_o \overrightarrow{v_1}) = 0 \tag{6.6}$$

Let $\nu_p = \nu_{pen} + \nu_{pei}$ in (6.5). Then (6.5) becomes

$$m_e n_o \frac{\partial \overrightarrow{v_1}}{\partial t} = -e n_o \overrightarrow{E_1} - \gamma k_B T_e \nabla n_1 - m_e \nu_p n_o \overrightarrow{v_1} \tag{6.7}$$

Looking for electrostatic waves of the form $\overrightarrow{E_1} = E_1 e^{i(kx-\omega t)}\hat{x}$, where $\hat{x}$ is in the direction of wave vector. We are considering a one dimensional problem.

$$v_1 = -\frac{ieE_1}{m_e(\omega + \nu_p)} + \frac{k\gamma k_B T_e}{m_e n_o(\omega + i\nu_p)} n_1 \tag{6.8}$$

$$v_1 = \frac{\omega n_1}{k n_o} \tag{6.9}$$

Combining (6.8) and (6.9), one gets

$$n_1 = \frac{-iken_oE_1}{\omega m_e(\omega + i\nu_p) - k^2\gamma k_BT_e} \tag{6.10}$$

The equation of motion and continuity equation of the cold electron beam fluid may be written as

$$m_e n_b\left[\frac{\partial\overrightarrow{v_b}}{\partial t} + (\overrightarrow{v_b}.\nabla)\overrightarrow{v_b}\right] = -en_b\vec{E} - m_e\nu_{ben}n_b\overrightarrow{v_b} - m_e\nu_{bei}n_b\overrightarrow{v_b} \tag{6.11}$$

$$\frac{\partial n_b}{\partial t} + \nabla.(n_b\overrightarrow{v_b}) = 0 \tag{6.12}$$

where ν_{ben} and ν_{bei} are the electron-neutral collision frequency and the electron-ion collision frequency of beam electrons, respectively. Other symbols have their usual meaning. Solving (6.11) and (6.12) by the process of linearization, where $n_b = n_{ob} + n_{1b}$, $\overrightarrow{v_b} = \overrightarrow{v_{ob}} + \overrightarrow{v_{1b}}$ and $\vec{E} = \overrightarrow{E_o} + \overrightarrow{E_1}$. Subscript zero represents the equilibrium quantities and the subscript one represents the first order perturbation. At equilibrium, $\overrightarrow{E_o} = \nabla n_{ob} = \partial n_{ob}/\partial t = 0$. Therefore, equation (6.11) and (6.12) takes the form

$$m_e n_{ob}\left[\frac{\partial\overrightarrow{v_{1b}}}{\partial t} + (\overrightarrow{v_{ob}}.\nabla)\overrightarrow{v_{1b}}\right] = -en_{ob}\overrightarrow{E_1} - m_e n_{ob}\overrightarrow{v_{1b}}(\nu_{ben} + \nu_{bei}) \tag{6.13}$$

$$\frac{\partial n_{1b}}{\partial t} + \overrightarrow{v_{ob}}.\nabla n_{1b} + n_{ob}\nabla.\overrightarrow{v_{1b}} = 0 \tag{6.14}$$

Let $\nu_b = \nu_{ben} + \nu_{bei}$, then equation (6.13) becomes,

$$m_e n_{ob}\frac{\partial \overrightarrow{v_{1b}}}{\partial t}+m_e n_{ob}(\overrightarrow{v_{ob}}.\nabla)\overrightarrow{v_{1b}}=-en_{ob}\overrightarrow{E_1}-m_e n_{ob}\overrightarrow{v_{b1}}\nu_b \tag{6.15}$$

Looking for electrostatic waves of the form $\overrightarrow{E_1}=E_1 e^{i(kx-\omega t)}\hat{x}$, where $\hat{x}$ is in the direction of wave vector, (6.14) and (6.15) becomes,

$$v_{1b}=-\frac{ieE_1}{m_e(\omega-kv_{ob}+i\nu_b)} \tag{6.16}$$

$$v_{1b}=\frac{(\omega-kv_{ob})}{kn_{ob}}n_{1b} \tag{6.17}$$

Combining (6.16) and (6.17), one gets

$$n_{1b}=-\frac{iekn_{ob}E_1}{m_e(\omega-kv_{ob}+i\nu_b)(\omega-kv_{ob})} \tag{6.18}$$

Writing the Gauss' law and considering electrostatic waves of the form $\overrightarrow{E_1}=E_1 e^{i(kx-\omega t)}\hat{x}$, where $\hat{x}$ is in the direction of wave vector and using (6.10) and (6.18), one gets the dispersion relation as

$$1-\frac{\omega_{pe}^2}{\omega\left(\omega+i\nu_p\right)-\frac{\gamma}{2}k^2v_{the}^2}-\frac{\eta\omega_{pe}^2}{(\omega-kv_{ob}+i\nu_b)(\omega-kv_{ob})}=0 \tag{6.19}$$

For one dimensional adiabatic process $\gamma=3$

$$1-\frac{\omega_{pe}^2}{\omega\left(\omega+i\nu_p\right)-\frac{3}{2}k^2v_{the}^2}-\frac{\eta\omega_{pe}^2}{(\omega-kv_{ob}+i\nu_b)(\omega-kv_{ob})}=0 \tag{6.20}$$

In a collisionless plasma with a finite temperature the dispersion relation becomes

$$1 - \frac{\omega_{pe}^2}{\omega - \frac{3}{2}k^2 v_{the}^2} - \frac{\eta \omega_{pe}^2}{(\omega - k v_{ob})^2} = 0 \quad (6.21)$$

where $v_{the}^2 = 2k_B T_e / m_e$ is the electron thermal speed.

In order to visualize the effect of temperature on the growth rate of the instability, equation (6.21) is numerically solved for real k for different ratio's of thermal energy of plasma electrons and beam energy.

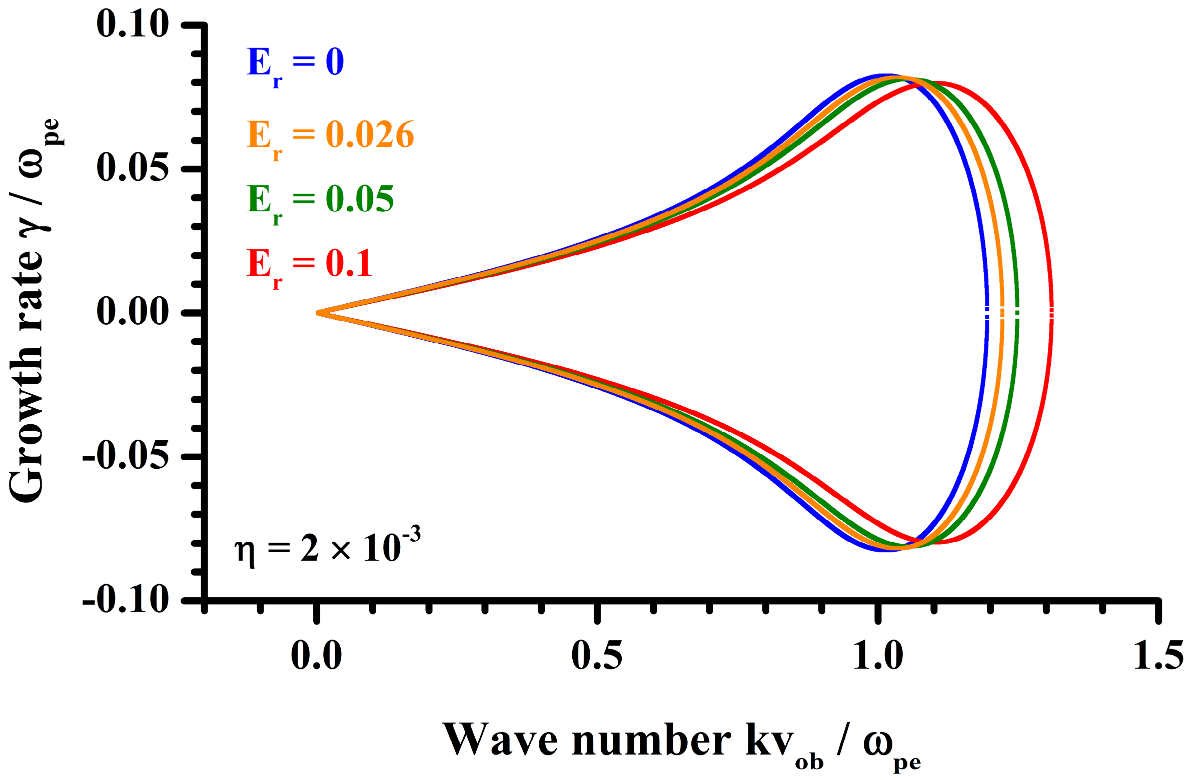

Figure 6.1: Variation of growth rate of the unstable modes for different beam energies.

Figure 6.1 shows the growth rate of the unstable modes in plasma with a finite temperature and $\eta = 2 \times 10^{-3}$ for different values of E_r, where E_r $\left(= \frac{1}{2} m_e v_{the}^2 / \frac{1}{2} m_e v_{ob}^2\right)$ is the ratio of the thermal energy to the beam energy. It is observed that on increasing the ratio of thermal energy to the beam energy, the wave number of the most unstable mode increases and the frequency of the unstable mode also shows a slight tendency of increasing with increase in E_r as shown in Figure 6.2. So with these perspectives in mind, the experiments on plasma oscillations have been carried out.

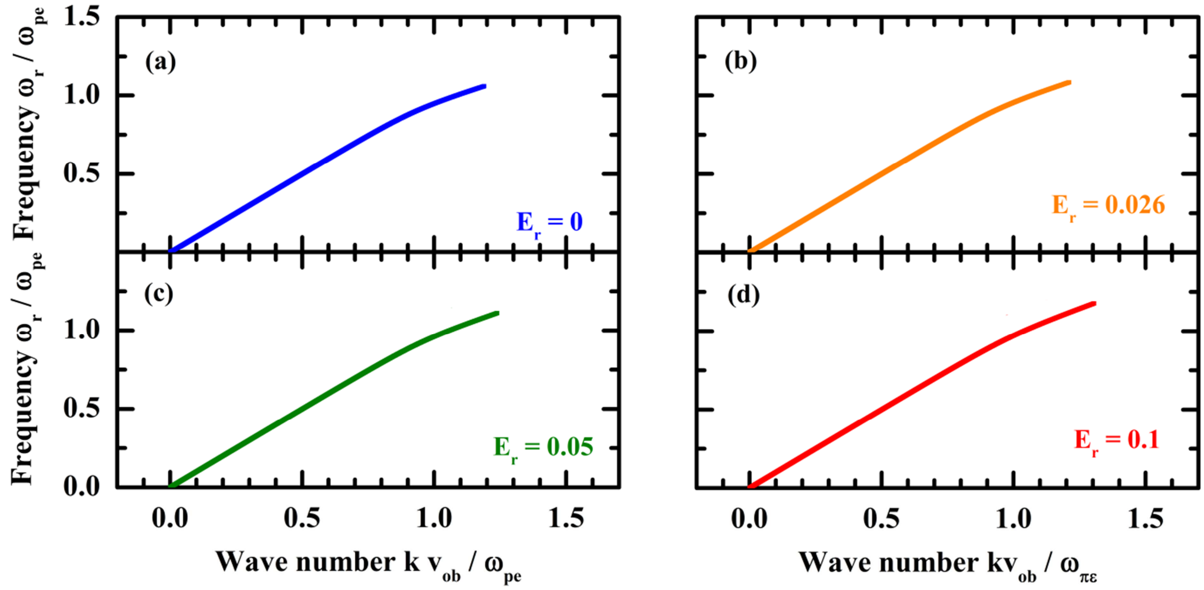

Figure 6.2: Variation of the frequency of the unstable mode with wave number for different values of E_r, when the ratio of the beam density to plasma density is 2×10^{-3}.

Electron beam for excitation of beam driven plasma oscillations is injected in the plasma from an electron emissive filament. A long straight filament of $3\,cm$ length and $0.125\,mm$ diameter is used for wave studies. Electron emission from the heated filament takes place when the heating current is varied from $1-3\,A$. The electron beam energy $[E_B = e(V_s - V_B)]$ is controlled by varying the filament biasing voltage V_B, which is negative with respect to the plasma potential V_s. The beam temperature is reduced by a factor of $\sim k_B T_{Fil}/E_B$ from the filament temperature $T_{fil}\sim 0.2\,eV$ when electrons emitted from the filament are accelerated to energy E_B [139]. Therefore, the cold beam approximation holds well compared with T_e and beam energies $\sim 115\,eV$. The beam is injected in the system along the axial magnetic field. The beam divergence is expected to be very small around few Larmor radii within few centimetres from the filament. Under typical operating conditions, the energy of the beam (E_{beam}) is $\sim 115\ eV$, beam current is $\sim 10\ mA$, plasma temperature is $\sim 2\ eV$. The beam density is estimated from the beam current is found to be $n_b \sim 3.07 \times 10^7\ cm^{-3}$, which is much less than the plasma density $n_0 \sim 1.6 \times 10^{10}\ cm^{-3}$. Thus, the weak beam approximation holds and hence, a single peak is expected in the frequency spectra. The frequency spectrum of the excited oscillation is shown in the Figure 6.3 which shows a sharp peak centered at plasma frequency.

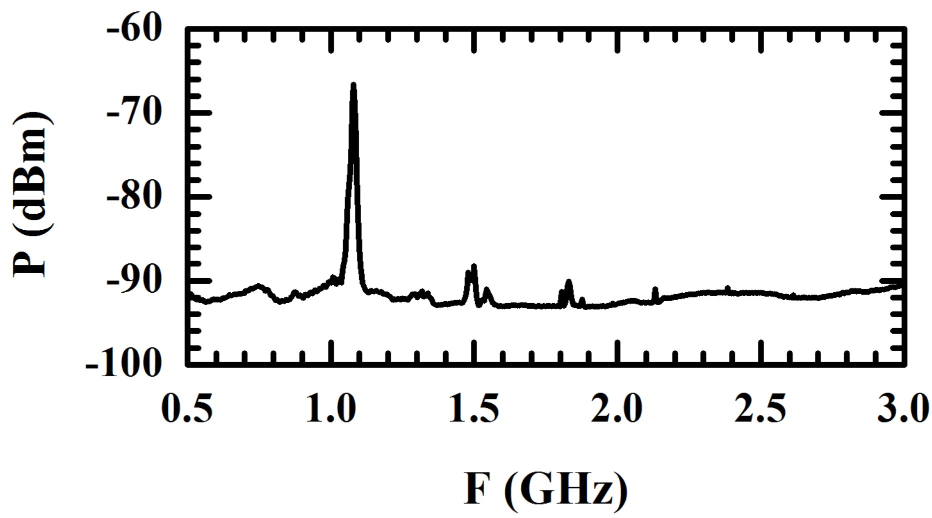

Figure 6.3: Frequency spectrum of the beam driven plasma oscillation.

Plasma oscillations driven by the electron beam are electrostatic waves of high frequencies ($\sim f_{pe} = 1\ GHz$) and short wavelength ($\sim 2\pi v_{ob}/\omega_p$, typically 6.4 mm) and are received by a high frequency probe. The probe had a straight $5\ mm$ long tip connected to a semi-rigid cable. The high frequency probe is directly connected to a spectrum analyser for identifying the frequency of the wave potential.

6.2 Interaction of plasma oscillations with a ion acoustic wave in the background

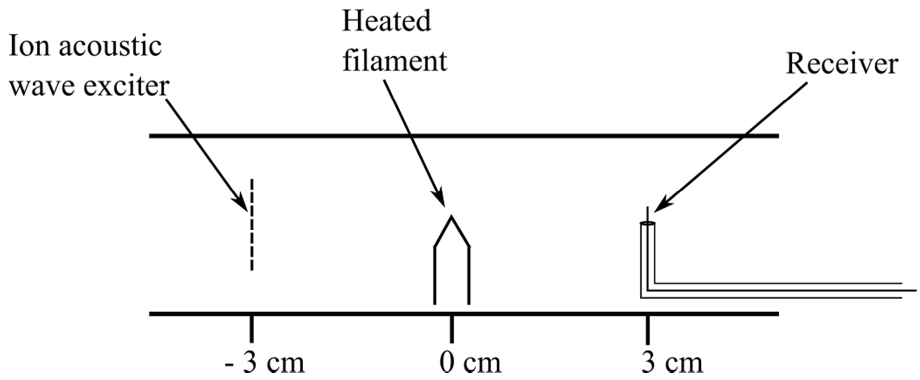

Figure 6.4: Schematic of the experimental set up for studying the plasma oscillation in the presence of an ion acoustic wave in the background.

The experimental study of the interaction of plasma oscillation with an ion acoustic wave in the background is conducted in the main chamber of IMPED [42]. The schematic of the experimental set up is shown in the Figure 6.4. It consist of a gridded exciter made from stainless steel mesh (SS 316) for exciting ion acoustic wave, followed by a 3 cm long biased heated tungsten filament for exciting the plasma oscillations and a high frequency receiver which can also be used to sense signal in the ion acoustic frequency range. For detecting signal in the ion acoustic frequency range the high frequency probe is biased at $-85\ V$ in the ion saturation region and the disturbance in the ion saturation current corresponding to the wave excitation signal is measured using a $1GHz$ oscilloscope. The heated filament used for excitation of the plasma oscillation can be moved radially and the gridded ion acoustic wave exciter and the receiver probe is movable be axially. For the experimental data presented below the grid is placed behind the biased heated filament at a distance of 3 cm. The receiver is placed in front of heated filament at a distance of 3 cm from the filament.

The experiments are conducted at $10^{-4}\ mbar$, in argon plasma. The magnetic field in the main chamber is held constant at $218\ G$ while the magnetic field near the plasma source is fixed at $29\ G$. The discharge voltage is held constant at $-90\ V$. The experiment is conducted in five steps. Initially ion acoustic waves are excited by applying a single burst to a gridded exciter at 100 kHz in the absence of the electron beam. The receiver is retracted and the propagating wave is sampled at different z locations. The ion acoustic waves observed are similar to waves shown in Figure 3.25.

After confirming that ion acoustic waves are propagating on application of oscillating voltage on the ion acoustic wave exciter grid. The power to the ion acoustic wave exciter grid is switched off and the receiver probe is brought back to z = 3 cm. Now without any power to the ion acoustic wave exciter grid and without any electron beam in the system the output of the high frequency receiver probe connected to a spectrum analyser is recorded. The spectrum analyser output is shown in Figure 6.5.

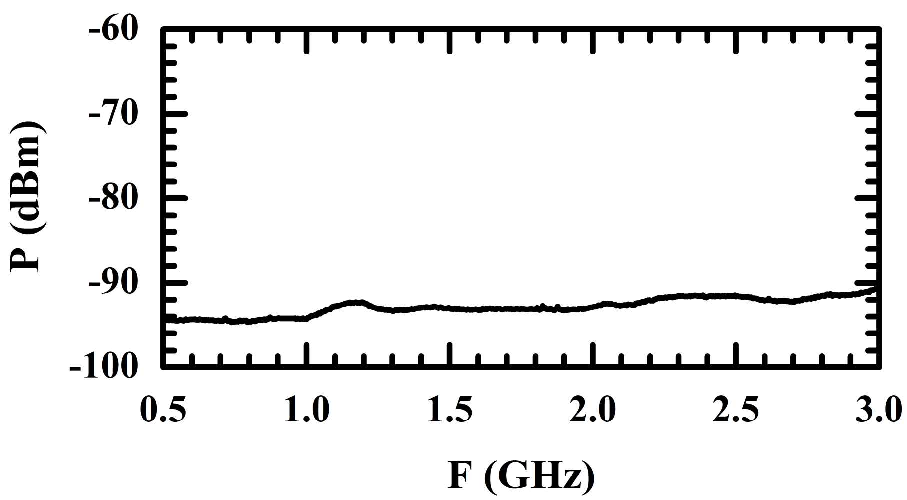

Figure 6.5: Frequency spectrum in the absence of electron beam in the plasma

This is followed by excitation of plasma oscillations by introducing an electron beam of density $3 \times 10^7\ cm^{-3}$ and energy $\sim 115\, eV$ along axis of the magnetic field using the heated tungsten filaments. The plasma oscillations excited by the beam is detected using same high frequency probe connected to the spectrum analyser. The output of the spectrum analyser is shown in Figure 6.7a. The output of the spectrum analyser shows a sharp peak at $1.079\, GHz$. The plasma density determined from the frequency peak is $\sim 1.6 \times 10^{10}\ cm^{-3}$. The plasma density is also measured using a Langmuir probe in the absence of the electron beam and as per Langmuir probe measurements the plasma density is $\sim 2 \times 10^{10}\ cm^{-3}$. The wavelength corresponding to the observed frequency peak determined from dispersion relation is $6.4\, mm$.

Following the excitation of plasma oscillations, ion acoustic waves are excited in the presence of the beam by applying an oscillating voltage at $\sim 100\, kHz$ to the grid. The existence of the propagating ion density perturbation in presence of the electron beam is confirmed by applying a single burst to the gridded exciter and detecting the corresponding ion acoustic wave using the time of flight technique. Figure 6.6 shows the propagation of ion acoustic wave on application of $28\, V_{pp}$ pulsed voltage on the gridded ion acoustic wave exciter in the presence of an electron beam. The wavelength of the wave is $14\, mm$ and the induced ion density perturbation ($\delta n_{pp}/n$) is 0.026.

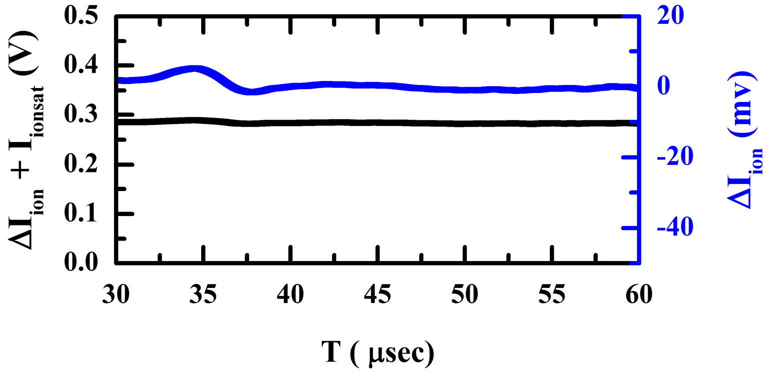

Figure 6.6: Propagating ion density perturbation as received by the receiver on application of a single *28* V_{pp} pulse voltage on the ion acoustic wave exciter

This is followed by the experimental study of plasma oscillations in the presence of ion acoustic waves in the background. Ion acoustic waves are excited by continuously applying oscillating voltage to the grid at 100 kHz. Ion acoustic waves of subsequently increasing amplitude are excited in the presence of plasma oscillation and its effect on the coherent power in the plasma oscillation is experimentally studied. The frequency spectrum of the high frequency probe for different exciter voltage applied to the grid is shown Figure 6.7 (a - f).

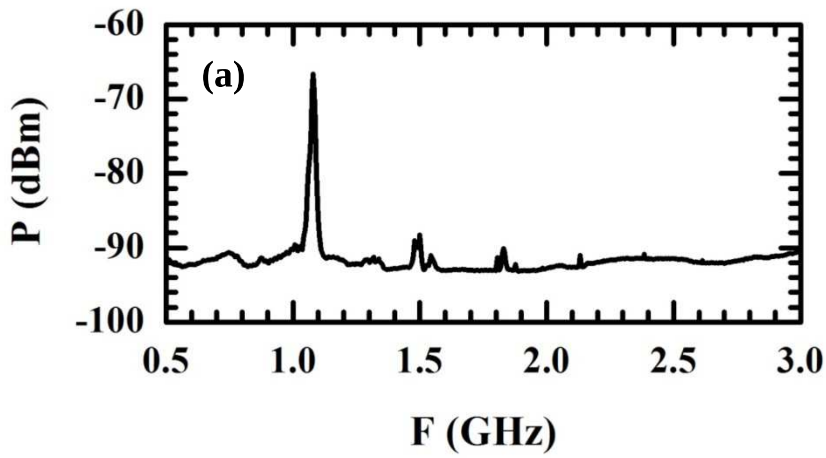

Exciter voltage = 0 V_{pp}

F = 1.079 GHz

Power = - 66.63 dBm

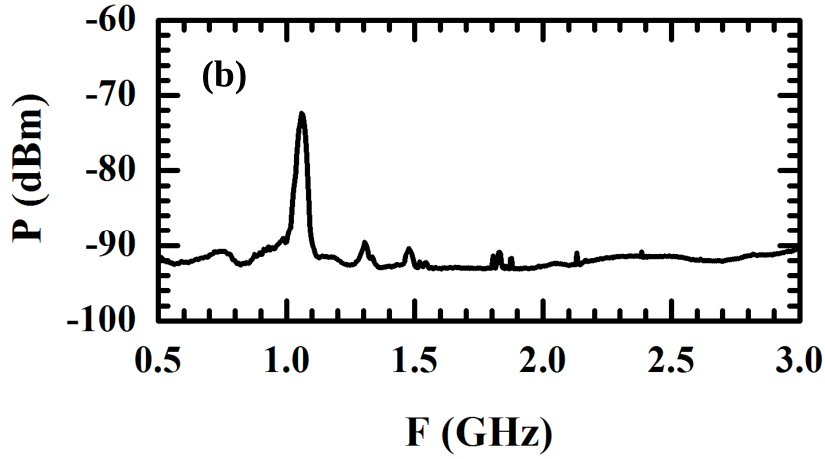

Exciter voltage= $11.8\ V_{pp}$

F = 1.059 GHz

Power = - 72.37 dBm

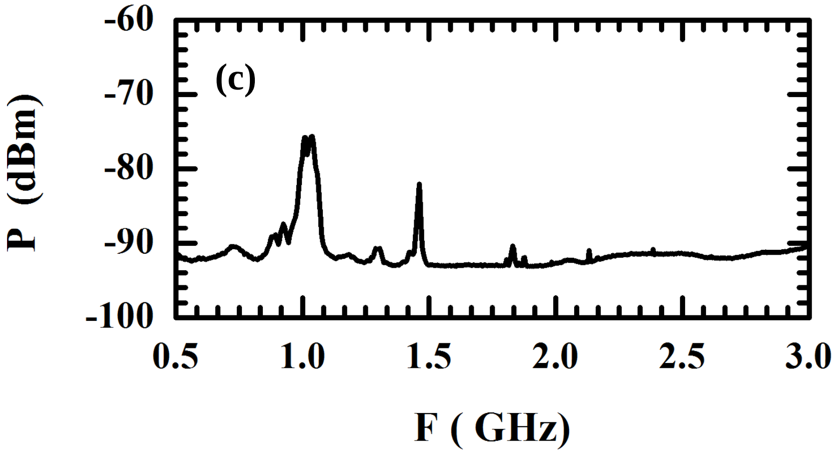

Exciter voltage= $28\ V_{pp}$

F = 1.03 GHz

Power = - 75.80 dBm

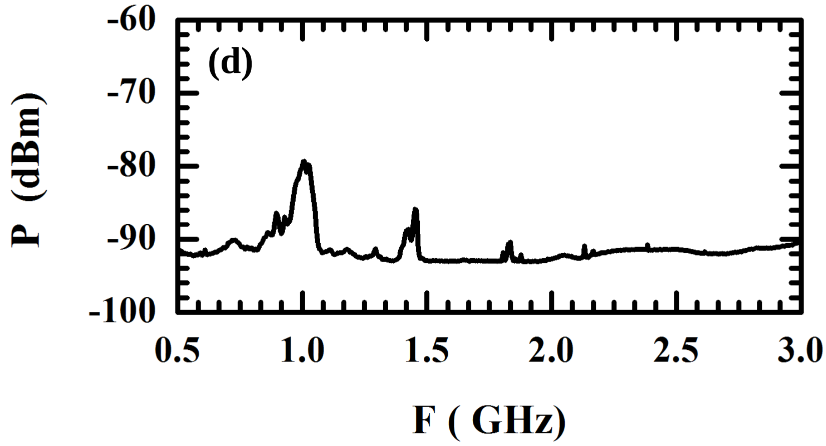

Exciter voltage = $38\ V_{pp}$

F = 1.079 GHz

Power = - 79.306 dBm

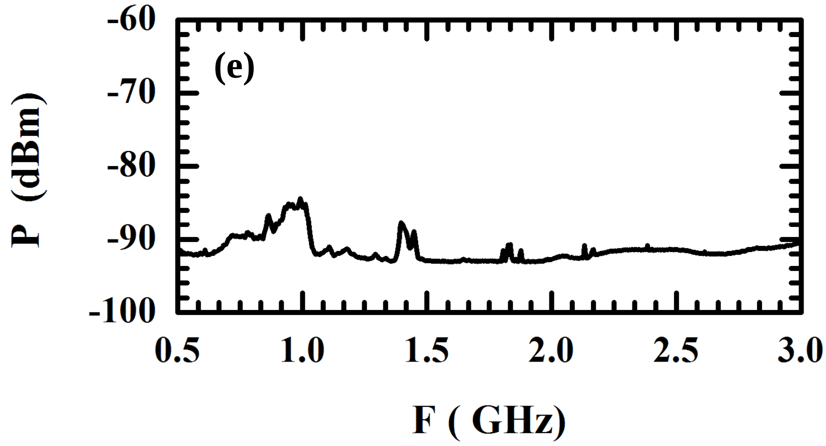

Exciter voltage = $48\ V_{pp}$

F = 0.99 GHz

Power = - 84.375 dBm

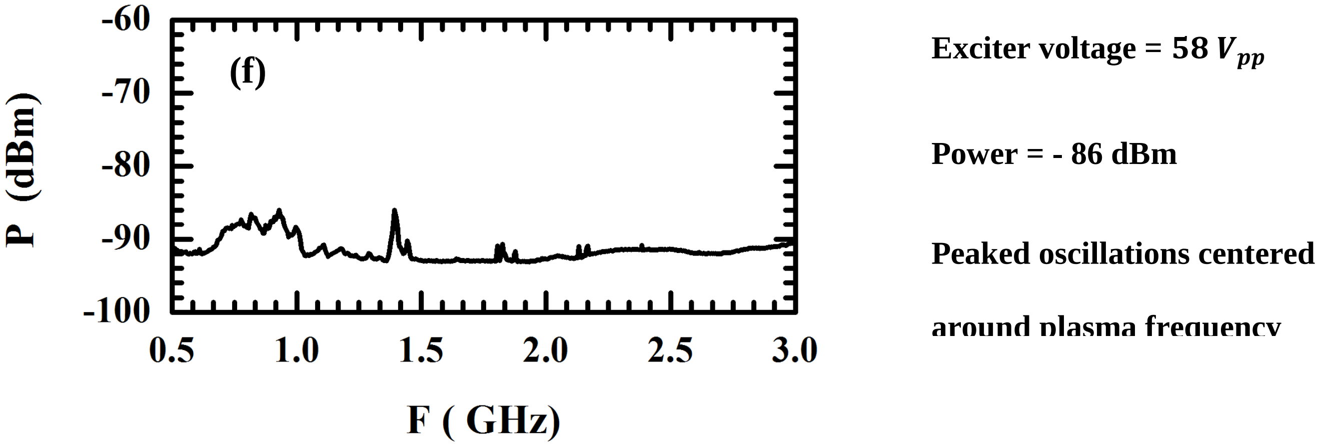

Figure 6.7: Variation of power in the coherent oscillation with increase in the applied voltage to the grid exciting ion acoustic wave.

The power in the coherent plasma oscillation decreases on increasing the background ion density perturbation as shown in Figure 6.7. Without any background ion density perturbation, the power in coherent plasma oscillation is $-66.6\ dBm$. As the background ion density perturbation is increased, the power in the coherent plasma oscillation decreases. For example, in the presence of background ion acoustic wave (ion density perturbation) of amplitude $\delta n_{pp}/n\ \sim 0.01$ excited by applying $11.8\,V_{pp}$ exciter voltage, the power in the coherent oscillation decreases to $-72.37\,dBm$. On increasing the amplitude of the background ion acoustic wave further to $\delta n_{pp}/n \sim 0.026$ by applying an exciter voltage $28\,V_{pp}$, the power in the coherent oscillation decreased to $-75.80\,dBm$. For a background ion acoustic wave $\delta n_{pp}/n \sim 0.03$ (Exciter voltage = $48\,V_{pp}$), the power in the coherent oscillation decreases further to $-84.375\,dBm$. On increasing the exciter voltage further to $58\,V_{pp}$ to excite a higher amplitude ion acoustic wave the peaked oscillation is no longer visible.

It is also experimentally observed that on increasing the amplitude of exciter voltage on the grid, the plasma frequency tends to decrease slightly. This may be due to the fact that the exciting grid draws more current from the plasma at higher amplitudes, thus decreasing the downstream plasma density slightly.

6.3 Intuitive explanation of the observed phenomena

In an inhomogeneous plasma the local plasma frequency varies spatially due to the dependence of local plasma frequency on density at that location. Because of the spatial dependence of the plasma frequency, the phase difference between the oscillators constituting the oscillation change with time, which eventually leads to fine scale mixing of various parts of the oscillation [11]. The time in which two oscillators separated by twice the amplitude of oscillation goes out of phase by 180^0 is defined as the phase mixing time. The phase mixing time of small amplitude plasma oscillation in a weakly inhomogeneous plasma [11] is given by $t_{mix} = \frac{\pi}{2\left(\frac{d\omega p}{dx}\right)X}$. This formula deduced by J.M. Dawson gives an interesting insight into the phenomenon of phase mixing. It shows that the rate of phase mixing is dependent on the displacement X of the oscillator from the equilibrium position, which implies that greater the distance traversed by an oscillator in a single period, more is the dephasing. This statement is true not only for small amplitude of oscillation, but also in case of large amplitude of oscillation. However, in case of large amplitude oscillation, the phase mixing may not have the simple inverse dependence as predicted by J.M. Dawson.

Experimentally, plasma oscillations are excited by using a weak electron beam. The beam excites the oscillations in the plasma as it propagates. Beam driven oscillations have a finite growth rate, thus, the amplitude of oscillation grows with time. As the amplitude grows, the oscillators constituting the oscillation traverse a greater distance from the mean position. In an inhomogeneous plasma the dephasing of the oscillators constituting the oscillation takes place and this dephasing is greater for higher amplitudes. Thus there is a driver, which is the weak electron beam and there is a damping mechanism due to phase mixing, which depends on the amplitude and the background density perturbation. For a given ion density perturbation, the beam driven growth rate of the oscillation can be more dominant at lower amplitudes while the phase mixing effect is dominant at higher amplitudes of oscillation. This leads to saturation of the oscillation at lower amplitude in presence of background ion density perturbation (inhomogeneous plasma) than what it would have been in the uniform plasma. Hence on increasing the ion density perturbation, the saturation amplitude of oscillation should decrease further. This is what we have observed experimentally, when a smaller ion density perturbation is excited (refer Figure 6.7b) the oscillation is equilibrating at a higher amplitude which is of course less than the amplitude of oscillation observed in a uniform plasma as shown in Figure 6.7a. On increasing the ion density perturbation further (refer Figure 6.7c, d and e) the oscillation is equilibrating at a much lower amplitude and beyond a certain limit, the peaked coherent oscillation is no longer observed.

6.4 Summary

Phase mixing of plasma oscillation is experimentally demonstrated in a unique experimental configuration for the first time, which allows one to investigate phase mixing as a steady state phenomenon instead of a transient phenomenon lasting only few nanoseconds to tens of nanoseconds. Oscillations in the plasma are excited using a weak electron beam ($\eta = n_b/n \ll 1$). The frequency of the most unstable mode in the weak beam approximation limit ($\eta \ll 1$) is $\sim f_{pe} (= 1\ GHz)$ and the wavelength is $\sim 6.4\ mm$. The non-uniformity in the density is externally induced in a controlled manner by exciting ion acoustic waves using a single grid exciter. The wavelength of the excited ion acoustic wave is $\sim 14\ mm$. The frequency of the ion acoustic wave is much less than the frequency of the plasma oscillation($\Omega \ll f_{pe}$). The variation of power in the coherent oscillation in presence of ion wave in the background of different amplitudes is experimentally studied. The power in the coherent oscillation is found to decrease with an increase in the amplitude of the background ion acoustic wave and beyond a certain limit, the coherent oscillation ceases to exist. The experimental results verify that phase mixing of plasma oscillation is dependent on both amplitude of oscillation and also on the non-uniformity of the background plasma density.

Chapter 7 Conclusion and Future Scope

This chapter is divided into two sections. The first section gives an account of summary of the work described in this thesis followed by the conclusions drawn from it. In the second section, a brief discussion on the further experiments that can be carried out is presented.

7.1 Summary

The physics of phase mixing of plasma oscillations [11] and breaking of nonlinear plasma oscillations [11] is a topic of considerable interest both from the fundamental point of view as well as from the application point of view. Fundamentally, it is the simplest collective irreversible phenomena observed in plasma yet a number of aspects of this phenomena are yet to be experimentally explored. The longitudinal electric field associated with plasma oscillations can be used to accelerate particles [34] and it finds applications in plasma based accelerators and certain laser fusion schemes. In this thesis, an experimental system, designed for the detailed experimental investigation of phase mixing of plasma oscillation, has been described.

The design process involved a theoretical study of phase mixing and breaking of plasma oscillation, followed by identification of unresolved issues that are to be addressed. This was followed by a detailed calculation for identifying the plasma parametric space necessary for a comprehensive experimental investigation of phase mixing and wavebreaking of the longitudinal wave. Accordingly, a set of requirements were determined that a laboratory experimental device must satisfy for the proposed wave experiments. The requirements can be summarized as follows:

i. Quiescence: $\frac{\delta n}{n} \sim 1\%$ or less
j. Density range: $5 \times 10^8 - 10^{11}\ cm^{-3}$ (for experimental purpose a three order density variation within the mentioned range may suffice)
k. Temperature: ~ few eV
l. Operating pressure: $5 \times 10^{-5} - 10^{-3}\ mbar$
m. Magnetic field: $50G$ to $1.2kG$
n. Extent of the flat top magnetic field: $1.2\ m$
o. Axial uniformity of the plasma: $L_{uniform} > 1.2\ m$
p. Plasma source to be compatible with different ion species

On the basis of the above requirement, an experimental device has been designed and constructed in two stages. The device consists of a multi-filamentary plasma source placed in the low magnetic field region connected to a main chamber having uniform magnetic field through a transition magnetic field region. The axial profile of the magnetic field can be tailored to obtain many different configurations by feeding current to the electromagnets independently. These independent variations of magnetic fields in the source, extension, and main chamber enable the machine operation with different mirror ratio ($R_m = B_{main}/B_{source}$) configurations thus, increasing the parametric range of operation.

A number of diagnostics have been developed for characterizing the plasma and carrying out wave experiments. A low noise Langmuir probe system has been developed for measuring time resolved density and temperature. A code has been written in MATLAB® for efficiently processing the single Langmuir probe I-V trace over a wide operating range for determining the plasma parameters. A set of rack probes for measuring density and potential fluctuations in the plasma has been developed along with codes for higher order spectral analysis of the fluctuation data for detailed experimental study of intrinsic instabilities in a magnetized plasma. Excitation and detection system for ion acoustic wave and plasma oscillation have been developed and operated.

A density variation of four orders $(10^9 - 10^{12}\ cm^{-3})$ has been experimentally achieved in IMPED using different control parameters, notably pressure, axial magnetic field, mirror ratio, mesh and filament heating current. Hence, the initial target of realizing four order density variations for parametric wave studies has been met experimentally. The plasma temperature (T_e) was varied from 0.8 eV to 5 eV using the above mentioned control features of IMPED. Thus, the required range of temperature $(\ 2 - 5\ eV)$ for the phase mixing experiment has been satisfied. Out of all the controlling features used for varying the plasma parameters usage of the flexible transition magnetic field (mirror ratio) in the absence of cusp confinement in the curved surface of the source chamber is unique to IMPED. Its effectiveness in varying both the density and temperature has been substantiated with experimental data and the cause of variations of plasma parameters has also been experimentally established. The effectiveness of a mesh in altering plasma parameters in the downstream magnetized plasma has been experimentally explored. Probe measurements show that the plasma is radially and axially uniform. The axial uniformity extends to 1.2 m in the main chamber thus, satisfying the uniform plasma requirement. In addition to producing argon plasma, plasma of other ion species like helium, neon, krypton, and xenon and their different combinations can also be produced in this device. Furthermore, this machine has been designed for accommodating many plasma sources and the present plasma source can easily be replaced by other sources such as duoplasmatron [53], microwave source [61], and oxide coated cathode [76]. Apart from steady state operation, the IMPED can also sustain afterglow plasmas for sufficiently long time compared to that required for wave studies.

A method for production of quiescent magnetized plasma has been proposed using the flexible transition magnetic field between the plasma source and the main chamber that allows independent variation of magnetic field in the source (B_{source}) and the main chamber (B_{main}). Plasma with low density fluctuation has been produced by operating the system in low mirror ratio (R_m) configuration. The effectiveness of this method has been substantiated with experimental data. The plasma quiescence has been maintained around $\delta n/n \lesssim 1\%$ over a wide operating range spanning from 5×10^{-5} to 10^{-3} $mbar$ pressure and $109\ G$ to $1090\ G$ magnetic field in the main chamber, by operating the system in low mirror ratio configuration. Density fluctuation as low as $\sim 0.2\%$ has been obtained in low mirror ratio operation $R_m \sim 29$ when the magnetic field in the main chamber is held constant at $872\ G$ at 1×10^{-4} $mbar$ operating pressure. The effect of low mirror operation on the nature of fluctuations in IMPED has been experimentally explored. Operation in low mirror ratio configuration was found to give rise to a sheared electric field at the edge of the plasma, which in turn induced a sheared $\vec{E} \times \vec{B}$ rotation. Kelvin-Helmholtz [131, 134] instability has been observed due to the sheared rotation at the plasma edge. Bicoherence spectrum [122] of density fluctuation revealed nonlinear coupling of KH with low frequency modes (may be DW) producing side bands. Strong interaction of the dominant spectral component of KH with itself was observed, resulting in harmonic generation. These results may be interesting to the wider physics community as the occurrence of KH instability due to velocity sheared layer is common in hydrodynamic systems. The dynamics of drift waves is similar to the dynamics of Rossby waves if Lorentz force is compared to Coriolis force [140]. However, it must be noted that nonlinear interactions due to self-excited modes were limited to the region away from the centre of plasma and density fluctuations near the axis were very less ($\delta n/n \lesssim 1\%$).

Phase mixing of plasma oscillation was experimentally demonstrated in a unique experimental configuration for the first time, which allows one to investigate phase mixing as a steady state phenomenon instead of a transient phenomenon lasting only few nanoseconds to tens of nanoseconds. Plasma oscillations in the plasma were excited using a weak electron beam ($\eta = n_b/n \ll 1$). The non-uniformity in the background density was externally induced by exciting plasma ion acoustic wave. The frequency of the beam excited wave was much greater than the frequency of the ion acoustic wave in the background ($f_{pe} \gg \Omega$). The experiments were carried out in the regime where the wavelength of the high frequency electrostatic wave driven by the weak electron beam and the low frequency ion wave were of the same order. The power in the coherent oscillation was found to decrease on increasing the amplitude of the background ion acoustic wave and beyond a certain limit the coherent oscillation ceases to exist signifying phase mixing of plasma oscillations. Our experimental results showed that phase mixing of plasma oscillations depends on both the amplitude of oscillation and the non-uniformity of the background plasma density.

Thus, it can be concluded that a plasma device has been successfully designed and constructed on the basis of a set of requirements dictated by the physics of nonlinear plasma oscillations. The device has met all its design criteria. Phase mixing of plasma oscillations has been experimentally demonstrated in a unique experimental configuration for the first time that clearly brings out the dependence of phase mixing on both the amplitude and the background density non-uniformity in a very controlled manner.

7.2 Future scope

A versatile experimental device has been built for the experimental study of waves and instabilities in plasma. The device uses a unique flexible transition magnetic field for the production of quiescent plasma by operating the system in low mirror ratio configuration. But KH instability was observed in low mirror ratio operations in region away from the axis of the main chamber. The KH instability was found to be caused by a sheared electric field. The cause of occurrence of this sheared electric field in the low mirror ratio operating regime should be experimentally explored.

We have observed coupling between KH instability and a low frequency mode at low mirror ratio operation. The range of frequencies of the low frequency mode suggests that it may be drift waves. Detailed experiments can be carried out to identify the low frequency mode and also the exact condition when KH and low frequency mode couples can be experimentally studied. The diagnostics necessary for the study of the above mentioned instabilities have been developed completely, hence one is only required to make measurements and interpret the result.

Experiments on interaction of plasma oscillation with an ion acoustic wave in the background have been successfully carried out. The power in the coherent oscillation was found to decrease with increases in amplitude of the background ion acoustic wave and beyond a certain amplitude of the background ion acoustic wave the coherent oscillations ceases to exists. The fundamental question that arises now is, where is energy of plasma oscillation going? Theoretically one expects the energy to be dumped in the plasma but experimentally that needs to be verified. The experimental configuration used for conducting the phase mixing experiment as described in this thesis enables one to study phase mixing as a steady state phenomenon instead of a transient one. This is particularly advantageous as one is required to measure the equilibrium plasma temperature both when phase mixing is happening and in its absence to get an indication as to where is the energy getting transferred.

Phase mixing of plasma oscillations have been theoretically explained with the help of mode coupling [12]. The power from the lower ‘k’ is supposed to go to higher ‘k’ and ultimately the energy is supposed to go to the plasma by resonant wave particle interaction. This can be experimentally verified in the current device. Role of ion inertia [13] on phase mixing of plasma oscillation in uniform plasma is yet to be explored experimentally.

A parametric experimental study of the wave breaking amplitude verifying Coffey’s limit [36] needs to be carried out. In addition, a number of unresolved issues are mentioned in Chapter 1 of this thesis that can be addressed in this device.

During the course of diagnostic development, two high frequency Langmuir probe systems were developed. One is based on the usage of triaxial cable for capacitance neutralization, as described in chapter 3 of this thesis and another system was based on the dual cable method [141]. The circuit of the dual cable method Langmuir system that has been developed is given in Figure 7.1. A comparative study of both the techniques can be done to find which technique is better suited under a wide variety of experimental conditions. This particular experiment will enable other researches in the field of experimental plasma physics to make an informed decision while designing a Langmuir probe system for measuring plasma parameters with a high temporal resolution.

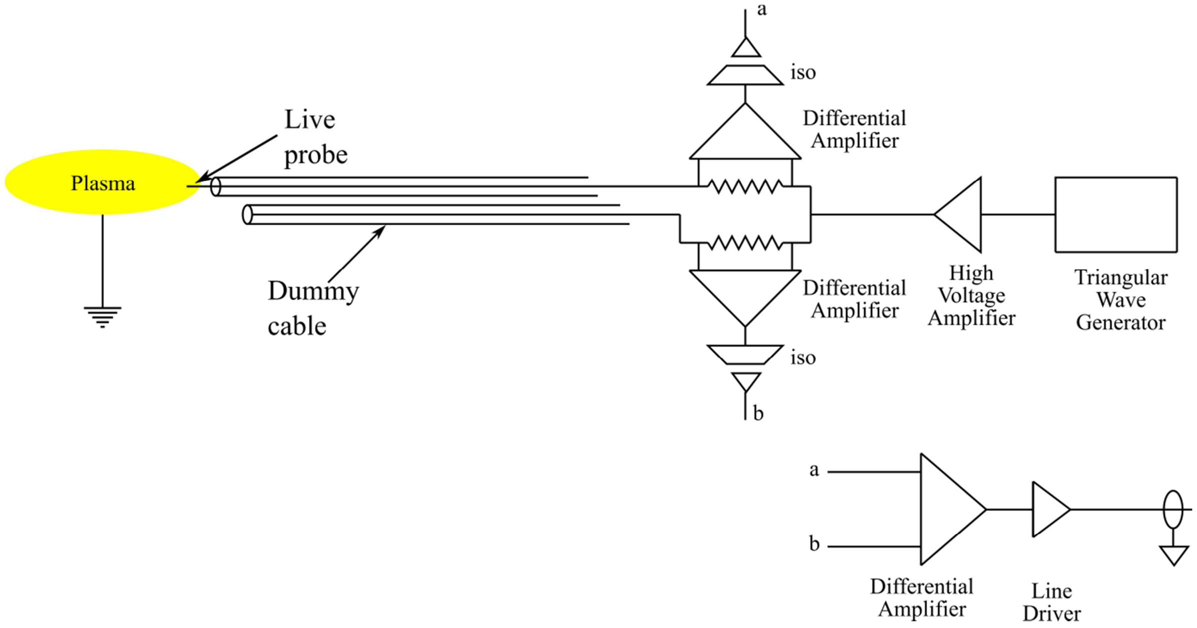

Figure 7.1: Capacitive current neutralization using the dual cable method.

REFERENCES

[1] L. Tonks and I. Langmuir, “Oscillations in ionized gases,” *Physical Review,* 33, 195 (1929).

[2] L. D. Landau, “On the vibrations of the electronic plasma,” *Journal of Physics,* 10, 25 (1946).

[3] J. Dawson, “On Landau Damping,” *Physics of fluids,* 4, 869 (1961).

[4] J. H. Malmberg and C. B. Wharton, “Dispersion of electron plasma waves,” *Physical review Letters,* 17, 175 (1966).

[5] T. O. Neil, “Collisionless Damping of Nonlinear Plasma Oscillations,” *Physics of Fluids,* 8, 2255 (1965).

[6] J. H. Malmberg and C. B. Wharton, “Collisionless damping of large amplitude plasma waves,” *Physical Review Letters,* 19, 775 (1967).

[7] C. B. Wharton, J. H. Malmberg and T. M. O' Neil, “Nonlinear effects of large amplitude plasma waves,” *Physics of Fluids,* 11, 1761 (1968).

[8] R. N. Franklin, S. M. Hamberger, G. Lampis and G. J. Smith, “Nonlinear behaviour of a finite amplitude electron plasma wave I. Electron trapping effect,” *Proceedings of Royal society,* 347, 1 (1975).

[9] R. N. Franklin, S. M. Hamberger, G. Lampis and G. J. Smith, “Nonlinear behaviour of a finite amplitude electron plasma wave II. Wave - wave interaction,” *Proceedings of Royal Society,* 347, 25 (1975).

[10] R. N. Franklin, R. R. Mackinlay, P. D. Edgley and D. N. Wall, “Nonlinear behaviour of a finite amplitude electron plasma wave. III. the side band instability,” *Proceedings of Royal Society A,* 360, 229 (1978).

[11] J. M. Dawson, “Nonlinear Electron Oscillations in a Cold Plasma,” *The Physical Review,* 113, 383 (1959).

[12] P. K. Kaw, A. T. Lin and J. M. Dawson, “Quasiresonant mode coupling of electron plasma waves,” *Physics of fluids*, 16, 1697 (1973).

[13] S. Sengupta and P. K. Kaw, “Phase Mixing of Nonlinear Plasma Oscillations in an Arbitrary Mass Ratio Cold Plasma,” *Physical Review Letter*, 82, 1867(1999).

[14] J. H. Malmberg, C. B. Wharton, R. W. Gould and T. M. O'Neil, “Plasma wave echo experiment,” *Physical Review Letters*, 20, 95 (1968).

[15] M. Tabak, J. Hammer, M. E. Glinsky, W. L. Kruer, S. C. Wilks, J. Woodworth, E. M. Campbell, M. D. Perry and R. J. Mason, “Ignition and high gain in ultrapowerful lasers,” *Phyics of Plasmas*, 1, 1626 (1994).

[16] R. Kodama, “Fast heating of ultrahigh density plasma a step towards laser fusion ignition,” *Nature*, 412, 798 (2001).

[17] E. Esarey, C. B. Schroeder and W. P. Leemans, “Physics of laser-driven plasma-based electron accelerators,” *Review Modern Physics*, 81, 1229 (2009).

[18] T. Tajima and J. M. Dawson, “Laser electron accelerator,” *Physical Review Letters*, 43, 267 (1979).

[19] J. D. Kimetec, C. L. Gordon, J. J. Macklin, B. E. Lemoff, G. S. Brown and S. E. Harris, “MeV x-ray generation with a femtosecond laser,” *Physical Review Letters*, 68, 1527 (1992).

[20] A. Y. Wong, P. Y. Cheung, M. J. McCarrick, J. Stanley, R. F. Wuerker, R. Close, B. S. Bauer, E. Fremouw, W. Kruer and B. Langdon, “Large scale resonant modification of polar ionosphere by resonant electromagnetic waves,” *Physical Review Letters*, 63, 271 (1989).

[21] A. Y. Wong, J. Steinhauer, R. Close, T. Fukuchi and G. M. Milikh, “Conservation of ozone in the upper atmosphere by selective ion removal,” *Comments on Plasma Physics and Controlled Fusion*, 63, 271 (1989).

[22] G. Botha, T. Arber, V. M. Nakariakov and F. P. Keenan, “A developed stage of alfven wave phase mixing,” *Astronomy and Astrophysics*, 363, 1186 (2000).

[23] H. Xu, Z.-M. Sheng and J. Zhang, “Phase mixing due to ion motion nad relativistic

effects in nonlinear plasma oscillations," *Physica Scripta,* 74, 673 (2006).

[24] P. Verma, S. Sengupta and P. Kaw, "Residual bernstein-greene-kruskal-like waves after one dimensional electron wave breaking in cold plasma," *Physics Review E,* 86, 016410 (2012).

[25] L. M. Gorbunov, A. A. Frolov, E. V. Chizhonkov and N. E. Andreev, "Breaking of Nonlinear Cylindrical Plasma Oscillations," *Plasma Physics Reports,* 36, 345 (2010).

[26] R. M. G. M. Trines and P. A. Norreys, "Wave-breaking limits for relativistic electrostatic waves in a one-dimensional warm plasma," *Physics of Plasmas,* 13, 123102 (2006).

[27] W. B. Mori and T. Katsouleas, "Wavebreaking of Longitudinal Plasma Oscilations," *Physica Scripta,* T30, 127 (1990).

[28] W. L. Kruer, "Introduction to the Physics of large Amplitude Plasma Waves," *Physica Scripta,* T30, 5 (1990).

[29] A. Schmitt and R. Ong, "The Effect of Collisions on Wave-Breaking in a Cold Plasma," *Applied Physics,* 22, 333 (1980).

[30] J. Albritton and P. Koch, "Cold plasma wavebreaking: Production of energetic electrons," *Physics of Fluids,* 18, 1136 (1975).

[31] B. S. Bauer, A. Y. Wong, V. K. Decyk and G. Rosenthal, "Experimental observation of superstrong electron plasma waves and wave breaking," *Physical Review Letter,* 68, 3706 (1992).

[32] M. J. Everett, A. Lal, D. Gordon, K. Wharton, C. E. Clayton, W. B. Mori and C. Joshi, "Evolution of Simulated Raman into Stimulated Compton Scattering of Laser light via Wave Breaking of Plasma Waves," *Physical review Letters,* 74, 1355 (1995).

[33] D. W. Forslund, J. M. Kindel and E. L. Lindman, "Theory of stimulated scattering process in laser-irradiated plasmas," *Physics of Fluids*, 18, 1002 (1975).

[34] A. Modena, Z. Najmudin, A. E. Dangor, C. E. Clayton, K. A. Marsh, C. Joshl, V. Malka, C. B. Darrow, C. Danson, D. Neely and F. N. Walsh, "Electron acceleration form the breaking of relativistic plasma waves," *Nature*, 377, 606 (1995).

[35] P. Michelsen, H. L. Pecseli and J. J. Ramussen, “Ion acoustic waves in the presence of electron plasma waves,” *Physics Letters,* 59A, 445 (1977).

[36] T. P. Coffey, “Breaking of large amplitude plasma oscillation,” *Physics of fluids,* 14, 1402 (1971).

[37] E. Infeld, G. Rowlands and S. Torven, “Ion density cavities can cause nonlinear plasma oscillations to peak,” *Physical Review Letters,* 62, 2269 - 2272 (1989).

[38] C. Nappi and d. Nicola, “Collisional drag can prevent plasma oscillation from breaking,” *Europhysics Letters*, 19, 381 (1992).

[39] S. Bose, M. Kaur, P. K. Chattopadhyay, J. Ghosh and Y. C. Saxena, “Inverse mirror plasma experimental device - A new magnetized linear plasma device with a wide operating range,” *Review of Scientific Instruments,* 86, 063501 (2015).

[40] W. Gekelman and R. L. Stenzel, “Large, quiescent, magnetised plasma for wave studies,” *Review of Scientific Instrument,* 46, 1386 (1975).

[41] T. Pierre, G. Leclert and F. Braun, “Magnetized double-plasma device for wave studies,” *Review of scientific instruments,* 58, 6 (1987).

[42] S. Bose, P. K. Chattopadhyay, J. Ghosh, S. Sengupta, Y. C. Saxena and R. Pal, “Inverse mirror plasma experimental device (IMPED) - a magnetized linear plasma device for wave studies,” *Journal of Plasma Physics,* 81, 345810203 (2015).

[43] E. Infeld and G. Rowlands, “Langmuir oscillations against a single-ion or cavity background,” *Physical Review A,* 42, 838 - 842, (1990).

[44] J. Dawson, “One dimensionla plasma model,” *Physics of Fluids,* 5, 445 (1962).

[45] R. C. Davidson, Methods in nonlinear plasma theory, New York: Academic Press, 1972.

[46] L. D. Landau, “On the vibrations of the electronic plasma,” *Journal of Physics*, 10, 25, 1946.

[47] Y. P. Raizer, Gas Discharge Physics, Springer-Verlag Berlin Heidelberg.

[48] R. Jones, “Laboratory plasma devices,” *Physics reports,* 61, 295 (1980).

[49] J. D. Cobine, Gaseous conductors, New York: Dover, 1958.

[50] F. F. Chen, *Production of laboratory plasmas,* New Jersy, 1964.

[51] L. M. Lidsky, S. D. Rothleder, D. J. Rose, S. Yoshikawa, C. Michelson and R. J. Mackin Jr, “Highly Ionized Hollow Cathode Discharge,” *Journal of Applied Physics,* 33, 2490 (1962).

[52] N. Sato, S. Iizuka, T. Koizumi and T. Takada, “Electron-temperature control by movable pins installed in hollow cathode discharge plasmas,” *Applied Physics Letters,* 62, 567 (1993).

[53] F. Boeschoten and F. Schwirzke, “Investigation of a stationay plasma in a magnetic field,” *Nuclear Fusion,* 2, 54 (1962).

[54] J. H. Malmberg, C. B. Wharton and W. E. Drummond, “Landau damping of electron plasma waves,” in *Plasma Physics and Controlled Nuclear Fusion Research,* Cullham, 1966.

[55] L. Jerde, S. Friedman, W. Carr and M. Seidl, “Plasma quiescence in a reflex discharge,” *Journal of Applied Physics,* 51, 965 (1980).

[56] F. F. Chen, “Helicon discharges and sources: a review,” *Plasma Sources Science and Technology,* 24, 014001 (2015).

[57] C. Watts, “Alpha: A large-area plasma helicon array,” *Review of Scientific Instruments,* 75, 1975 (2004).

[58] M. Light, F. F. Chen and P. L. Colestock, “Quiescenet and unstable regimes of a helicon plsama,” *Plasma Sources Science and Technology,* 11, 273 (2002).

[59] K. K. Barada, P. K. Chattopadhyay, J. Ghosh, S. Kumar and Y. C. Saxena, “A linear helicon plasma device with controllable magnetic field gradient,” *Review of Scientific Instruments,* 83, 063501 (2012).

[60] E. R. Ault and K. R. Mackenzie, “A large volume quiescent plasma in a uniform magnetic field,” *Review of Scientic Instruments,* 44, 1697 (1973).

[61] R. Pal, S. Biswas, S. Basu, M. Chattopadhyay, D. Basu and M. Chaudhuri, "The MaPLE device of Saha Institute of Nuclear Physics: Construction and its plasma aspects," *Review of Scientific Instruments,* 81, 073507 (2010).

[62] S. Biswas, S. Chowdhury, A. M. Pal, S. Bhattacharya, S. Basu, M. Chattopadhyay, N. Chakrabarti and R. Pal, "The MapLE device: A linear machine for laboratory plasma studies of magnetized plasma physics phenomena," *Journal of Plasma Physics,* 81, 345810205 (2015).

[63] A. Ganguli, M. K. Akhtar, R. D. Tarey and R. K. Jarwal, "Absorption of left-polazrized microwaves in electron cyclotron resonance plasmas," *Physics Letter A,* 250, 137 (1998).

[64] M. Y. Tanaka, M. Bacal, M. Sasao and T. Kuroda, "High-density plasma production for neutralizing negative ion beam," *Review of scientific Instruments,* 69, 980 (1998).

[65] G. Lisitano, R. A. Ellis Jr, W. M. Hooke and T. H. Stix, "Production of Quiescent Discharge with High Electron temperature," *Review of Scientific Instruments*, 39, 295 (1968).

[66] I. Langmuir and K. H. Kingdon, "Thermionic Effects Caused by Vapours of Alkali Metals," *Proceedings of Royal Society London A,* 107, 61 (1925).

[67] A. M. Levine, A. F. Kuckes and R. W. Motley, "Electron-Cyclotron resonance Heating of Alkali Plasmas," *Journal of Applied Physics*, 38, 4435 (1967).

[68] P. J. Barrett, H. G. Jones and R. N. Franklin, "Dispersion of electron plama waves," *Plasma Physics,* 10, 911 (1968).

[69] P. J. Paris and N. Rynn, "An improved Q-Machine source," *Review of Scientific Instruments,* 61, 1095 (1990).

[70] N. Rynn and N. D'Angelo, "Device for Generating a Low Temperature, Highly Ionized Cesium Plasma," *Review of Scientific Instruments,* 31, 1326 (1960).

[71] N. Rynn, "Improved quiescent plasma source," *Review of Scientific Instruments*, 35, 40 (1964).

[72] T. Kaneko, H. Ishida, R. Hatakeyama and N. Sato, "An improved Q - machine source

with a rotating cathode system," *Review of Scientific Instruments,* 72, 3854 (2001).

[73] F. F. Chen, "Coaxial cathode design for plasma sources," *Review of Scientific Instruments,* 40, 1049 (1969).

[74] R. J. Taylor, K. R. Mackenzie and I. Ikezi, "A large double plasma device for plasma beam and wave studies," *Review of Scientific Instruments,* 46, 1675 (1972).

[75] R. Limpaecher and K. R. Mackenzie, "Magnetic Multipole Containment of Large Uniform Collisionless Quiescent Plasmas," 44, 1697 (1973).

[76] W. Gekelman, H. Fister, Z. Lucky, Z. Bamber, D. Leneman and Z. Maggs, "A large volume quiescent plasma in a uniform magnetic field," *Review of Scientific Instruments,* 62, 12 (1991).

[77] R. L. Stenzel and J. M. Urrutia, "Currents between tethered electrons in a magnetized laboratory plasma," *Journal of Geophysical research,* 95, 6209 (1990).

[78] A. G. Lynn, M. Gilmore, C. Watts, J. Herrea, R. Kelly, S. Will, S. Xie, L. Yan and Z. Yue, "The HelCat dual-source plasma device," *Review of Scientific Instruments,* 80, 103501 (2009).

[79] L. M. Awasthi, G. Ravi, P. K. Srivastava and S. K. Matto, "A large area multifilamentary plasma source," *Plasma Sources Science and Technology,* 12, 158 (2003).

[80] T. Pierre, G. Leclert and F. Braun, "Magnetized double plasma device for wave studies," *Review of Scientific Instruments,* 58, 6 (1987).

[81] R. F. Holsinger and K. Halbach, "Download Area for Poisson Superfish," Los Alamos National Laboratory, 18 October 2013. [Online]. Available: http://laacg.lanl.gov/laacg/services/download_sf.phtml.

[82] *Indian Standard Copper Specification,* New Delhi: Bureau of Indian Standards, 2007.

[83] H.M. Mott-Smith and I. Langmuir, "The Theory of Collectors in Gaseous Discharges", *Physical Review,* 28, 727 (1926).

[84] P. M. Chung, L. Talbot and K. J. Touryan, "Electric probes in Stationary and Flowing

Plasmas: Part1. Collisionless and Transitional Probes," *AIAA Journal*, 12, 133 (1974).

[85] C. H. Su and R. E. Kiel, "Continuum Theory of Electrostatic Probes," *Journal of Applied Physics*, 37, 4907 (1966).

[86] R. E. Kiel, "Continuum Electrostatic Probe Theory for Large Sheaths on Spheres and Cylinders," *Journal of Applied Physics*, 40, 3668 (1969).

[87] B.-W. Koo, N. Hershkowitz and M. Sarfaty, "Langmuir probe in low temperature, magnetized plasmas: Theory and experimental verification," *Journal of Applied Physics*, 86, 1213 (1999).

[88] J. R. Sanmartin, "Theory of a probe in a strong magnetic fielld," *Physics of Fluids*, 13, 103 (1970).

[89] P. M. Chung, L. Talbot and K. J. Touryan, Electric Probes in Stationary and Flowing Plasmas-Theory and Application, Springer-Verlag Berlin Heidelberg, 1975.

[90] E. W. Peterson and L. Talbot, "Langmuir Probe Respose in a Turbulent Plasma," *AIAA Journal*, 8, 1391 (1970).

[91] I. H. Hutchinson, Principles of Plasma Diagnostics, Cambridge, 2002.

[92] J. D. Swift and M. R. Schwar, Electrical Probes for Plasma Diagnostics, London: Iliffe, 1970.

[93] N. Hershkowitz, "Chapter 3 - How Langmuir Probes Work," in *Plasma Diagnostics: Discharge Parameters and Chemistry*, Academic Press, 1989, pp. 113 - 183.

[94] V. I. Demidov, S. V. Ratynskaia and K. Rypdal, "Electric probes for plasmas: The link betwen theory and instrument," *Review of Scientific Instruments*, 73, 3409 (2002).

[95] F. F. Chen, "Electric Probes," in *In Plasma Diagnostic Techniques, edited by Huddlestone, R.H. and Leornard, S.L*, New York, Academic Press, 1965.

[96] B. E. Cherrington, "The use of electrostatic probes for plasma diagnostics—A review," *Plasma Chemistry and Plasma Processing* , 2, 113 (1982).

[97] J. E. Allen, "Probe Theory - The Orbital Motion Approach," *Physica Scripta*, 45, 497 (1992).

[98] J. E. Allen, R. F. Boyd and P. Reynolds, "The Collection of Positive Ions by a Probe Immersed in a Plasma," *Proceedings of the Physical Society. Section B,* 70, 297 (1957).

[99] F. F. Chen, *Journal of Nuclear Energy Part C,* 7, 47 (1965).

[100] I. B. Bernstein and I. N. Rabinowitz, "Theory of Electrostatic Probes in a Low-Density Plasma," *Physics of Fluids,* 2, 112 (1959).

[101] J. G. Laframboise, "Theory of Spherical and Cylindrical Langmuir Probe in Collsionless Maxwellian Plasma at Rest," Rept 100 (1966).

[102] A. A. Sonin, "Free-Molecule LangmuirProbe and Its Use in Flowfield Studies," *AIAA Journal,* 4, 1588 (1966).

[103] M. G. Dunn and J. A. Lordi, "Measurements of Electron Temperature annd Number density in Schock Tunnel flows. Part I, Development of Free-Molecular Langmuir Probes," *AIAA Journal,* 7, 1458 (1969).

[104] K. A. Graf and J. H. deLeeuw, "Comparision of Langmuir Probe and Microwave Diagnostics Techniques," *Journal of Applied Physics,* 39, 4466 (1967).

[105] R. E. Kiel, "Electrostatic Probe Theory for Free Molecular Cylinders," *AIAA Journal,* 6, 708 (1968).

[106] E. W. Peterson and L. Talbot, "Collisionless Electrostatic Single-Probe and Double-Probe Measurements," *AIAA Journal,* 8, 2215 (1970).

[107] C. Steinbrüchel, "A new method for analyzing Langmuir probe data and the determination of ion densities and etch yields in an etching plasma," *Journal of Vacuum Science and Technology A,* 8, 1663 (1990).

[108] A. Karamcheti and C. Steinbrüchel, "Parametrization of Laframboise's results for spherical and cylindrical Langmuir probes," *Journal of Vacuum Science and Technology A*, 17, 3051 (1999).

[109] G. Narasimhan and C. Steinbrüchel, "Analysis of Langmuir probe data: Analytical parametrization, and the importance of end effect," *Journal of Vacuum Science and Technology A*, 19, 376 (2001).

[110] M. Mausbach, “Parametrization of the Laframboise theory for cylindrical Langmuir probe analysis,” *Journal of Vaccum Science and Technology A,* 15, 2923 (1997).

[111] F. F. Chen, “Langmuir probe analysis for high density plasmas,” *Physics of Plasmas,* 8, 3029 (2001).

[112] T. E. Sheridan, “How big is a small Langmuir probe?,” *Physics of Plasmas,* 7, 3084 (2000).

[113] F. F. Chen and D. Anrush, “The floating potential of cylindrical Langmuir probes,” *Physics of Plasmas,* 8, 5051 (2001).

[114] I. G. Brown, A. B. Compher and W. B. Kunkel, “Response of a Langmuir Probe in a Strong Magnetic Field,” *Physics of Fluids,* 14, 1377 (1971).

[115] F. F. Chen, “Saturation Ion Currents to Langmuir Probes,” *Journal of Applied Physics,* 36, 375 (1965).

[116] G. Neumann, M. Kammeyer and B. Schneemann, “Personal-computer-based control and evaluation of langmuir probe characteristics,” *Measurement Science and Technology,* 6, 391 (1995).

[117] R.B Lobbia and A.D. Gallimore, “Temporal limits of a rapidly swept langmuir probe”, *Physics of Plasmas*, 17, 073502 (2010)

[118] K. Hansen, T. Klinger and A. Piel, “Computer controlled probe diagnostic system and applications in a magnetized laboratory plasma,” *Review of Scientific Instruments,* 65, 2615 (1994).

[119] I. Langmuir, “The pressure effect and other phenomena in gaseous discharges,” *Journal of the Franklin Institute,* 196, 751 (1923).

[120] J. R. Smith, N. Hershkowitz and P. coakley, “Inflection-point method of interpreting emissive probe characteristics,” *Review of Scientific Instrument,* 50, 210 (1979).

[121] J. P. Sheehan and N. Hershkowitz, “Emissive Probes,” *Plasma Sources Science and Technology,* 20, 063001 (2011).

[122] Y. C. Kim and E. J. Powers, “Digital Bispectral Analysis and its applications to Nonlinear Wave Interactions,” *IEEE Transactions on Plasma Science,* 7, 120 (1979).

[123] J. M. Beall, Y. C. Kim and E. J. Powers, “Estimation of wave number and frequency spectra using fixed probe pairs,” *Journal of Applied Physics*, 53, 3933 (1982).

[124] H-Y Chang, C. Lien, A. Seyhoonzadeh, P. Forsling and K. E. Lonngren, “On the Double-Grid Excitation of Linear and Nonlinear Ion-Acoustic Waves,” *IEEE Transactions of Plasma Science,* 16, 50 (1988).

[125] I. Alexeff and W. D. Jones, “Electron-emitting and electron-collecting probes as ion wave detectors,” *Physics Letters,* 20, 269 (1966).

[126] A. Y. Wong, “Observation of the Electron Contribution to Ion Acoustic Waves,” *Physical Review Letters,* 14, 252 (1965).

[127] H. Derfler and T. C. Simonen, “Experimental verification of Landau waves in an isotropic electron plasma,” *Journal of Applied Physics,* 5014 (1967).

[128] J. R. Thompson, “Nonlinear Evolution of Collisionless Electron Beam-Plasma Systems,” *Physics of Fluids,* 14, 1532 (1971).

[129] M. A. Lieberman and A. J. Lichtenberg, Principles of plasma discharges and materials processing, New York: John Wiley & Sons, Inc., 1994.

[130] K. R. Mackenzie, R. J. Taylor, D. Cohn, E. Ault and H. Ikezi, “Plasma electron heating by absorption of cold electrons,” *Applied physics Letters,* 18, 529 (1971).

[131] F. Brochard, E. Gravier and G. Bonhomme, “Transition from flute modes to drift waves in a magnetized plasma column,” *Physics of Plasmas,* 12, 062104 (2005).

[132] S. Chandrasekhar, “Hydrodynamic and Hydromagnetic Stability,” in *Chap 11*, Oxford, Claredon, 1961.

[133] C. C. Lin, The Theory of Hydrodynamic Stability, Cambridge: Cambridge University Press, 1966.

[134] D. L. Jassby, “Transverse Velocity Shear Instabilities within a Magnetically Confined Plasma,” *Physics of Fluids,* 15, 1590 (1972).

[135] R. J. Goldston and P. H. Rutherford, Introduction to plasma physics, Bristol and Philadelphia: Institute of Physics Publishing, 1995.

[136] J. M. Beall, Y. C. Kim and E. J. Powers, “Estimation of wavenumber and frequency spectra using fixed probe pairs,” *Journal Applied Physics*, 53, 3933 (1982).

[137] Y. C. Kim and E. J. Powers, “Digital Bispectral Analysis and Its Applications to Nonlinear Wave interactions,” *IEEE Transactions on Plasma Science*, PS-7, 120 (1979).

[138] J. R. Thompson, “Nonlinear Evolution of Collisionless Electron Beam-Plasma Systems,” *Physics of Fluids*, 14, 1532 (1971).

[139] T. Shirakawa and H. Sugai, “Plasma Oscillation Method for Measurement of Absolute Electron Density in Plasma,” *Japanese Journal Applied Physics* , 32, 5129 (1993).

[140] W. Horton and A. Hasegawa, “Quasi-two-dimensional dynamics of plasmas and fluids,” *Chaos*, 4, 227 (1994).

[141] T. F. Yang, Q. X. Zu and P. Liu, “A dual-cable noise reduction method for Langmuir probes,” *Review of Scientific Instruments*, 66, 3879, (1995).